UNIVERSITY OF MILANO BICOCCA
Department of Earth and Environmental Sciences

Modelling the suitability for ice core drilling of mountain glaciers and development of new spectroscopy systems for cold room laboratory and environmental monitoring

Roberto Garzonio

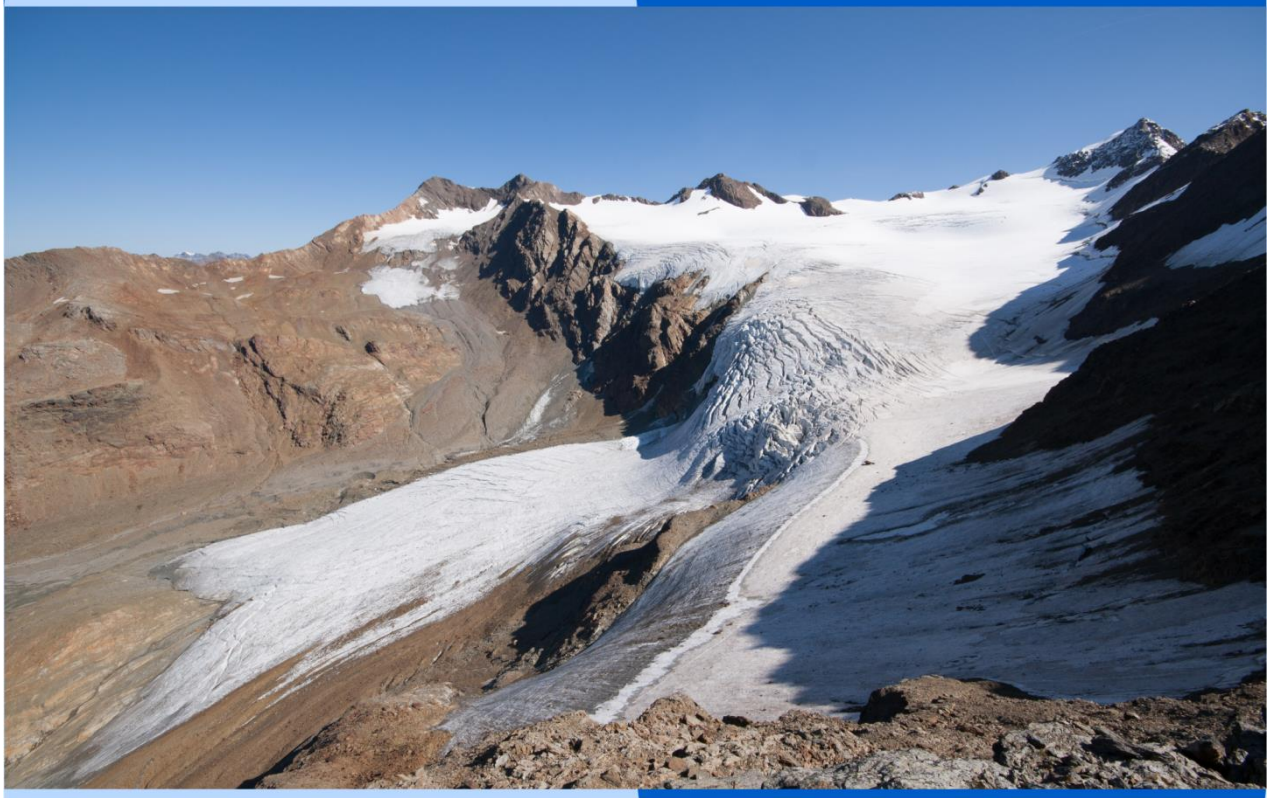

Tutor: Dr. Roberto Colombo

Ph.D. Dissertation

Ph.D. SCHOOL OF ENVIRONMENTAL SCIENCES, XXVIII CICLE

University of Milano-Bicocca

Department of Earth and Environmental Sciences

PH.D. SCHOOL OF ENVIRONMENTAL SCIENCES, XXVIII CYCLE

Ph.D. Dissertation

MODELLING THE SUITABILITY FOR ICE CORE DRILLING OF MOUNTAIN GLACIERS AND DEVELOPMENT OF NEW SPECTROSCOPY SYSTEMS FOR COLD ROOM LABORATORY AND ENVIRONMENTAL MONITORING

CANDIDATE:

Roberto Garzonio

TUTOR: DR. ROBERTO COLOMBO

ADVISOR: DR. MICHELE MERONI

COORDINATOR: PROF. VALTER MAGGI

Ringraziamenti

Grazie a tutti voi che avete
condiviso con me questi anni,
Biagio, Dani, Max, Teo e Marco
per la vostra amicizia, il vostro aiuto sincero…

Grazie a tutti gli amici del
laboratorio di telerilevamento e di geomatica,
per l'entusiasmo, la simpatia e l'amicizia offerta…

Grazie a chi mi ha permesso di arrivare fino a qui
e di fare questa preziosa esperienza
per le cose imparate, i valori veri trasmessi…

Grazie agli amici di strada
e a tutti quelli che leggeranno
per il vostro cercare, le vostre intuizioni…

Grazie a Te… che sei bellezza per occhi nuovi…

per il vostro cammino, le infinite possibilità di vita
per la vostra ricerca, le soddisfazioni, le corse e le attese
per gli anni che verranno, le cose che rimarranno e quelle che cambieranno
per le vostre scelte, mai banali e intrise di realtà

per la strada che verrà.

TABLE OF CONTENTS

Abstract

Mountain glaciers and non-polar ice cores are very detailed sources of paleo-proxy data essential to achieve a complete overview of climate and environmental changes. The increase in the glaciers melting leads to a loss of information, affecting the possibility to predict the climate evolution. In this context, it is important to define a set of guidelines and create dedicated maps to identify suitable glaciers for future ice core drillings. In the first year of my research, the Suitability for Ice Core Drilling (SICD) was defined as the likelihood of drilling a glacier to retrieve an ice core with preserved stratigraphic information that allows the reconstruction of historical climate and environmental conditions. Environmental variables related to the SICD were selected on the basis of previously drilled sites, according to available scientific literature and glaciologists opinions. Two different spatial multi-criteria analysis—one knowledge-driven and one data-driven method—were implemented to combine key variables (slope, local relief, temperature and direct solar radiation) in order to map the potential drilling sites in the European Alps and in the Asian High Mountain glaciers. Accuracy of the models were evaluated and first indications of potential drilling sites were reviewed. Results can be considered valuable for future selection of potential drilling sites.

In the second year of my PhD, a light UAV was developed for collecting spectral measurements in support of field spectroscopy surveys. The system, namely HyUAV, is based on a four-rotors platform with hovering capability, equipped with a non-imaging spectrometer and a RGB camera. The HyUAV collects simultaneously hyperspectral data (350-1000 nm, ~1.5 nm spectral resolution) of Earth reflected radiance and RGB images. The Entrance Optics Receptor (EOR) was specifically developed to optimize the spectrometer field of view and to collect in-flight dark current. The geometric, radiometric and spectral performances of the system were characterized through

dedicated laboratory tests. Then, the accuracy of the hyperspectral data were evaluated during flight tests comparing spectral data collected from HyUAV with ground-based measurements. Two methods to estimate surface reflectance from HyUAV were investigated and discussed providing suggestions for an accurate retrieval of surface reflectance. The results showed: i) good systems stability of the system (in terms of geometric, radiometric and spectral features); ii) accurate spectra measurements (in terms of radiance and reflectance); iii) similar results for the delineated methods to calculate reflectance. The HyUAV was demonstrated to be a reliability systems for supporting field spectroscopy surveys and a promising platform for a wide range of environmental applications.

Imaging spectroscopy is a powerful technique that provides insights information of surfaces properties and materials composition. This technique aims to investigate spectral features at very detailed spatial resolution. Applied to ice cores analysis, hyperspectral imaging can be considered an innovative technique. During the third year of my PhD, a fully automated Hyperspectral systems for Imaging Ice core (HYCE) in a cold-room environment was developed. The system is composed by an high-precision linear stage that embeds a imaging hyperspectral sensor (Headwall Photonics VINR spectrometer, 380-1000 nm, 2-3 nm spectral resolution, 1004 spatial pixels) and a dedicated stable halogen light source. Several tests were performed on the system to evaluate the components and verify the efficiency in cold environments. First hyperspectral imaging of ice cores were collected. The Snow Darkening Index (SDI) was calculated observing its spatial relation with impurity layers. The research provided important results in the development of a new hyperspectral system, inspecting the powerful to estimate past atmospheric depositions such as mineral dust.

Riassunto

I ghiacciai montani sono importanti fonti di dati paleoclimatici, essenziali allo studio dei cambiamenti climatici e ambientali. L'aumento della fusione dei ghiacciai sta portando alla perdita di preziose informazioni utili a predire l'evoluzione del clima. In questo contesto, è fondamentale definire le linee guida e creare mappe per l'identificazione delle aree idonee ad essere perforate. Nel primo anno di dottorato, ho definito l'idoneità di un ghiacciaio alla perforazione (SICD) come la probabilità di estrarre un campione di ghiaccio che possiede una stratigrafia ben conservata, utile alla ricostruzione del clima del passato. Le varabili ambientali introdotte nel modello, relazionate con la perforabilità, sono state selezionate in accordo alle perforazioni già effettuate, e alla letteratura scientifica, considerando l'opinione degli esperti. Due modelli spaziali sono stati sviluppati: il promo basato sulla conoscenza di esperti, il secondo di tipo probabilistico. Le variabili scelte (pendenza, rilievo locale, temperatura, radiazione solare diretta) sono state così combinate al fine di mappare le aree potenzialmente perforabili presenti nelle Alpi e in Asia. L'accuratezza del modello è stata valutata e sono state indicati i siti più idonei ad essere perforati. La ricerca ha permesso di fornire preziose informazioni utili alla scelta dei prossimi siti di perforazione.

Nel secondo anno di dottorato un Sistema Aeromobile a Pilotaggio Remoto (SAPR) è stato sviluppato per acquisire misure spettrali durante campagne di spettroscopia di campo. Il sistema, nominato HyUAV, è basato su una piattaforma APR equipaggiata con uno spettrometro e una camera RGB. HyUAV è in grado di acquisire simultaneamente dati iperspettrali (350-1000 nm, 1.5 nm di risoluzione spettrale) della radiazione riflessa dalla Terra e immagini RGB. Un'ottica specifica (EOR) è stata sviluppata al fine di ottimizzare il campo di vista dello spettrometro e di misurare il

segnale di Durk Current durante il volo. Le performance geometriche, radiometriche e spettrali del sistema sono state caratterizzate attraverso alcuni test di laboratorio ed è stata valutata l'accuratezza e la precisione dei dati iperspettrali raccolti attraverso un test di volo. Due metodi per la stima della riflettanza da UAV sono stati proposti e discussi. I risultati raggiunti mostrano: i) un'ottima stabilità del sistema (in termini geometrici, radiometrici e spettrali); ii) misure spettrali accurate (sia in termini di radianza che di riflettanza); iii) risultati simili tra i due metodi di stima della riflettanza. Lo studio ha dimostrato che il sistema HyUAV può essere considerato affidabile al fine di supportare indagini di spettroscopia di campo e promettente per un'ampia gamma di applicazioni ambientali.

La spettroscopia ad immagine è una tecnica efficace che fornisce importanti informazioni per la caratterizzazione delle proprietà ottica delle superfici a scala spaziale di dettaglio. Applicata all'analisi delle carote di ghiaccio, essa può essere considerata una tecnica innovativa utile a migliorare la conoscenza dei cambiamenti climatici. Durante il terzo anno di dottorato, ho sviluppato un sistema automatico per acquisire immagini iperspettrali (HYCE) in camera fredda. Il sistema è composto da una un motore lineare ad alta precisione spaziale, il quale trasporta uno spettrometro iperspettrale ad immagine (Headwall Photonics VINR, 380-1000 nm, 2-3 nm di risoluzione spettrale, 1004 pixels spaziali) e una lampada alogena dedicata. Test di laboratorio sono stati effettuati al fine di valutare le componenti del sistema. Le prime immagini iperspettrali di una carota di ghiaccio sono state acquisite in camera fredda ed analizzate. In particolare è stato calcolato lo Snow Darkening Index (SDI) ed è stata verificare la sua applicabilità per la stima delle concentrazione di deposizioni atmosferiche minerarie nelle carote di ghiaccio.

1. INTRODUCTION

1.1 High mountain glaciers archives of environmental data

Glaciers play a central role in the global environmental system and they are linked with changing patterns of the ocean–atmosphere circulation, climate, sea level and landscape. There is a strong relationship between glaciers and climate (Figure 1.1): climate controls glacier behaviours including size, thermal and hydrological regime, movement and geomorphic activity, and glaciers exert control over climate by affecting the albedo, the surface energy balance and the composition and circulation of the atmosphere. Because they reflect aspects of the global system, glaciers can be used as a tool to reconstruct past environmental conditions. In particular, mountain glaciers respond very quickly to different climate forcing, preserving atmospheric compositions and environmental components stored in the ice (Knight, 2004).

Figure 1.1: The retreat of Morteratsch Glacier, Switzerland from 1985 to present. From 1980 a significant increase in temperature has led to glacier retreat rapidly. Glacier are linked with changing patterns in landscape and climatic circulation.

Drilling glaciers to extract ice cores is a main source of data for paleo-environmental reconstruction both for glaciologists and for other environmental scientists (Figure 1.2). The mainly information contained in the glaciers regards: local air temperature and precipitation rate; regional atmospheric circulation, origin of the precipitation and dust transportation; chemical composition of the atmosphere including greenhouse

gas concentrations; volcanic and solar activity. Being often adjacent to densely inhabited regions, ice cores collected from mountain glaciers are more susceptible to the influence exerted by human activities. Thus, they are an excellent indicators of anthropogenic forcing on climate (Jouzel and Masson-Delmotte, 2010a).

Figure 1.2: Ice core drilling to climate studies. A) A 2 meter section of ice core from Combatant Col (British Columbia) is removed from an electrothermal drill. Credit: Doug Clark, Univ. Washington. B) The drilling dome built near the summit of Mt. Ortles. Four 60-75 m deep ice cores were retrieved at an altitude of 3860 m. Credit: Paolo Gabrielli. C) Drill head and ice core from a depth of 2,874 meters at Dome C Station in East Antarctica. This ice core is about 491,000 years old. The entire core contains a continuous record of greenhouse gases for the past 650,000 years. Credit: Laurent Augustin. Laboratoire de Glaciologie et Géophysique de l'Environnement. D) Colle Gnifetti drilling sites, Monte Rosa Massif. Credit: Stefano Roverato.

Ice cores preserved layered sequences of information that extends into the Pleistocene including the Ice Age and previous warmer interglacial periods. Deep ice cores, retrieved from Antarctica and Greenland ice sheets, allow to go back in time providing the reconstruction of climate variability over hundreds of thousands of years (Epica, 2004; Jouzel and Masson-Delmotte, 2010b). While, ice core cores drilled from high-altitude glaciers yield continuous high-resolution seasonal records, that can be considered a unique set of fundamental regional observations (Figure 1.3) (Thompson, 2000, 2010; Thompson and others, 2013).

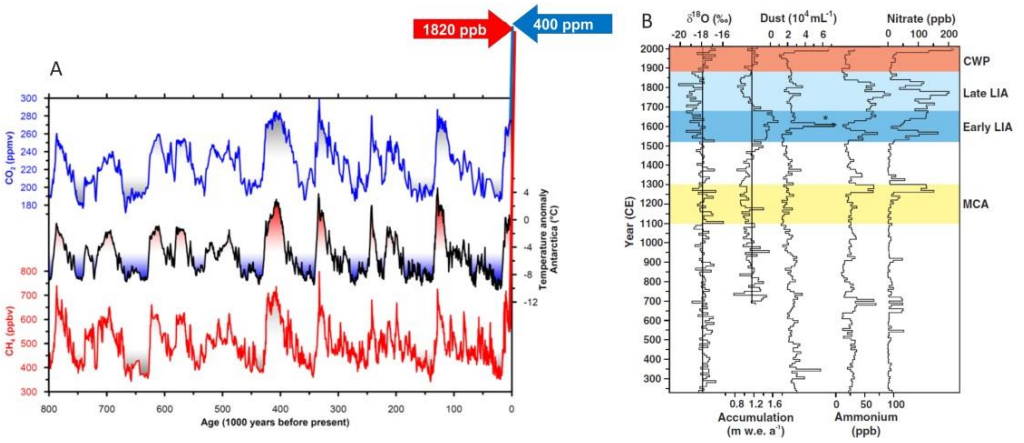

Figure 1.3: A) Results from the Antarctic EPICA Dome C ice core showing the development of temperature and the concentrations of the atmospheric greenhouse gases carbon dioxide (CO_2, in blue) and methane (CH4, in red) over the past 800 thousand years. Modern values are indicated by arrows (CO_2 concentration 400 ppm, CH4 concentration 1820 ppb, data from 2015). The temperature record shows the temperature anomaly from present day temperature. The natural variability of past temperatures and greenhouse gas concentrations is related to the glacial cycles. In recent times, the greenhouse gas concentrations are seen to show a very abrupt rise as compared to the natural levels of the past 800 thousand years. The rise is caused by mankind's extended use of fossil fuels since the industrial revolution. Credit: Professor Thomas Blunier, Centre for Ice and Climate, Niels Bohr Institute, University of Copenhagen. B) Annually resolved ice core records from the Quelccaya ice cap (5670 meters above sea level) in Peru. It extend back ~1800 years and provide a high-resolution record of climate variability there. Decadal averages of $\delta^{18}O$, net accumulation, insoluble dust, ammonium, and nitrate in the ice core. The asterisk on the dust profile indicates the 1600 CE eruption of Huaynaputina (Peru) (Thompson and others, 2013).

The conservation and the reliability of the glacial records can be attributed to the permanent freezing state of the glaciers. In recent decades, in the most regions of the world, glaciers have been retreating, thinning, and disappearing at an accelerated rate (Figure 1.4). Such trends are predicted to continue. This widespread glacier decline has resulted in numerous environmental consequences such as: freshwater supply crises, natural calamities, and sea level rise. Furthermore, glacial archives information is vanishing with rapid glaciers reduction; the possibility to obtain past environmental records is greatly affected as the possibility to predict the future climate evolution (Stocker and others, 2013).

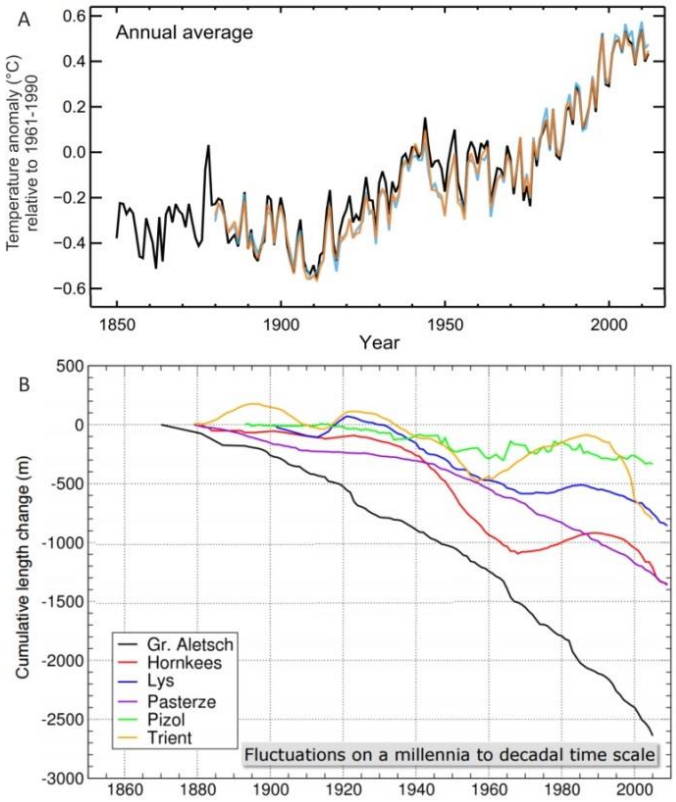

Figure 1.4: A) Observed global mean temperature combined land and ocean surface temperature anomalies relative to the mean of 1961–1990 from 1850 to 2012. B) Glacier retreat from 1880 to 2012. The graph show the cumulative length of glaciers changes in the Alps. The increasing in the Earth temperature produce glacier retreat in the most regions of the world (Stocker and others, 2013).

Despite the progress in remote sensing and analytical techniques, our reconstructions of past glaciations remain tentative, our understanding of modern glacial processes incomplete and our modelling of their future unreliable. Vanishing records represent unique memories of the most recent and intensive human impact on the earth's system. Therefore, they are invaluable reference for the introduction of new environmental policies and to confirm their efficacy in the future.

In this context, it is important to identify a set of potentially valuable drilling sites in order to obtain new ice cores from mountain glacier. In fact, collecting more ice cores from mid-latitude mountains glaciers spatially located around the Earth could provide

highly resolved climatic records, fundamental to improve the current knowledge of climate forcing and future variability at global and local scale. Furthermore, the development of new advanced techniques to collect essential glacial end environmental information, and for analysing ice cores is certainly a scientific challenge. Changes in the climate systems, in fact, cause impacts on a huge part of the Earth's populations and on natural ecosystems. Understanding climate and environmental variations is necessary for the development and the implementation of sustainable policies with the essential purpose to preserve environment to new generations. (Field and others, 2014; Zhang and others, 2015).

1.2 New hyperspectral tools in environmental change

In the last decade, the Unmanned Aerial Vehicles (UAVs) are becoming a commonly used platforms for collecting proximal sensing data. This new technology is very useful for Earth observation studies to a wide range of scientific disciplines. It represent a low-cost and low-impact solution to environmental management in a variety of ecosystems. Although many types of satellite imagery are already available – low resolution (Landsat, MODIS) and high resolution (WorldView, Quickbird) – they sometimes cannot offer sufficiently high resolution, cover the specific area of study, or capture the time series necessary to the purpose of the research. With changing ecosystems and disaster dynamics caused by the climate change and the anthropogenic impacts, the on-demand of aerial data collection and real-time environmental monitoring will become increasingly important (Trevors and Weiler, 2013).

With an high level of flexibility and the abilities to high spatial resolution imaging UAVs are advantageous tools for environmental monitoring. They might be employed for autonomous/routinely operations, real time monitoring, to collect data with different observation requirements (i.e. different scale/resolution, view angle and revisit time), and to facilitate data collection in hardly accessible sites. Specific environmental

applications that use UAV systems concern: vegetation and precision farming, photogrammetry and creation of 3D models, geomorphology, glaciers and landslides monitoring, ecology, civil applications as disaster and risk managements (Colomina and Molina, 2014).

UAVs equipped with different type of sensors (e.g. RGB camera, multi- or hyper-spectral sensor, thermal camera, miniaturized LIDAR, etc.) can be exploiting for collecting high resolution data over glaciers and every types of ecosystems (Figure 1.5). This technologies could provide exciting new information from which can be investigated the climate change evolution, the relationship between glaciers and environment, and the impact of anthropogenic activities.

Figure 1.5: UAV in environmental research. A) Anteos UAV produced by Aermatica S.P.A. B) Use of the UAV in snow covered area during a field campaigns organized to measure spectral reflectance of snow after mineral dust depositional events (Di Mauro and others, 2015).

Field spectroscopy is an essential technique in remote sensing to gain valuable insight on Earth's surface optical properties. The hyperspectral sensors capture data in contiguous narrow bands of the electromagnetic spectrum. Therefore, hyperspectral remote sensing provides spectral features that can be investigated to quantify surfaces materials and compositions. The field-based spectral measurements are useful in calibration of remote sensing sensors, development/testing of models and evaluating the optimum spectral bands for particular applications. The development and the progress of significant new remote sensing technology can provide potential

advancements of imaging spectroscopy in the Earth sciences (Schaepman and others, 2009; Greenberger and others, 2015).

Hyperspectral imaging, traditionally used for airborne remote sensing, is now becoming a valuable tool for in-line inspection instruments and quality control investigations. It allows to capture wavelength intensity images of a scene with exceptional spatial resolution (Figure 1.6). Therefore, it provides significantly more analytical power than currently available single-point spectroscopy tools. Hyperspectral imaging is emerging analytical technique in applications such as: agriculture, food safety and quality, life sciences, mineral exploration, etc. Because this systems were originally designed for airborne applications (performed in field conditions such as available sunlight), new applications required innovative instrument designs to achieve stable sample illumination and to optimize efficiency and dynamic parameters of the sensor (Bannon, 2009).

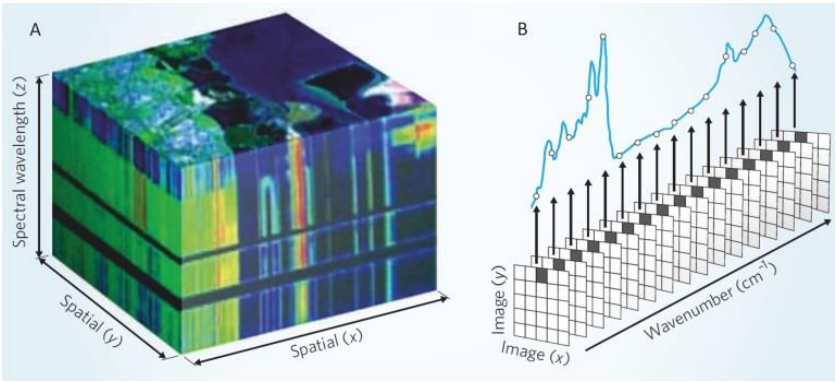

Figure 1.6: Hyperspectral imaging allows for the differentiation, display and classification of objects based on their chemical composition. A) the hyperspectral image cube is built up as the sensor passes over the ground or as products pass in front of the sensor. B) The hyperspectral datacube is a three-dimensional image comprised of spatial data (x and y coordinates) and spectral data (created by the diffraction grating, which disperses the wavelengths of light). Credit: (Bannon, 2009).

In order to assets the climatic and environmental changes, as well as glaciers retreats and consequently impacts on Earth's ecosystems and populations, new technology should be developed. Hyperspectral spectroscopy can be considered a powerful

techniques for these propose. Spectral data, in fact, can be analysed in order to identify spectral features related to concentrations of various snow and ice components such as: mineral dust, tephra volcanic eruption, nuclear fallout, anthropogenic particulate matter and pollutants, pollens, etc. Spectral data collected on the cryosphere can be used to develop new algorithms for accurate estimation of various snow and glacier parameters such as: grain size, fractional snow cover area, snow albedo, snow cover mapping, snow melts, etc. Furthermore, analyses of ice core features and microstructure could be used to identify annual layers thickness, grains, discontinuity, bubbles, refers to past climatic conditions such as atmospheric components, snow accumulation rate and circulation patterns.

UAVs can be considered new platform to investigate Earth's surface optical properties. The hyperspectral cameras integrated on UAVs, in fact, allow collection of high spectral resolved data with high spatial and temporal resolution. While, hyperspectral imaging applied to ice cores can be considered an innovative technique, that could provide valuable information improving the understanding of climate and environmental change.

1.3 Objectives and thesis structure

The main objective of this thesis is proposed a methodology to map the suitability of mountain glacier for ice core drilling and the development of new spectroscopy systems for environmental monitoring and ice core investigations. Each chapter of the Ph.D. thesis is structured as a scientific papers with its own introduction, methods, results, discussion and conclusions.

In Chapter 2, I present the activity mainly conduced in the first year of my Ph.D. This activity is a part of the NextData project, that aims to develop a national system for retrieval, storage, access and diffusion of environmental and climate data from mountain and marine areas. The research was aimed to define the suitability for ice core drilling in order to identify the potential drilling sites in the European Alps and in

the Asian High Mountain glaciers. First I defined the criteria governing the selection of a drilling site, referring to the available literature and collecting glaciologists' opinions. Then, I proposed a methodology to map potential drilling sites combining selected environmental variables (related to the SICD) based on spatial multicriteria analysis methods. Maps of suitable drilling sites and first indication of more potential glacier were proposed and discussed to provide useful information in the selection of future drillings.

In the Chapter 3 is presented the activity aimed to developed a new light UAV for collecting visible to near-infrared spectral measurements during field spectroscopy surveys. The Hyperspectral UAV (HyUAV) was equipped with an optical payload developed combining a high-resolution non-imaging VIS-NIR spectrometer with a RGB digital camera. I designed a specific entrance optics receptor and I conduced laboratory tests and flight tests to evaluate the accuracy of the systems in terms of geometrical, radiometrical an spectral performances and the reliability of collected data. Then, I developed the software for the processing of the spectral data and I investigated two methods to estimate surface reflectance from HyUAV with the aim of providing suggestions for an accurate retrieval of surface reflectance from UAVs.

In last year of my Ph.D., using the knowledge about hyperspectral spectroscopy reaching with the HyUAV, I developed an innovative hyperspectral system for imaging ice cores in cold room laboratory. The Chapter 4 describe the system and a set of experiments. The system is fundamentally composed by an high-precision linear stage, which embeds a imaging VNIR hyperspectral spectrometer and a dedicated halogen stable light source. The tests were done with the aims to evaluate the capability of the systems to provide high quality hyperspectral data from ice core. First hyperspectral measurements of ice cores were collected and first investigations of spectral features related to atmospheric component (e.g. mineral dust and tephra from volcanic eruption) was performed and presented in this research.

With this thesis, I present a contribution in the selection of future potential drilling sites and in the development of new systems for collecting valuable data from glacier and ice cores. All this tools are essential to study future climate and environmental changes. In the Chapter 5, the conclusions gained from my research and future prospective are presented.

Bibliography

Bannon D (2009) Hyperspectral imaging: Cubes and slices. *Nat. Photonics* 3(11), 627–629 (doi:10.1038/nphoton.2009.205)

Colomina I and Molina P (2014) Unmanned aerial systems for photogrammetry and remote sensing: A review. *ISPRS J. Photogramm. Remote Sens.* 92, 79–97 (doi:10.1016/j.isprsjprs.2014.02.013)

Di Mauro B, Fava F, Ferrero L, Garzonio R, Baccolo G, Delmonte B and Colombo R (2015) Mineral dust impact on snow radiative properties in the European Alps combining ground, UAV, and satellite observations. *J. Geophys. Res. Atmos.*, 1–18 (doi:10.1002/2015JD023287)

Epica CM (2004) Eight glacial cycles from an Antarctic ice core. Nature 429(6992), 623–628 (doi:10.1038/nature02599)

Field CB, Barros VR, Dokken, D J, Mach KJ, Mastrandrea MD, Bilir TE, Chatterjee M, Ebi KL, Estrada YO, Genova RC, Girma B, Kissel ES, Levy AN, MacCracken S, Mastrandrea PR, White LL and (eds) (2014) IPCC, 2014: Summary for policymakers. Cambridge University Press, Cambridge, United Kingdom and New York, NY, USA (doi:10.1016/j.renene.2009.11.012)

Greenberger RN, Ehlmann BL, Blaney DL, Cloutis E a, Wilson JH, Green RO and Fraeman A a (2015) Imaging spectroscopy of geological samples and outcrops: Novel insights from microns to meters. *Gsa Today* (12) (doi:10.1130/GSATG252A.1)

Jouzel J and Masson-Delmotte V (2010a) Paleoclimates: what do we learn from deep ice cores? *Wiley Interdiscip. Rev. Clim. Chang.* 1(5), 654–669 (doi:10.1002/wcc.72)

Jouzel J and Masson-Delmotte V (2010b) Deep ice cores: the need for going back in time. *Quat. Sci. Rev.* 29(27-28), 3683–3689 (doi:10.1016/j.quascirev.2010.10.002)

Knight PG (2004) Glaciers: art and history, science and uncertainty. *Interdiscip. Sci. Rev.* 29(4), 385–393 (doi:10.1179/030801804225012527)

Schaepman ME, Ustin SL, Plaza AJ, Painter TH, Verrelst J and Liang S (2009) Earth system science related imaging spectroscopy-An assessment. *Remote Sens. Environ.* 113(SUPPL. 1), S123–S137 (doi:10.1016/j.rse.2009.03.001)

Stocker TF, Qin D, Plattner G-K, Tignor M, Allen SK, Boschung J, Nauels A, Xia Y, Bex V, Midgley PM and (eds.) (2013) IPCC, 2013: Climate Change 2013: The Physical Science Basis. Contribution of Working Group I to the Fifth Assessment Report of the Intergovernmental Panel on Climate Change. Cambridge University Press, Cambridge, United Kingdom and New York, NY, USA,

Thompson LG (2000) Ice core evidence for climate change in the Tropics: implications for our future. *Quat. Sci. Rev.* 19(1-5), 19–35 (doi:10.1016/S0277-3791(99)00052-9)

Thompson LG (2010) Understanding global climate change: paleoclimate perspective from the world's highest mountains. *Proc. Am. Philos. Soc.* 154(2), 133–57 http://www.ncbi.nlm.nih.gov/pubmed/21553594

Thompson LG, Mosley-Thompson E, Davis ME, Zagorodnov VS, Howat IM, Mikhalenko VN and Lin P-N (2013) Annually Resolved Ice Core Records of Tropical Climate Variability over the Past 1800 Years. *Science (80-.).* 340(6135), 945–950 (doi:10.1126/science.1234210)

Trevors J and Weiler P (2013) A new eye in the sky: Eco-drones. *Environ. Dev.* 7(May), 155–164 (doi:10.1016/j.envdev.2013.05.011)

Zhang Q, Kang S, Gabrielli P, Loewen M and Schwikowski M (2015) Vanishing High Mountain Glacial Archives: Challenges and Perspectives. *Environ. Sci. Technol.* 49(16), 9499–9500 (doi:10.1021/acs.est.5b03066)

2. Mapping the suitability for ice core drilling of glaciers in the European Alps and in the Asian High Mountains

Abstract

Mountain glaciers and non-polar ice cores are very detailed sources of paleo-proxy data essential to achieve a complete overview of climate change. The increase in glaciers melting leads to a loss of information stored in the ice, and affects the possibility to predict the evolution of climate. In this context, it is important to define a set of guidelines and create dedicated maps to identify potentially suitable areas for future ice core drilling. In this study, the Suitability for Ice Core Drilling (SICD) was defined as the likelihood of drilling a glacier to retrieve an ice core with preserved stratigraphic information that allows the reconstruction of historical climate conditions. Environmental variables related to SICD were selected on the basis of previously drilled sites, according to available scientific literature and on the basis of glaciologists' opinion. Two different spatial multi-criteria analysis—one knowledge-driven and one data-driven method—were optimised and key variables (slope, local relief, temperature and direct solar radiation) were combined to map the potential drilling sites in the European Alps and in the Asian High Mountain glaciers. The performance of the models were evaluated and first indications of potential drilling sites were reviewed. Results will serve as an indication for potential future drilling sites in non-polar mountain glacier.

2.1 Introduction

Ice cores from non-polar mountain glaciers are one of the most sensitive and highly resolved records of the Earth's climatic and environmental conditions. Mountain glaciers responds very quickly to natural and anthropogenic climate changes, offering extensive time series, some reaching back hundreds of thousands of years (before reliable instrumental records), essential to study past climate, environmental conditions and future variations. Ice fields with the proper characteristics for ice core drilling are not limited to the polar regions: glaciers and ice sheets can be found on all the continents, mainly where temperatures remain generally below freezing, but also where some melt can still preserve annual layers and paleoclimate information, providing climatic data over a large part of the Earth (Petit and others, 1999; Lowell, 2000; Neff and others, 2012).

Ice cores contain important information regarding: precipitation rate and regional atmospheric circulation, temperature records derived from isotopes of oxygen and hydrogen, atmospheric chemical composition including greenhouse gas concentrations (i.e. carbon dioxide, methane, etc.), atmospheric component such as: mineral dust, carbonaceous particles, salts, fallout from volcanic eruptions, emissions from biological activity, information about volcanic and solar activity and even cosmic energy bombardment of chemical species present in the atmosphere (Steig, 2003; Tian and others, 2003; Thompson, 2010). This information is essential to achieve a complete understanding of climate variability in the last centuries, enabling scientists to study the climate through glacial cycles and large climatic fluctuations. (Schuster and others, 2002; Maggi and others, 2006; Kaspari and others, 2007; Jenk and others, 2009; Thevenon and others, 2009; Gabrieli and others, 2011; Faïn and others, 2014; Buffen and others, 2014).

Although Antarctic and Greenland ice cores contain important climatic record that describe the long-time history of Earth's climate (hundreds of thousands of years ago), collecting more ice cores from mid-latitude mountains glaciers could provide highly

resolved climatic records, that are fundamental to improve the current knowledge of climate forcing (including solar activity, volcanism, aerosol, and dust atmospheric concentrations) and future variability at local scale. These ice cores, in fact, can preserve histories of local climate, regional conditions and also broader environmental information; furthermore, it is important to distinguish natural variation of the climate system from the anthropogenic forcing superimposed during the last century (Thompson, 2000; Alley, 2000; Brook, 2007; Jouzel and Masson-Delmotte, 2010). Obtaining a standardized suite of multiple measurements, on accurately dated ice cores, it is also important for analysing the local variability of climate affected by global climate patterns. From this point of view, some geographical regions are crucial because they are located in transition zones between different climatic systems (e.g. Westerlies and Indian monsoon characterised the Karakoram mountains range), related to atmospheric circulation patterns (Thompson, 1996; Gregory and Noone, 2008; Vimeux and others, 2009; Thompson and others, 2011, 2013). Additionally, some glaciers adjacent to densely inhabited regions, are more susceptible to the influence exerted by human activities and thus serve as indicators of anthropogenic impacts.

Changes in climate have caused impacts on human and natural systems. Understanding how the climate will evolve in the future is relevant for the development and the implementation of environmentally sustainable policies (Field and others, 2014). The melting of glaciers, which rapidly increased in recent years (Vincent and others, 2005; Immerzeel and others, 2010; Bolch and others, 2012; Stocker and others, 2013; Zhang and others, 2015), could lead to a dramatic loss of information stored in the ice, affecting the possibility to foresee the evolution of future climate (Thompson and others, 2003). Despite the existence of technical requirements to drill and to store ice cores, the criteria governing the choice of a drilling site and the environmental factors related to the possibility to drill the glacier, are poorly defined in the literature and, to date, no attempt to map candidate ice core drilling sites has been conducted. The available literature mainly describes the analysis of paleo-proxy data;

whereas, the criteria supporting the choice of a drilling site, to collect high quality data, are only marginally presented from the authors.

As a consequence, it is necessary to identify new areas of non-polar mountain glaciers for potential ice core drillings in order to retrieve paleoclimates data. The capability to easily identify these areas is important for climate studies, especially in wide remote areas, where exploration is difficult and most standard investigations are impossible to carry out at large scale (such as Himalayan glaciers). Therefore it is important to outline a methodology to map mountain glaciers using simple, global and spatially distributed variables, to give primary indications of potential drilling sites.

The goal of this study is to develop a novel methodology to identify suitable areas for ice core drilling. For this purpose, we firstly identified the criteria and selected the variables to be included in spatial analysis, then Suitability for Ice Core Drilling (SICD) maps were produced for Alpine and Asian High Mountain glaciers. Finally, the indication of more potential drilling sites was proposed and discussed for the Alps and for the Asia.

2.2 Review on the suitability for ice core drilling

When snow falls and accumulates on the glacier surface, the climatic signal is stored in the snow. Glaciers preserve, in each layer, differences in chemistry and ice texture related to environmental and atmospheric past conditions. The morphological and physical features of a specific drilling site (i.e. slope, glacier dynamics, flow velocity, ice thickness etc.), as well as the climatic variables (snow accumulation rate, wind exposure, pressure and temperature etc.), can modify the quality of the ice core stratigraphy.

Thompson (2000) claims that the stratigraphy can be modified by different factors such as: i) surface processes (drifting and removal of snow by wind), ii) densification, iii) temperature gradient metamorphism (temperature gradients from day to night and

summer to winter), iv) glacier flow (Thompson and others, 2002, 2005). Other authors (Oerter and others, 1983; Schwikowski, Döscher, and others, 1999; Schwikowski, Brütsch, and others, 1999; Preunkert and others, 2000; Kaspari and others, 2008; Thevenon and others, 2009; Gabrielli and others, 2010, 2012; Konrad and others, 2013) mentioned further elements to explain the selection of a drilling site: i) firn temperature profile, that allows to evaluate if a high elevation, mid-latitude glacier site, is located in the recrystallization and cold infiltration zone, ii) mass balance reconstruction and snow accumulation rate, implying preservation of layers with temporal resolution, iii) preferential wind erosion of snow, iv) glacier thickness related to geophysical investigations, v) ice flow dynamics and alteration of snow layers, vi) glacio-chemical analysis of various chemical species deposits.

Lacking of a physical model to define new drilling sites, the choice of suitability areas can be interpreted as the interaction between different environmental, climatic and social variables. Those are described in the next paragraph.

The most important requirement in the selection of a drilling site is that the suitable area should not be characterised by glacier processes, that can modify the preserved stratigraphy, making the ice core not appropriate to reconstruct the past climate. The most important variables related to the quality of the stratigraphy are summarised in Table 1.

The second criterion in the selection of a drilling site is the temporal resolution of the stratigraphy. It can be expressed as the numbers of years described by the layers (i.e. they cover a long period reaching back hundreds of thousands of years) or the seasonal detail (i.e. they cover fewer years, with a high seasonal detail). This feature is related to glacier thickness, snow annual accumulation and seasonal distribution of the precipitations.

Variables	*Influence on the quality of the stratigraphic conservation*
Temperature and Solar Radiation	High temperatures produce snow melting, infiltration, percolation and refreezing phenomena that blur the original stratigraphy. The suitable areas are characterized by negative temperature, mainly located at high altitude areas less exposed to solar radiation.
Snow melting	The persistence of snow cover allows the formation of snow layers. The Equilibrium Line Altitude (ELA) is the elevation at which snow accumulation exactly balances ablation, contingent upon snowfall precipitation and air temperatures. The suitable areas are necessarily placed above the ELA within the accumulation zone.
Wind transport and Avalanche mixing	Spatial heterogeneity of snow is the result of the redistribution of snow operated by wind and avalanches. These processes cause the alteration of the stratigraphy. Prevailing wind exposure produces differences in snow accumulation through erosion of snow in windy areas (e.g. ridge and saddle) and subsequent transport and deposition in the sheltered areas. Avalanches cause mixing of snow and destruction of the stratigraphy layers; while also posing hazard to the drilling operations. The suitable areas are manly characterised by low wind exposure and low wind deposition and little to no risk of avalanches.
Glacier dynamics and Ice flow	The glacier dynamics and the ice flow can wrap and mix the layers making complex the reading of the stratigraphic information. Ice flow is related to slope gradient and relief energy: great velocity are present in steepest slope associated with high relief energy. For this reason suitable sites are placed principally in flat summit areas characterised by low flow.

Table1: Variables that affect the quality of the ice core stratigraphic conservation.

Another consideration regards the climatic importance of a drilling site, concerning the specific research interests (i.e. altitude, latitude, relevance of the geographic location). Finally, the last requirement is the logistical possibility to drill the glacier, that can be evaluated according to the capability of reaching the area (i.e. accessibility) as well as the political and environmental criticalities (i.e. permission, elevation, environmental risk).

All these requirements are difficult to formalize and many parameters are nearly impossible to obtain spatially at the global scale. The rationale of this study is to combine a limited subset of variables, identified through literature research and information collected from glaciologists, and to propose a SICD index in order to map the potential drilling sites of non-polar mountain glaciers.

2.3 Data collection and methodology

The study was applied to the European Alps and to the Asian High Mountains. The overall area of study is represented in Figure 2.1.

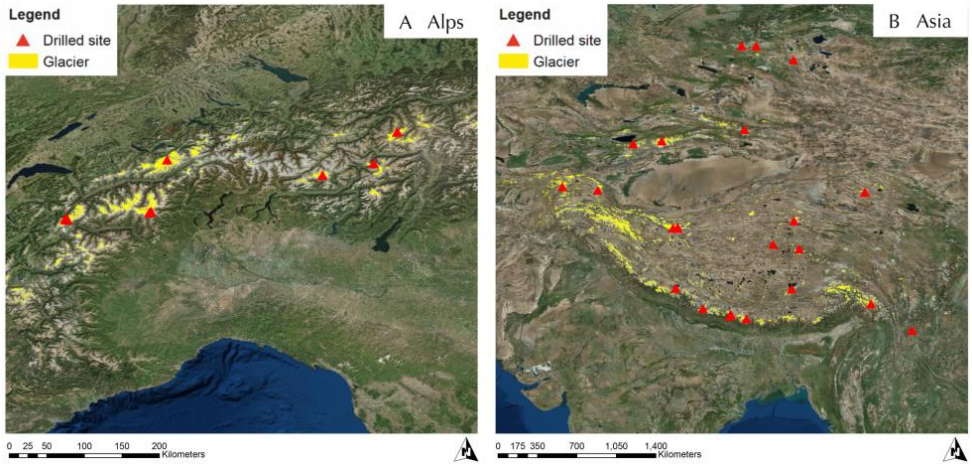

Figure 2.1: Study area: the Alps and the Asia region (figure A and B, respectively). The extent of glaciers (yellow polygons) with the position of the ice core drilled sites (red points) retrieved from IDB.

The Alps are a complex system of mountains that extends about 1000 kilometres throughout south-central Europe, with a maximum elevation of 4800 meters (at the Mont Blanc summit). Major glaciers are located at the highest elevations along the crest of mountains, especially where areas persist above the snowline. Numerous smaller glaciers are, however, distributed throughout the Alps, with fewer fragmented glaciers located on southern slopes due to the seasonal weather patterns and the greater intensity of solar radiation. (Williams and Ferrigno, 2006).

The Asian High Mountains correspond to the regions of Himalaya, Karakoram, Tibet, Pamir, Tien Shan and Altay Sayan. The Indian Monsoon supplies high amounts of precipitation from the Indian Ocean over the Himalayas. The Westerlies system becomes more important in the West Himalaya and in the Karakoram; whereby the northern and western air masses flow from Siberia and Central Asia to Tien Shan and Pamir Mountains, characterising the continental climate of these regions. This complex

circulation pattern determines the snow accumulation and divides Asian glaciers into summer-accumulation and winter-accumulation types with spatially heterogeneous fluctuation among the regions (Bolch and others, 2012; Sakai and others, 2015).

2.3.1 Data harmonization and variables selection

Ice Core Database

The complete archive of data from non-polar ice cores was created starting from the information of the Tropical ICE COREs National Oceanic and Atmospheric Administration (NOAA) Paleoclimatology (http://www.ncdc.noaa.gov/paleo/icgate.html) and the National Ice Core Laboratory (NICL http://www.icecores.org) databases. In addition, the Ice Core Database (IDB) was produced by collecting ice core data from scientific literature; amounting to 178 ice cores from: North America (27); South America (29); European Alps (46); Africa (8) and Asia (68) were included (Strigaro and others, 2014) (http://geomatic.disat.unimib.it/wp2.3). In the IDB, the spatial accuracy of drilled sites was improved: some points were discarded due to coordinate inaccuracies, while other sites were relocated using map figures retrieved from original manuscripts. The drilled ice core sites (i.e. areas of glacier where different ice core drillings were performed) and its geographic coordinates were extracted from IDB. The Alps and Asian regions were chosen due to their abundance of drilled sites and the good accuracy of their locations. This study employs 24 drilled sites in the Alps and 42 in the Asian High Mountains (Table 2).

EUROPEAN ALPS	*N drilled site*
Ortles-Cevedale	1
Mount Blanc	7
Monte Rosa	11
Bernese-Oberland	1
Bernina-Morteratsch	1
Oetztal Alps	3
Total	*24*

ASIAN HIGH MOUNTAINS	*N drilled site*
Altay and Sayan	4
Pamir (Safed Khirs)	3
West Tien Shan	4
East Tien Shan (Dzhungaria)	2
West Kun Lun	7
East Kun Lun (Altyn Tagh)	1
Qilian Shan	4
Inner Tibet	6
Central Himalaya	7
East Himalaya	1
Hengduan Shan	3
Total	*42*

Table 2: Ice cores drilled sites used in the study for the Alps and for the Asian High Mountains regions.

Digital Elevation Model

The ASTER Global Elevation Model (ASTER G-DEM) used in this study is characterized by 30 meters of spatial resolution (∼1 arc-second) and ∼15-30 meters of vertical accuracy (ASTER GDEM Validation Team, 2011). ASTER G-DEM was chosen in order to have a global coverage with a standard spatial resolution and accuracy. This offers a higher geomorphologic detail, especially in mountain areas characterised by a complex topography. (Bolch and others, 2005; Hayakawa and others, 2008).

Glacier outlines

We used the Randolph Glacier Inventory (RGI 4.0) (Arendt and others, 2014; Pfeffer and others, 2014) as it is a globally complete collection of digital outlines of glaciers, supplemental to the Global Land Ice Measurements from Space (GLIMS), that is designed to monitor the world's glaciers (Kargel and others, 2014). The European Alps contain 3812 glaciers, extended over a total surface of about 2052 Km^2, with a vertical altitudinal range from about 1500 to 4800 meters. The Asian High Mountains include 85492 glaciers, that extend over about 120070 Km^2, with the elevation ranging from 2500 to 8800 meters.

Climate data

WorldClim climate data is a set of global climatic data layers, with a spatial resolution of ∼1 square kilometre, generated through interpolation of average monthly data from weather stations (1960-90 period) (Hijmans and others, 2005). For the purpose of this study, the most relevant variables are represented by monthly and annual precipitation, monthly mean, minimum and maximum temperature and some derived bioclimatic variables (e.g. mean diurnal range, mean temperature of warmest quarter, precipitation seasonality, precipitation of warmest quarter, etc.).

Selected variables

Due to the complexity of defining suitable areas for ice core drilling characterised by a preserved stratigraphy, we reduced the delineated process (Section 2) in a simplified scheme, identifying some relevant variables, then used in the spatial analysis. The following morphometric and climatic variables were used in this study:

- *Slope [degrees].* Degree of surface inclination from the horizontal plane generated from DEM using GIS function (Hofierka and others, 2009) (http://grass.osgeo.org/grass64/manuals/r.slope.aspect.html). Areas with lower slope gradients are more favourable to ice core drilling because they are associated with flat surfaces with a preserved stratigraphy and parallel ice layers that easily refer to climate history. These sites are also suitable for the technical drilling operations (i.e. location of drilling camp, drill requirements, etc.).
- *Local Relief [meters].* Vertical difference in elevation between the highest and lowest points of a land surface within a specified horizontal distance (9x9 pixel window) (Wilson and Gallant, 2000). Higher values indicate the presence of steep slopes with great relief energy corresponding to a major glacier flow velocity that can modify the original stratigraphy. These areas are not favourable to ice core drilling. In addition, steep slopes are also predisposing factors for avalanche triggering that can disrupt the layers and constitute a risk for the technical operations.
- *Mean Temperature of Warmest Quarter [°C].* Average temperature of the three warmest months. The suitable areas for ice core drilling are especially characterized by negative temperatures. As temperature is correlated with elevation, drilling sites are generally placed in more elevated areas. On the contrary, positive temperatures (higher than 0°C) favour snow melting (with refreezing phenomena) and, consequently, they can modify the ice core stratigraphy. The mean temperature of warmest quarter was chosen from WordClim data set in order to evaluate the mean higher temperature that the site reaches during the years.

- *Direct Solar Radiation [W/m^2 day].* Raster map of solar direct radiation was calculated using GRASS-GIS software for a given day, latitude, surface and atmospheric conditions (http://grass.osgeo.org/grass64/manuals/r.sun.html) (Hofierka and Šúri, 2002). This variable allows the evaluation of areas characterized by different intensities of solar radiation, considering topographic exposure and shadows at the local scale. The function is evaluated on the 15th of August, when the mean temperatures are usually higher in both the Alps and the Asian Mountain areas, and the effect of heat accumulation in the glacier body favourites the ice melting. The suitable areas for ice core drilling are ideally located in areas less exposed to higher intensity of solar radiation.

These variables were selected through preliminary analysis and characterisation of the drilled sites present in the IDB database, through the analysis of cumulative distribution functions (CDF) and by collecting glaciologists' opinion. In particular, the values from each variables map were extracted from drilled sites (area of 5x5 pixel around the drilled point, ~150x150 meters) and from RGI glacier polygons. Differences between the already drilled site CDF and the whole glaciers CDF were evaluated to characterize drilled sites compared with glacier areas. A questionnaire was submitted to the CRYOLIST network (an international email list of researchers in the fields of snow and ice, http://cryolist.org/) and 12 responses were received from glaciologists.

For both the study areas, each variable was classified into 8 classes with uniform intervals (based on the CDF), in order to apply the spatial analysis and to define its relative importance in the selection of a drilling site.

2.3.2 Spatial Multi-criteria Analysis and derivation of the SICD index

Spatial Multi-criteria Analysis (SMA) is a set of systematic procedures and mathematical tools for analysing complex spatial decision making problems. Generally, in multi-criteria problems, the decision maker considers one criterion to be more

important than the another. This relative importance is usually expressed in terms of weight. (Karnatak and others, 2007).

The Suitability for Ice Core Drilling (SICD) was defined here as the likelihood of drilling a glacier to retrieve an ice core with preserved stratigraphic information, that allows the reconstruction of the climate history.

SICD index was derived as the result of a combination between the environmental variables previously described in Section 3.1.5. The assumption is that areas suitable for the future drilling have the similar conditions of already drilled areas. Two methods for SICD modelling are proposed and compared. In particular, we used (1) a Knowledge-Driven model based on both, glaciologist knowledge and an Analytic Hierarchy Process (KD-AHP), and (2) the Weight of Evidence (WoE) method, that is instead based on a data-driven approach.

KD-AHP method

Knowledge-driven approaches have been successfully used to describe natural phenomena (Giordano and others, 1991; Vogt and others, 2003) or to develop environmental vulnerability indices (Aller and others, 1987; Babiker and others, 2005; Hasiniaina and others, 2010; Saidi and others, 2011; Shirazi and others, 2012).

The Analytic Hierarchy Process (AHP) (Saaty, 1980, 2008; Ishizaka and Labib, 2011) is an interactive approach where a decision-maker (or a group) give their preferences to compare objectives, quantitative or qualitative criteria and alternatives. It is based on a series of pairwise comparisons and it has been successfully used to solve complex decision problems in several areas of applications, among those, environmental and natural resources (Thirumalaivasan and others, 2003; Vaidya and Kumar, 2006; You-Hailin and others, 2011; Sener and Davraz, 2012; Neshat and others, 2014).

In the KD-AHP methodology, the selected environmental variables were combined exploiting glaciologist knowledge by the questionnaire sent to the CRYOLIST. The

primary aim was to understand: i) which variable of each pair is more important in the choice of a drilling site, and ii) to what extent this variable is more important? (using a 1-9 scale). We used 12 complete respondents, from which we were able to generate the weight of each variable by AHP, describing its relative importance to the SICD.

The consistence of AHP is evaluated by the consistency ratio (CR) and the consensus between participant (Saaty, 1980). If the CR is lower than 0.1 the model can be considered consistent. The balanced scale (Salo and Hämäläinen, 1997) was used to improve the accuracy of the results (CR) of the AHP comparisons.

In addition to the AHP weight, a rating system was defined to assess the relative importance of each class of each variable. The scores (ranging from 1 to 10) were assigned on the basis of the corresponding CDF. In some cases, the scores were modified to enhance the importance of a particular class in the model. For example, classes of slope lower than 15 degrees are poorly represented in the dataset; nevertheless we consider this class very important for the SICD and, therefore, we assigned higher scores to these classes.

Weight of Evidence method

WoE is a family of methods that are widely used in multiple fields. Different scientific disciplines have adopted different methods, both qualitative and quantitative, for synthesizing individual lines of evidence (i.e. human health, ecological risk, etc.). Qualitative methods do not attempt to integrate evidence (e.g. variable), while quantitative methods include integration of multiple variable using weighting, ranking, or indexing (Linkov and others, 2009, 2015). According with these authors, a quantitative WoE scoring was developed in this research. A statistical approach was used to assign a weight to each class of each variable used in the model and to spatially integrate evidence into a single value referred as SICD-index. Similar approaches were mainly used in geology for the identification of mineral potential (Bonham-Carter and others, 1989; Agterberg and others, 1990; Bonham-Carter, 1994; Asadi and Hale, 2001)

and for landslide susceptibility mapping (Thiery and others, 2007; Dahal, Hasegawa, Nonomura, Yamanaka, Dhakal, and others, 2008; Dahal, Hasegawa, Nonomura, Yamanaka, Masuda, and others, 2008; Pradhan and others, 2010; Regmi and others, 2010, 2013; Sorichetta and others, 2012; Stevenazzi and others, 2015; Youssef and others, 2015; Hussin and others, 2015). In this method, the spatial relationship between a variable (evidence) and SICD is evaluated using a statistical approach based on the Bayesian probability theorem:

$$P\{D|B\} = \frac{P\{B|D\} \times P\{D\}}{P\{B\}}$$

Where the suitability of locating an occurrence (D) given the presence or the absence of variables (B) can be estimated by the conditional probabilities $P\{D|B\}$, $P\{B|D\}$. The assumption here is that, in the future, ice core drilling will be possible under similar conditions to those contributing to the selection of previously drilled sites. The model is based on the calculation of positive and negative weights for each variable as follows:

$$W^+ = log_e \frac{P\{B|D\}}{P\{B|\overline{D}\}} \qquad W^- = log_e \frac{P\{\overline{B}|D\}}{P\{\overline{B}|\overline{D}\}}$$

Where P is the probability, B is the presence of a class of selected variable, $\overline{B}$ is the absence of a class of selected variable (e.g. slope), and D and $\overline{D}$ are respectively the presence and the absence of occurrences (i.e. drilled sites). The difference between the two weights is the weight contrast or total weight $\mathrm{W^t} = W^+ - W^-$ which provides a measure of the spatial association between the class variable and the occurrences. The two areas of study are separately treated; drilled sites (area of 5x5 pixel around the point) were overlapped with variable maps and only the area of glacier extension was considered. The weights of each class of each variable were defined computing the WoE method (Table 4).

SICD index derivation

The SICD index was calculated as a linear combination of scores and weights defined for the selected variables. The following equations show the SICD index for the KD-AHP and the WoE model, respectively.

$$SIDCI_{KD-AHP} = S_S S_W + R_s R_w + T_s T_w + D_s D_w$$

$$SIDCI_{WoE} = S_{W^t} + R_{W^t} + T_{W^t} + D_{W^t}$$

Where S, R, T, D are the four variables (Slope, local Relief, Temperature, Direct radiation); the subscripts s and w are the corresponding scores and weights, defined using KD-AHP; $\mathrm{W^t}$ is the total weight assigned to the class of the variable calculated using the WoE method.

All variable maps were prepared and combined in a GIS (Geographic Information System) environment. The SICD index maps were created (implementing a GRASS-GIS script) for the European Alps and the Asian High Mountain glaciers. Larger SICD values indicate a higher suitability for ice core drilling. Normalization (between 0 and 1) was performed for the maps of SICD to evaluate and compare the model. Finally, first indications of more potential glaciers suitable for ice core drilling were established by ranking the glaciers, computing the sum of pixel with values of SICD > 0.7, for both the European Alps and the Asian High Mountains, and results of potential sites are discussed.

2.3.3 Model evaluation

The RMSE (root-mean-square error) was computed to evaluate the generated maps. The RMSE value was calculated for the proposed model using the values of SICD estimated in the drilled sites and considering 1 the expected value of SICD in these points.

The ability of proposed method to indicate suitable areas for ice core drilling was verified using the success rate curve. This methodology was applied by several authors

to compare models and to assess predictive capability (prediction rate curve) of models (Chung and Fabbri, 1999; Fabbri and others, 2003; Remondo and others, 2003; Dahal, Hasegawa, Nonomura, Yamanaka, Dhakal, and others, 2008; Pradhan and others, 2010; Sterlacchini and others, 2011; Youssef and others, 2015).

In this study, the success rate curve is used to evaluate the goodness of fit of the model. It indicates how well the model fits the occurrences by calculating the percentage of the drilled sites that occurs in the area classified with higher values of SICD. If the curve and the diagonal coincide, the model should be deemed equivalent to a totally random model. Likewise, greater slope in the first part of the curve indicates higher model quality. The curve was created by crosschecking the distribution of the total set of drilled sites with the SICD maps: after sorting SICD values of each pixel in descending order, the cumulative percentage of drilled sites was plotted against the cumulative percentage of the total study area.

The Area Under the Curve (AUC) represents the quality of the model to reliably fit the occurrence: the larger is the area, the greater is the goodness of fit of the model. The AUC allows the comparison among different success rate curves. The model with the highest AUC is considered to be better, a total area equal to 100 denotes perfect accuracy, whereas values below 50 represent a random fit.

2.4 Results and discussion

2.4.1 Spatial variability of the selected variables

Spatial variability of the selected variables, used in this study, is shown as example in Figure 2.2, focusing in Mount Rosa massif (European Alps). Low slope values (range from 0 to 20 degrees) are present in glacier tongues as well as in other more elevated areas in the accumulation basins. High local relief values (higher than 70 meters) are found along the mountain ridges and in the vicinity of steep northern slopes. The temperature depicts a local pattern that may be related to the elevation; in fact, lower

temperature (lower than -4 °C), are common in the more elevated summit areas. Regarding solar radiation, elevated flat areas are exposed to solar radiation because they cannot be shielded by the effect of topography (i.e. prevailing exposure and shadows).

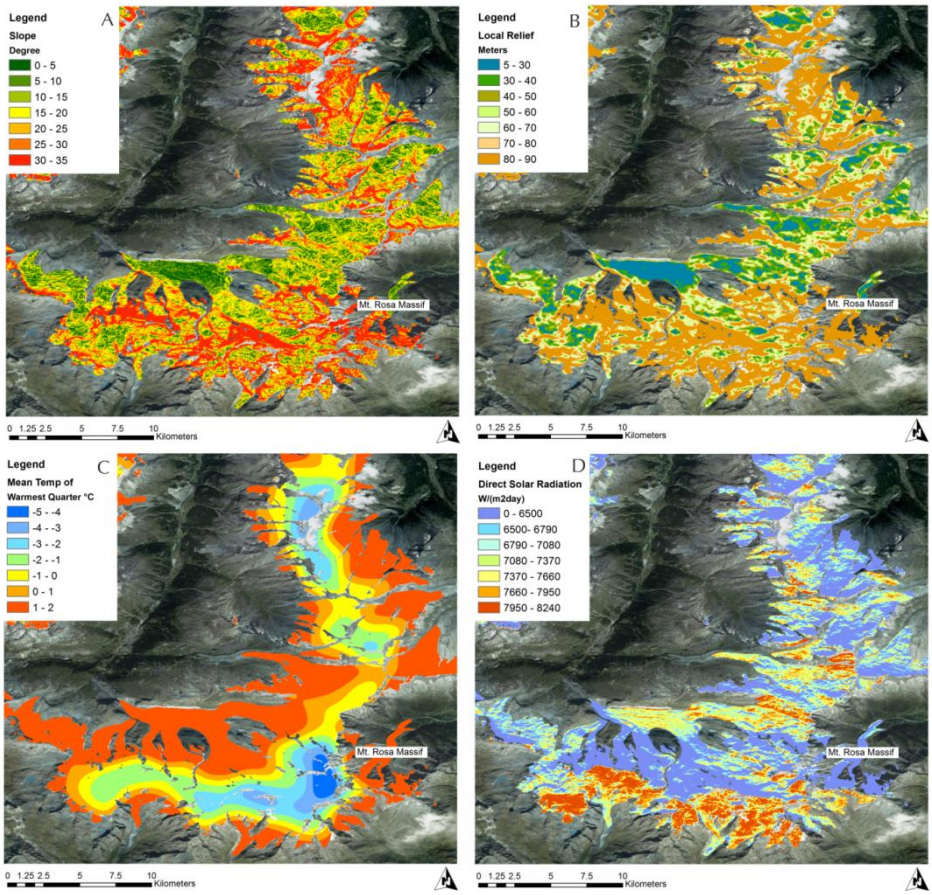

Figure 2.2: Environmental variables included in the model: A) Slope; B) Local Relief; C) Mean Temperature of Warmest Quarter; D) Direct Solar Radiation; (Example for the Monte Rosa massif, European Alps).

Figure 2.3 shows the CDF of each variable in the drilled sites. The curve enables determination of which values characterise the drilled sites. Based on the CDF, each variable was classified into the same uniform intervals used in the KD-AHP and WoE models.

CDF plots of slope and local relief show similar behaviour between the Alps and the Asian High Mountains; whereas, some differences are present for mean temperatures and direct solar radiation. Regarding the slope, we can observe that 80% of drilling

sites are characterised by values lower than 20 degrees (Figure 2.3a). Local relief CDF shows that the drilled sites are mainly characterised by low values of local relief (Figure 2.3b). Temperature (Figure 2.3c) in the drilled Alpine sites range from -4 to 2 °C with 85% of sites under 0°C, while for the Asian glaciers the CDF of temperatures shift to a more-positive value range from -2 to 4 °C. Similar differences could be seen for direct radiation (Figure 2.4d). These differences could be ascribed to the variability in geomorphological features between the drilled sites of the Alps and the Asian High Mountains. The latter, in fact, covers a broader altitudinal and latitudinal range, resulting in higher Warm Temperatures and Direct Radiation, with respect to the European Alps. These differences were considered in order to adjust interval classes of these variables for the areas of study. This classification is reported in Table 4.

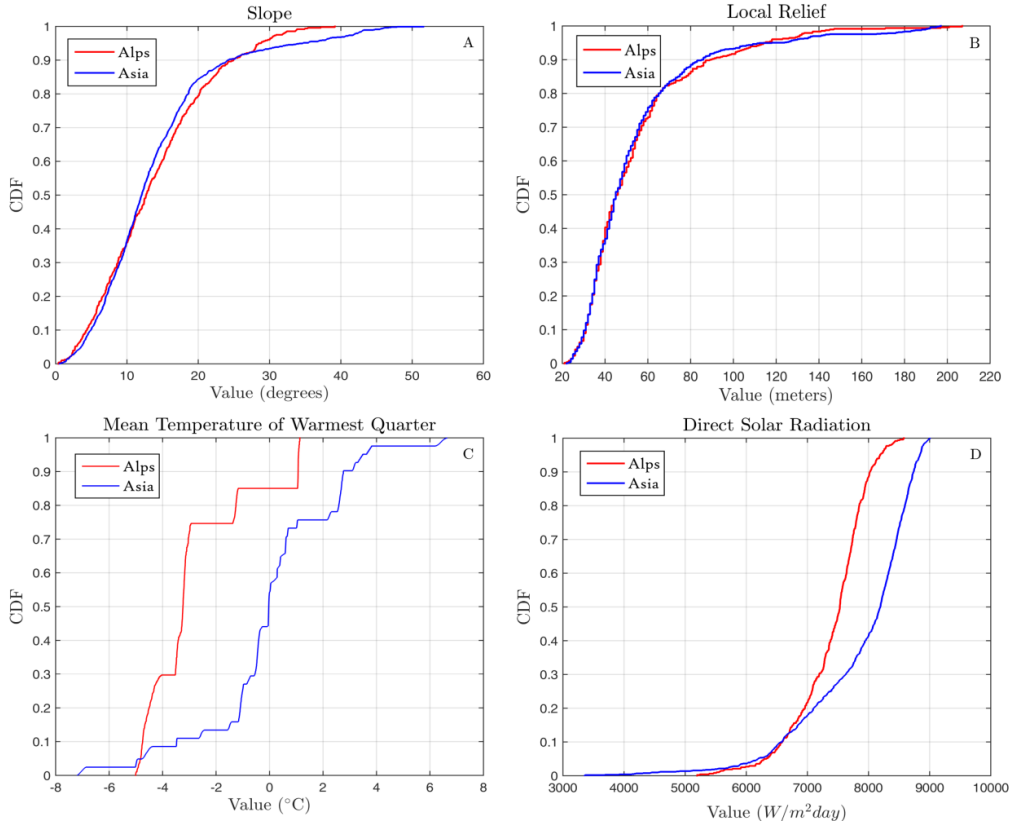

Figure 2.3: CDF of selected variables for Alps (red line) and Asia (blue line). The curve show the distribution of values of each variable in the all available drilling site. A) Slope; B) Local Relief; C) Mean Temperature of Warmest Quarter; D) Direct Solar Radiation.

2.4.2 Weights definition and comparison between methods

Results from the KD-AHP and the WoE methods are reported in this section. Table 3 shows the weights of each variable defined by AHP. The balanced scale improved the CR from 3.3, of the linear scale, to 0.8, leading to a consensus among participants of 83%.

Variable	*Rank*	*Weight*
Mean Temperature of Warmest quarter	1	45.9
Slope	2	24
Direct Radiation	3	15.6
Local Relief	4	14.5

Table 3: Environmetal variables and relative weight defined by AHP. The CR index of AHP is 0.8 %, consensus between participants 83.8 %.

Results from the AHP, showed that air temperature is considered the most crucial variable, while slope, local relief and mean temperature of warmest quarter have lower importance in the model. Table 4 summarize the scores assigned to each class used to compute the SICD index. High scores are associated with classes more suitable for ice core drilling. We can see that low slope values (lower than 15 degrees) and temperatures below 0°C are the most important classes in the computed model. Overall, this simple model allows the selection of suitable sites where gentle slopes, low relief energy, cold air temperature and reduced solar radiation coexist in the same area.

The results of the WoE are shown in Table 4. Variable classes with negative weights are negatively spatially associated with SICD, while positive values indicate that the presence of class is favourable for ice core drilling. Weights that are close to zero evidence a little relation between the class and SICD. Weight values between the Alps and the Asian region show a good agreement. Regarding the slope, low values (from 0 to 15 degrees) have positive weights, indicating that these classes are suitable for ice core drilling, whereas values above 25 degrees are negatively related with SICD. Local relief shows that values from 30 to 50 meters are positively associated with SICD while high values are less favourable (negative weights) to ice core drilling. WoE model shows that areas

more exposed to solar radiation evidence a positive relation with the SICD. Temperature is the most important variable: lower temperature presents higher positive weights.

ALPS					ASIA				
Variable class	*KD-AHP Score*	*W+*	*W-*	*WoE Wt*	*Variable class*	*KD-AHP score*	*W+*	*W-*	*WoE Wt*
Slope [degrees]									
> 35	1	-3.123	0.146	-3.269	> 35	1	-1.659	0.245	-1.904
30-35	2	-1.058	0.067	-1.125	30-35	2	-1.797	0.088	-1.885
25-35	3	-0.839	0.081	-0.920	25-35	3	-1.229	0.081	-1.310
20-25	4	-0.328	0.049	-0.377	20-25	4	-0.647	0.059	-0.706
15-20	6	0.174	-0.037	0.211	15-20	6	0.402	-0.072	0.474
10-15	8	0.460	-0.112	0.572	10-15	8	0.807	-0.209	1.016
5-10	9	0.676	-0.141	0.817	5-10	9	0.797	-0.178	0.975
< 5	10	0.998	-0.086	1.084	< 5	10	0.686	-0.055	0.741
Local Relief [meters]									
> 90	1	-1.431	0.435	-1.867	> 90	1	-1.865	0.676	-2.541
80-90	2	-0.659	0.041	-0.700	80-90	2	-0.416	0.021	-0.437
70-80	4	-0.881	0.053	-0.934	70-80	4	-0.221	0.013	-0.234
60-70	5	0.121	-0.012	0.133	60-70	5	0.238	-0.019	0.257
50-60	7	0.628	-0.085	0.713	50-60	7	0.767	-0.092	0.859
40-50	8	0.874	-0.137	1.011	40-50	8	1.164	-0.195	1.359
30-40	9	1.325	-0.270	1.595	30-40	9	1.365	-0.250	1.615
< 30	10	-0.205	0.016	-0.221	< 30	10	0.200	-0.015	0.215
Mean Temperature of Warmest quarter [°C]									
> 2	1	---	0.933	---	> 4	1	-2.839	0.513	-3.352
1 - 2	2	-0.205	0.041	-0.245	3 - 4	2	-0.641	0.073	-0.714
0 - 1	3	---	0.119	---	2 - 3	3	0.081	-0.013	0.094
-1 - 0	4	---	0.054	---	1 - 2	4	-1.627	0.107	-1.734
-2 - -1	6	1.318	-0.082	1.399	0 - 1	6	0.724	-0.115	0.838
-3 - -2	8	0.929	-0.018	0.947	-1 - 0	8	1.716	-0.286	2.002
-4 - -3	9	4.730	-0.541	5.271	-2 - -1	9	1.654	-0.104	1.759
< -4	10	5.112	-0.351	5.463	< -2	10	1.894	-0.124	2.018
Direct Solar Radiation [W/(m^{2}day)]									
> 8240	1	1.927	-0.033	1.960	> 8840	1	2.906	-0.049	2.956
7950-8240	3	0.615	-0.050	0.665	8450-8840	3	1.012	-0.199	1.210
7660-7950	5	1.018	-0.183	1.201	8060-8450	5	0.385	-0.105	0.491
7370-7660	6	0.796	-0.151	0.947	7670-8060	6	-0.344	0.061	-0.404
7080-7370	7	0.277	-0.040	0.317	7280-7670	7	-0.648	0.076	-0.724
6790-7080	8	-0.058	0.006	-0.064	6890-7280	8	-0.291	0.029	-0.320
6500-6790	9	-0.150	0.014	-0.164	6500-6890	9	-0.143	0.011	-0.154
< 6500	10	-1.743	0.518	-2.262	< 6500	10	-0.932	0.164	-1.097

Table 4: Model parameters for the Alps and the Asia areas of study. Class of selected thematic variables: Slope, Local Relief Mean Temperature of Warmest quarter, Direct Solar Radiation. Weights assigned with the WoE method.

For both the Alps and the Asian High Mountains, an overall good agreement was found between the scores defined with KD-AHP and the weight results of WoE. A particular difference can be highlighted for the direct solar radiation, that presents a different trend between the two models. This difference may be caused by the presence of drilled sites in more elevated summit flat areas, which implies more exposure to direct solar radiation and contributes to increase the weights in WoE model. In the KD-AHP model, these areas are considered less favourable for ice core drilling because the radiation contributes to rising local surface temperatures.

2.4.3 SICD maps and model evaluation

Figure 2.4 shows a focus of the SICD map on the Mont Rosa Massif, for the Alps area of study, and Figure 2.5 on the Dasuopu and Yala glaciers (located in Central Himalaya) for the Asian High Mountains (KD-AHP and the WoE model). Green colours represent areas that are not suitable for ice core drilling; yellow and orange colours evidence sites where the SICD is moderate; and red colours indicate potential drilling sites, corresponding to high values of suitability for ice core drilling (ranging from 0.7 to 1).

A good agreement between drilled site and high value of SICD can be highlighted: higher SICD values are located in the vicinity of the already drilled sites. Furthermore, other potentially drillable areas are represented in the maps. Areas available for ice core drilling are mostly placed in elevated flat areas whereas, southern exposed glaciers and steep northern slopes are characterised by lower value of SICD. The maps depict appropriate results of the proposed methods and hot spots of high value of SICD identified suitable areas for ice core drilling. High values of SICD, estimated by WoE model are more concentrated throughout the drilled sites than those of KD-AHP model. This feature is more accentuated in the Alps with respect to the Asian glaciers, and could be due the wide extent of Asia and the relatively lower number of drilled sites compared with the Alps.

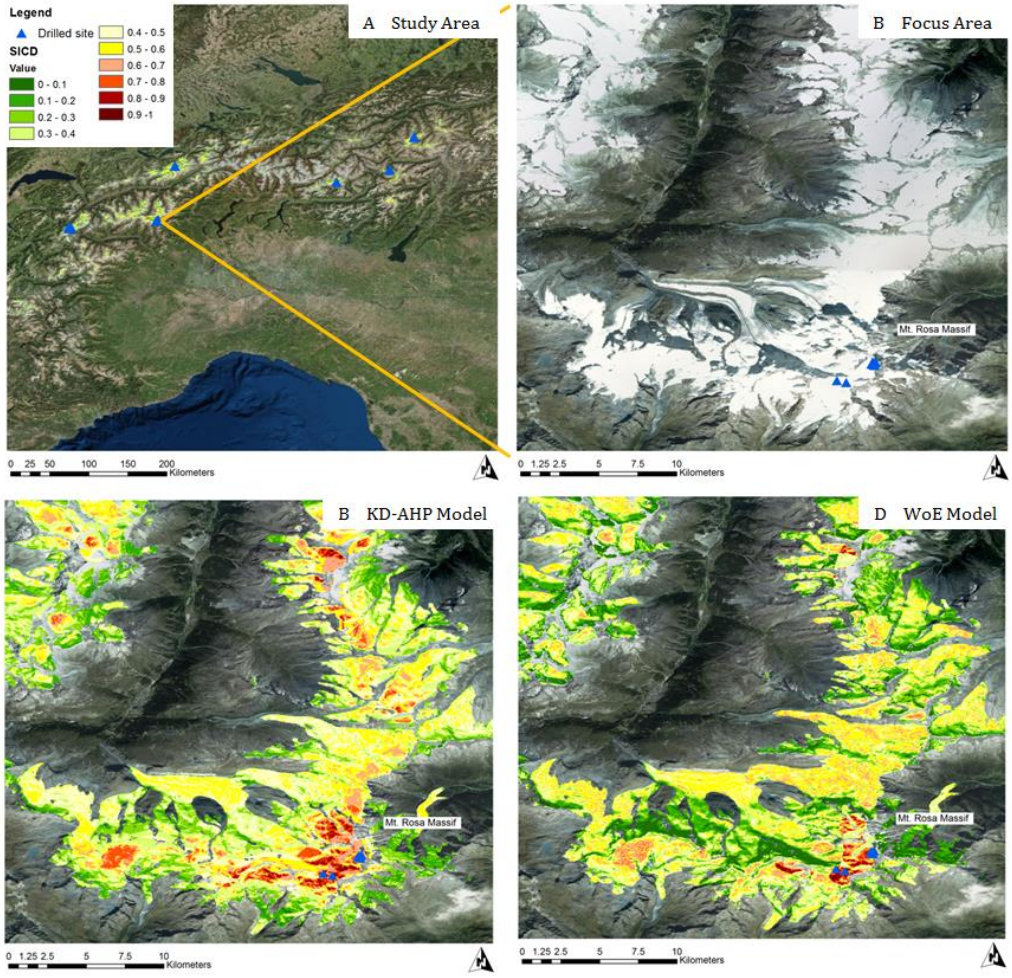

Figure 2.4: Suitability map for ice core drilling in the Alps focused in Mt. Rosa Massif. Green colours are associated with areas unsuitable for ice core drilling, yellow and orange colours evidence moderate SICD and red colours indicate high suitability for ice core drilling corresponding to values ranging from 0.7 and 1. A) The Alpine area of study; B) Focus in Mt. Rosa Massif; C) Focus of KD-AHP SICD map; D) Focus of WoE SICD map.

Regarding the model evaluation, we found RMSE values of 0.30 for KD-AHP and 0.29 for WoE model for the Alps, while for Asia RMSE resulted 0.41 and 0.35 for KD-AHP and WoE, respectively. A lower value of RMSE indicates a better result of the related model.

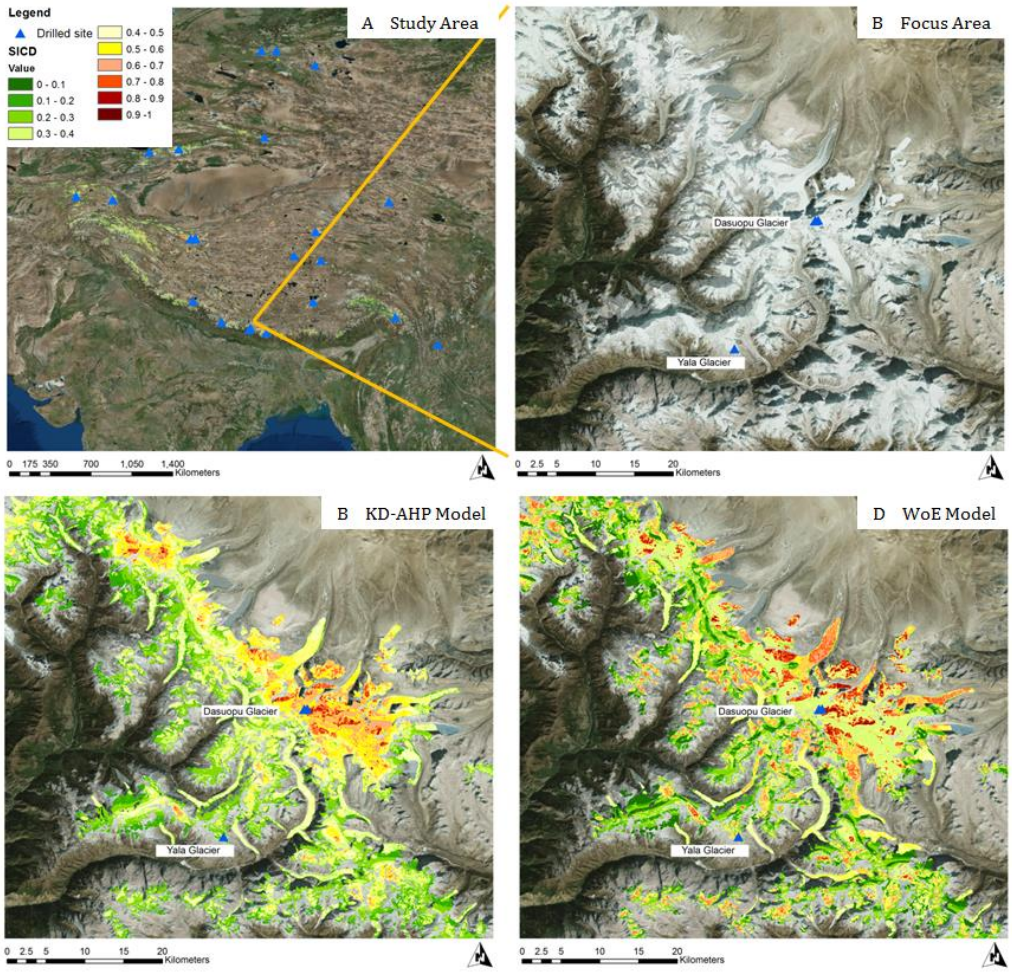

Figure 2.5: Suitability map for ice core drilling in Asia zoomed in Dasuopu and Yala glaciers. Green colours are associated with areas unsuitable for ice core drilling, yellow and orange colours evidence moderate SICD and red colours indicate high suitability for ice core drilling corresponding to values range from 0.7 and 1. A) The Asian area of study; B) Focus in Dasuopu and Yala glaciers; C) Focus of KD-AHP SICD map; D) Focus of WoE SICD map.

The success rate curve is used to evaluate the goodness of fit of the model and is represented in Figure 2.6. For the Alps, the success rate curve shows that 13% of most suitable part of the study area contains 90% of the drilled sites (red line) while, regarding the Asian High Mountains, 21% of the most suitable part of the study area contains 90% of the drilled sites (blue line). The graphs delineate that the two models provide similar results in terms of goodness of fit with slightly better results founded

for WoE. Better results were also found for the Alps compare with Asia. These consideration are also supported by the AUC values. In particular, considering the WoE model, the AUC show values of 95.86 and 89.77 for the Alps and for the Asia, respectively. With AUC values larger than 85, the models proposed in this study can be considered an appropriate approach to map the glaciers areas potential for ice core drilling.

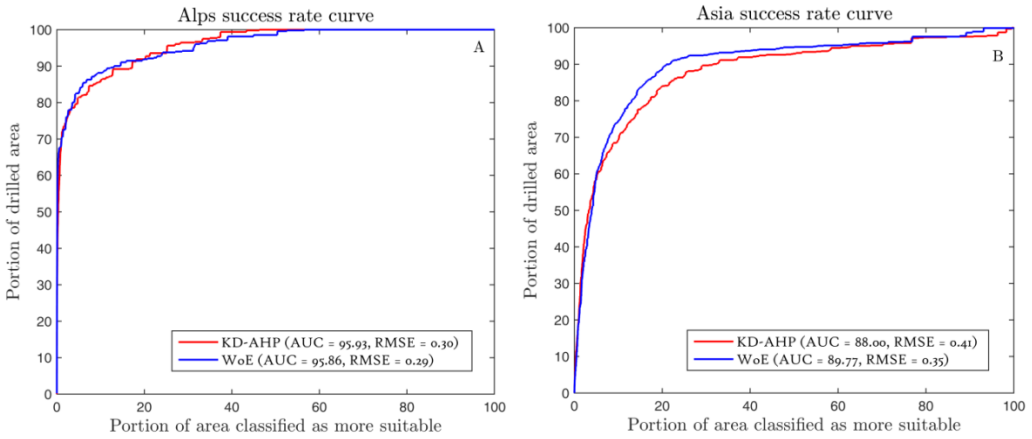

Figure 2.6: Success rate curves and AUC values for KD-AHP model (red line) and WoE model (blue line) for Alps (A) and Asia (B). The model in the Alps performs slightly better compared with Asia. AUC values indicate an appropriate accuracy of the models, with values lower than 85 for both the study areas.

In sum, slightly better results of the model are delineated for the Alps compared to the Asian High Mountains and the WoE model performs slightly better compared to KD-AHP. Evaluation methods of KD-AHP and WoE, such as the VoI (Keisler and others, 2014), should be applied in the future in order to estimate the value of the new information produced through glacier ice core drilling.

2.4.4 Discussion of potential drilling sites

The most potential glaciers for ice core drilling were identified through a ranking of estimated SICD. Only the WoE model were considered in this analysis because it performs better. The maps (Figure 2.7) show the suitable glaciers identified by the

model (blue points) in the European Alps and in the Asian High Mountains and the already drilled sites of these regions (red triangles).

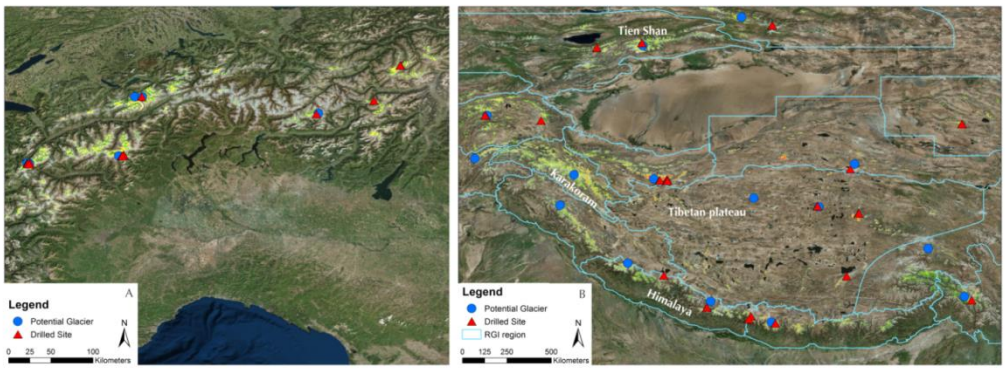

Figure 2.7: Indication of the potential drilling glaciers for Alps and Asia, and position of already drilled.

In the Alps, the major part of suitable drilling sites have been already exploited. Our model suggested new hot spot of SICD within already drilled glaciers, such as in the Mt. Bianco and Mt. Rosa massifs. In some cases (e.g. Aletsch and Fellaria Glacier) potential site were found in the accumulation zone near already drilled sites.

Referring to the selection of potential drilling site, the Alps can be classified in three geographical regions with different characteristics. The Western Alps are the most elevated and are influenced primarily by air masses coming from the Atlantic Ocean. In this region potential sites are still available, but most of them are placed near already drilled sites. Although the vicinity of two drilling site, differences in the preserved ice core records (i.e. resolution of the stratigraphy) can be related to local topographic effects. For example, Col du Lys and Colle Gnifetti drilled sites (Figure 2.4) are distant about 1.5 Km, but present accentuated difference in accumulation rate due to local topography and wind erosion effects. If compared with Western Alps, the glaciers of the Central Alps are less elevated and are threatened by global warming. Many of them, in fact, remain above the ELA and present negative mass balance. In this region it is urgent collect ice core before the melting leads to loss information. Finally,

although the Eastern part of the Alpine chain is influenced by cold air from Siberia, in this region the possibility to find potential drilling sites is low.

In summary, although the possibility to collect new ice cores from the European Alps is quite limited, Alpine glacier are at risk of climate change, thus saving information collecting new ice cores is necessary to improve the understanding of local climate and environmental variability. The Alps, in fact, are placed in the center of the Europe, and they are the principal sources of records to study the anthropogenic forcing on natural climate system.

Compared with the Alpine glaciers, the Asian High Mountains regions, remain for the most part unexplored. Interesting paleoclimates data could be extracted from Asia and a larger number of potential drilling sites are still available. The Figure 2.7 shows the most suitable glacier for each geographic region (as defined in the RGI database). The proposed methodology provides important indication for the selection of new drilling sites, that are fundamental especially in a wide remote area, such as in the Asia, where limited information is available. A discussion of potential drilling sites in the Asia is thus proposed in the next paragraphs.

The climate of the Asian High Mountains is affected by different regional weather systems and glaciers are sensitive to the related climate variability. The Himalaya is principally interested by the Indian Monsoons. This system, characterised by a very high seasonality, bring warm and moist air from ocean to glaciers. Temperature and ELA of this region are increasing, consequently the potential site are more threatened of melting and have higher priority for drilling than the other Asian glaciers. Some drillings were performed in this region, but a lot of drilling sites should be exploited in the next years (Figure 2.8A). Easternmost, other potential glaciers, that received the contribution of the South-East Asian air masses, are identified. The direct influence of densely inhabited areas (i.e. China or India) could be stored in these glaciers, providing important information of environmental conditions. Furthermore, a comparison between Europe with the emerging economies (i.e. India or China) could be suggested.

The Karakoram region is influenced by two weather systems: the Westerlies and the Monsoons, that are modulated by the El Niño–Southern Oscillation (ENSO) and the North Atlantic Oscillation (NAO) systems (Wang and others, 2000), respectively. These regions is poorly explored and, to date, no ice cores were collected for Karakoram glaciers (Figure 2.8B). Identified potential sites should be drilled to collect information for studying the relation between the regional climate conditions and the variability of the principal circulation patterns, which have a strong impacts on meteorological phenomena that directly or indirectly affect most regions on the planet and their populations. In this context, ice core records are fundamental to calibrate regional and global climate models, in fact, more data are necessary for improving the accuracy and the scale of these models.

The air masses flow from Siberia and Central Asia to Tien Shan and Pamir Mountains, characterize the continental climate of these northern regions. The potential glaciers (i.e. Altay mountains, Tien Shan, Figure 2.8C) could be investigated in order to understand regional conditions of these high latitudinal regions. Finally the climate of the Tibetan plateau, placed at the north of the Himalayan and surrounded by mountains, is dry and isolated from the other Asian regions. The selection of a glacier could provide regional characterisation and the effect of the extreme events of climatic circulation systems.

In summary, large part of the Asian High Mountains glaciers could be investigated. Potential drilling sites can provide important information regarding the regional climate variability, anthropogenic impacts, climate circulation patterns. Glaciers preserve this information, that are essential to understand climate and environment variation. Remote location of glaciers, rugged terrain, and a complex political situation, could make physical access difficult. These issues (especially social and political problems) should be overcome to gain valuable information to study future climate and environmental.

The proposed methodology gives indication of more potential drilling site combining morphometric and climatic variables, that are globally and freely distributed from on line repositories. Some limitations in the model could be caused by ASTER DEM and RGI glaciers outlines. ASTER shows low vertical accuracy that introduce errors in the calculated morphometric variables. This dataset was chosen in order to have a globally covered DEM with high spatial resolution. ASTER, in fact, offers a more detail compared to the other global dataset (i.e. Shuttle Radar Topography Mission digital elevation model, SRMT), fundamental for studying mountain complex topography. In the identification of a potential drilling site, the uncertainty of this errors were reduced considering an area of high value of SICD. Furthermore, errors of some pixel can be considered not so significant in the analysis. About the glacier outlines, artifacts such as internal rocks, or snow-covered bedrock, are included in the RGI dataset. Despite this limitation, the RGI was chosen because it is the most complete outlines database. In order to overcome this issues, the evaluation of a drilling site and the identification of potential glaciers were made also observing satellite images. In the future, the model could be applied using more detailed glaciers outlines.

Other variables such as glacier thickness, snow accumulation, wind erosion, warming temperatures, are also important but are not globally and uniformly distributed. These variables should be further investigated at regional or local scale, to provide a detailed characterisation of the potential drilling sites and accurately locate the drillings. The glacier thickness is a very important parameter in the location of a drilling site and is traditional explored using geo-radar soundings. High thicknesses are necessary to collect deep ice cores. The temporal resolution of ice core stratigraphy depends on the accumulation rate and ablation processes (e.g. operated by wind erosion). Generally, higher annual accumulations are associated with high resolved seasonal stratigraphy; otherwise, the sites characterised by low accumulation rate preserved long time history cores. A seasonal resolution drilling site can be selected investigating these parameters at glacier scale; the integration of climatic records from weather stations and mass balance data should be also performed in this directions.

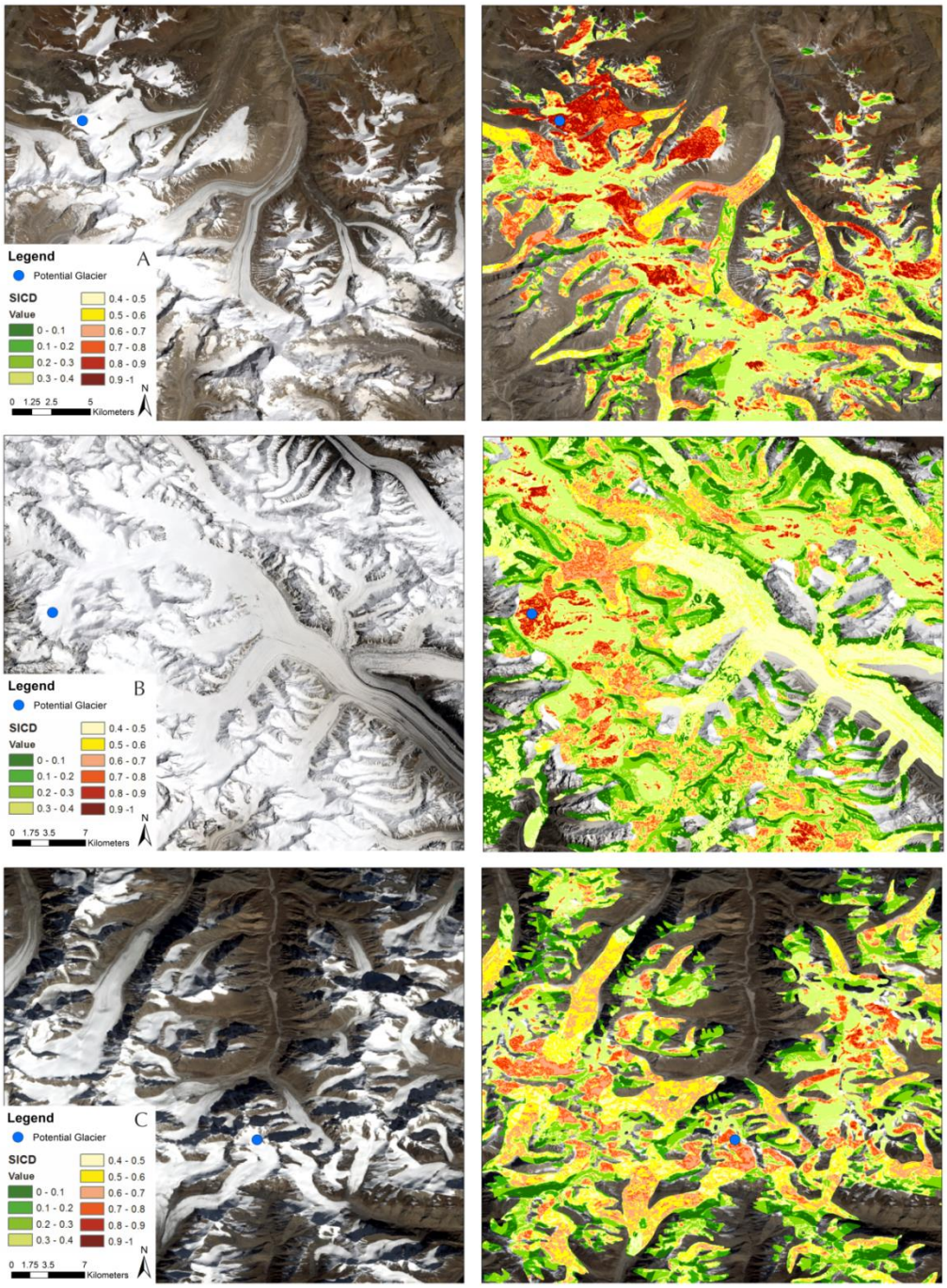

Figure 2.8: Suitability maps for ice core drilling for the Asian High Mountains glaciers: A) Central Himalaya, B) Karakoram regions, C) Altay mountains in Tien Shan. The figure shows the glaciers area collected by the Landsat 8 imagery and the SICD maps. The potential areas, indicated by the blue points are placed within high value of SICD (red colours).

2.5 Conclusions and perspectives

Ice cores are very important sources of paleoclimates information. This data are essential to study previous climate, describe current environmental conditions, in order to predict future climate change. The rapid glaciers melting poses the threat of losing fundamental information stored in the ice. Therefore, emerge the necessity to collect ice core for new potentially valuable drilling sites. To date, the issue of the identification of the suitable sites for ice core drilling has not been addressed quantitatively in available scientific literature. In this paper, we propose a first step toward developing methodology, to assess the suitability for ice core drilling of mountain glaciers, in order to collect ice cores with preserved stratigraphy.

Two methods for mapping potential drilling were developed: (1) exploiting a multi-criteria analysis and (2) combining by WoE morphometric and climatic variables. Selected variables (i.e. slope, local relief, mean temperature of warmest quarter and direct solar radiation) are globally available and freely distributed from on line repositories. The methods were optimised for mapping SICD of glaciers in the European Alps and in the Asian High Mountains.

Results from SICD estimation were satisfactory. In particular, considering the WoE model, the success rate curves show that the model correctly classified more than 85% of the total drilled pixels. The first maps of SICD of the more suitable glaciers was thus proposed. Furthermore, useful indication for the selection of the next drilling sites are suggested, also referring to the importance to perform new drillings.

This study suggests a valuable contribution to current research efforts and can be used to facilitate selection and prioritisation of the sites to be drilled in the next years. These results could be relevant, especially in remote areas where little information is available and many potential drilling sites are still to be exploited. Furthermore, the results encourage the application of the method to other mountain chains (i.e. North and South America) to map the potential sites at global scale.

Acknowledgements:

The present study was performed in the framework of the Project of Interest NextData: a national system devoted to assess the effects of climate and environmental change in mountain areas. A final version of this chapter is in review for *Journal of Glaciology*.

I would like to thank Giuseppe Orombelli, Barbara Delmonte, Giovanni Baccolo, Marco Filippazzi, Matteo Mattavelli (DISAT-UNIMIB, Italy) and all the Cryolist members that kindly compiled the questionnaire. The complete map of SICD is accessible at the following url, http://geomatic.disat.unimib.it/home/geomatic/idb2/, or can be request to the corresponding author. The complete questionnaire is available at http://geomatic.disat.unimib.it/home/geomatic/drill/.

Bibliography

Agterberg FP, Bonham-Carter GF and Wright DF (1990) Statistical Pattern Integration for Mineral Exploration. Computers and Geology. 1–21 (doi:http://dx.doi.org/10.1016/B978-0-08-037245-7.50006-8)

Aller L, Bennett T, Lehr JH, Petty R. and Hackett G (1987) DRASTIC: a standardized system for evaluating groundwater pollution potential using hydrgeologic settings. EPA-600/2-87-035., 1–58 (doi:EPA/600/2-87/035)

Alley RB (2000) Ice-core evidence of abrupt climate changes. Proc. Natl. Acad. Sci. 97(4), 1331–1334 (doi:10.1073/pnas.97.4.1331)

Arendt A, Bliss A, Bolch T and Cogley JG (2014) Randolph Glacier Inventory – A Dataset of Global Glacier Outlines: Version 4.0. GLIMS Tech. Rep. (December), 1–56

Asadi HH and Hale M (2001) A predictive GIS model for mapping potential gold and base metal mineralization in Takab area, Iran. Comput. Geosci. 27(8), 901–912 (doi:10.1016/S0098-3004(00)00130-8)

ASTER GDEM Validation Team (2011) ASTER Global Digital Elevation Model Version 2 – Summary of Validation Results. http://www.jspacesystems.or.jp/ersdac/GDEM/ver2Validation/Summary_GDEM2_validation_report_final.pdf

Babiker IS, Mohamed M a a, Hiyama T and Kato K (2005) A GIS-based DRASTIC model for assessing aquifer vulnerability in Kakamigahara Heights, Gifu Prefecture, central Japan. Sci. Total Environ. 345, 127–140 (doi:10.1016/j.scitotenv.2004.11.005)

Bolch T, Kamp U and Olsenholler J (2005) Using ASTER and SRTM DEMs for studying geomorphology and glaciation in high mountain areas. New Strateg. Eur. Remote Sens., 119–128 (doi:ISBN 90 5966 003 X)

Bolch T, Kulkarni a., Kaab a., Huggel C, Paul F, Cogley JG, Frey H, Kargel JS, Fujita K, Scheel M, Bajracharya S and Stoffel M (2012) The State and Fate of Himalayan Glaciers. Science (80). 336(6079), 310–314 (doi:10.1126/science.1215828)

Bonham-Carter GF (1994) Geographic Information Systems for Geoscientists: Modelling with GIS. Elsevier, 1994 (doi:0080424201, 9780080424200)

Bonham-Carter GF, Agterberg FP and Wright DF (1989) Weights of Evidence Modelling: A new approach to mapping mineral potential. Statistical Applications in the Earth Sciences 89, 171-183

Brook EJ (2007) Ice Core Methods. Encycl. Quat. Sci., 1145–1156 (doi:10.1016/B0-44-452747)

Buffen AM, Hastings MG, Thompson LG and Mosley-Thompson E (2014) Investigating the preservation of nitrate isotopic composition in a tropical ice core from the Quelccaya Ice Cap, Peru. J. Geophys. Res. Atmos. 119(5), 2674–2697 (doi:10.1002/2013JD020715)

Chung CF and Fabbri AG (1999) Probabilistic Prediction Models for Landslide Hazard Mapping. Photogramm. Eng. Remote Sens. 65(12), 1389–1399

Dahal RK, Hasegawa S, Nonomura A, Yamanaka M, Dhakal S and Paudyal P (2008) Predictive modelling of rainfall-induced landslide hazard in the Lesser Himalaya of Nepal based on weights-of-evidence. Geomorphology 102(3-4), 496–510 (doi:10.1016/j.geomorph.2008.05.041)

Dahal RK, Hasegawa S, Nonomura A, Yamanaka M, Masuda T and Nishino K (2008) GIS-based weights-of-evidence modelling of rainfall-induced landslides in small catchments for landslide susceptibility mapping. Environ. Geol. 54(2), 311–324 (doi:10.1007/s00254-007-0818-3)

Fabbri AG, Chung CJF, Cendrero A and Remondo J (2003) Is prediction of future landslides possible with a GIS? Nat. Hazards 30, 487–499 (doi:10.1023/B:NHAZ.0000007282.62071.75)

Faïn X, Chappellaz J, Rhodes RH, Stowasser C, Blunier T, McConnell JR, Brook EJ, Preunkert S, Legrand M, Debois T and Romanini D (2014) High resolution measurements of carbon monoxide along a late Holocene Greenland ice core: Evidence for in situ production. Clim. Past 10(3), 987–1000 (doi:10.5194/cp-10-987-2014)

Field CB, Barros VR, Dokken, D J, Mach KJ, Mastrandrea MD, Bilir TE, Chatterjee M, Ebi KL, Estrada YO, Genova RC, Girma B, Kissel ES, Levy AN, MacCracken S, Mastrandrea PR, White LL and (eds) (2014) IPCC, 2014: Summary for policymakers. Cambridge University Press, Cambridge, United Kingdom and New York, NY, USA (doi:10.1016/j.renene.2009.11.012)

Gabrieli J, Carturan L, Gabrielli P, Kehrwald N, Turetta C, Cozzi G, Spolaor a., Dinale R, Staffler H, Seppi R, Dalla Fontana G, Thompson L and Barbante C (2011) Impact of Po Valley emissions on the highest glacier of the Eastern European Alps. Atmos. Chem. Phys. 11(15), 8087–8102 (doi:10.5194/acp-11-8087-2011)

Gabrielli P, Barbante C, Carturan L, Cozzi G, Fontana GD, Dinale R, Dragà G, Gabrieli J, Kehrwald N, Mair V, Mikhalenko V, Piffer G, Rinaldi M, Seppi R, Spolaor A, Thompson LG and Tonidandel D (2012) Discovery of cold ice in a new drilling site in the eastern European Alps. Geogr. Fis. e Din. Quat. 35, 101–105 (doi:10.4461/GFDQ.2012.35.10)

Gabrielli P, Carturan L, Gabrieli J, Dinale R, Krainer K, Hausmann H, Davis M, Zagorodnov V, Seppi R, Barbante C, Fontana GD and Thompson LG (2010) Atmospheric warming threatens the untapped glacial archive of Ortles mountain, South Tyrol. J. Glaciol. 56(199), 843–853 (doi:10.3189/002214310794457263)

Giordano A, Bonfils P, Briggs DJ, de Sequeira EM, de Laburu CR and Yassoglou N (1991) The methodological approach to soil erosion and important land resources evaluation of the European community. Soil Technol. 4(1), 65–77 (doi:10.1016/0933-3630(91)90040-T)

Gregory S and Noone D (2008) Variability in the teleconnection between the El Niño–Southern Oscillation and West Antarctic climate deduced from West Antarctic ice core isotope records. J. Geophys. Res. 113, 1–17 (doi:10.1029/2007JD009107)

Hasiniaina F, Zhou J and Guoyi L (2010) Regional assessment of groundwater vulnerability in Tamtsag basin , Mongolia using drastic model. J. Am. Sci. 6(11), 65–78

Hayakawa YS, Oguchi T and Lin Z (2008) Comparison of new and existing global digital elevation models: ASTER G-DEM and SRTM-3. Geophys. Res. Lett. 35(17), L17404 (doi:10.1029/2008GL035036)

Hijmans RJ, Cameron SE, Parra JL, Jones PG and Jarvis A (2005) Very high resolution interpolated climate surfaces for global land areas. Int. J. Climatol. 25(15), 1965–1978 (doi:10.1002/joc.1276)

Hofierka J, Mitàsovà H and Neteler M (2009) Geomorphometry in GRASS GIS. Geomorphometry concepts, software, Appl. Hengl, T.; Reuter, I.H.). Amsterdam Elsevier. (Developments soil Sci. 33) 387-410. ISBN 9780123743459 handle http//hdl.handle.net/10449/19241, 387–410

Hofierka J and Šúri M (2002) The solar radiation model for Open source GIS: implementation and applications. Open source GIS - GRASS users conference in Trento, Italy, September 2002.

Hussin HY, Zumpano V, Reichenbach P, Sterlacchini S, Micu M, van Westen C and Bălteanu D (2015) Different landslide sampling strategies in a grid-based bi-variate statistical susceptibility model. Geomorphology 253, 508–523 (doi:10.1016/ j.geomorph.2015.10.030)

Immerzeel WW, van Beek LPH and Bierkens MFP (2010) Climate change will affect the Asian water towers. Science 328(5984), 1382–5 (doi:10.1126/science.1183188)

Ishizaka A and Labib A (2011) Review of the main developments in the Analytic Hierarchy Process. Expert Syst. Appl. 38(11), 14336–14345

Jenk TM, Szidat S, Bolius D, Sigl M, Gäggeler HW, Wacker L, Ruff M, Barbante C, Boutron CF and Schwikowski M (2009) A novel radiocarbon dating technique applied to an ice core from the Alps indicating late Pleistocene ages. J. Geophys. Res. Atmos. 114, 1–8 (doi:10.1029/2009JD011860)

Jouzel J and Masson-Delmotte V (2010) Paleoclimates: what do we learn from deep ice cores? Wiley Interdiscip. Rev. Clim. Chang. 1(5), 654–669 (doi:10.1002/wcc.72)

Kargel JS, Leonard GJ, Bishop MP, Kaab A and Raup BH (2014) Global Land Ice Measurements from Space. Springer Berlin Heidelberg, Berlin, Heidelberg (doi:10.1007/978-3-540-79818-7)

Karnatak HC, Saran S, Bhatia K and Roy PS (2007) Multicriteria spatial decision analysis in web GIS environment. Geoinformatica 11(4), 407–429 (doi:10.1007/s10707-006-0014-8)

Kaspari S, Hooke RL, Mayewski PA, Kang S, Hou S and Qin D (2008) Snow accumulation rate on Qomolangma (Mount Everest), Himalaya: synchroneity with sites across the Tibetan

Plateau on 50–100 year timescales. J. Glaciol. 54(185), 343–352 (doi:10.3189/002214308784886126)

Kaspari S, Mayewski P, Kang S, Sneed S, Hou S, Hooke R, Kreutz K, Introne D, Handley M, Maasch K, Qin D and Ren J (2007) Reduction in northward incursions of the South Asian monsoon since ~1400 AD inferred from a Mt. Everest ice core. Geophys. Res. Lett. 34(16), n/a–n/a (doi:10.1029/2007GL030440)

Keisler JM, Collier Z a., Chu E, Sinatra N and Linkov I (2014) Value of information analysis: the state of application. Environ. Syst. Decis. 34(1), 3–23 (doi:10.1007/s10669-013-9439-4)

Konrad H, Bohleber P, Wagenbach D, Vincent C and Eisen O (2013) Determining the age distribution of Colle Gnifetti, Monte Rosa, Swiss Alps, by combining ice cores, ground-penetrating radar and a simple flow model. J. Glaciol. 59(213), 179–189 (doi:10.3189/2013JoG12J072)

Linkov I, Loney D, Cormier S, Satterstrom FK and Bridges T (2009) Weight-of-evidence evaluation in environmental assessment: Review of qualitative and quantitative approaches. Sci. Total Environ. 407(19), 5199–5205 (doi:10.1016/j.scitotenv.2009.05.004)

Linkov I, Massey O, Keisler J, Rusyn I and Hartung T (2015) From ' Weight of Evidence ' to Quantitative Data Integration using Multicriteria Decision Analysis and Bayesian Methods. ALTEX Altern. to Anim. Exp. 32(1), 3–8

Lowell T V (2000) As climate changes, so do glaciers. Proc. Natl. Acad. Sci. U. S. A. 97(4), 1351–1354 (doi:10.1073/pnas.97.4.1351)

Maggi V, Villa S, Finizio a., Delmonte B, Casati P and Marino F (2006) Variability of anthropogenic and natural compounds in high altitude-high accumulation alpine glaciers. Hydrobiologia 562(1), 43–56 (doi:10.1007/s10750-005-1804-y)

Neff PD, Steig EJ, Clark DH, McConnell JR, Pettit EC and Menounos B (2012) Ice-core net snow accumulation and seasonal snow chemistry at a temperate-glacier site: Mount Waddington, southwest British Columbia, Canada. J. Glaciol. 58(212), 1165–1175 (doi:10.3189/2012JoG12J078)

Neshat A, Pradhan B and Dadras M (2014) Groundwater vulnerability assessment using an improved DRASTIC method in GIS. Resour. Conserv. Recycl. 86, 74–86 (doi:10.1016/j.resconrec.2014.02.008)

Oerter H, Reinwarth O and Rufli H (1983) Core drilling through a temperate alpine glacier (Vernagtferner, Oetztal Alps) in 1979. Zeitschrift für Gletscherkd. und Glazialgeol. 18 (1)(1983), 1–11 (doi:10013/epic.38420.d001)

Petit JR, Jouzel J, Raynaud D, Barkov NI, Barnola JM, Basile I, Bender M, Chappellaz J, Davis M, Delaygue G, Delmotte M, Kotlyakov VM, Legrand M, Lipenkov VY, Lorius C, PEpin L, Ritz C, Saltzman E and Stievenard M (1999) Climate and atmospheric history of the past 420,000 years from the Vostok ice core, Antarctica. Nature 399(6735), 429–436 (doi:10.1038/20859)

Pfeffer WT, Arendt A a., Bliss A, Bolch T, Cogley JG, Gardner AS, Hagen J-O, Hock R, Kaser G, Kienholz C, Miles ES, Moholdt G, Mölg N, Paul F, Radic V, Rastner P, Raup BH, Rich J and Sharp MJ (2014) The Randolph Glacier Inventory: a globally complete inventory of glaciers. J. Glaciol. 60(221), 537–552 (doi:10.3189/2014JoG13J176)

Pradhan B, Oh H-J and Buchroithner M (2010) Weights-of-evidence model applied to landslide susceptibility mapping in a tropical hilly area. Geomatics, Nat. Hazards Risk 1(3), 199–223 (doi:10.1080/19475705.2010.498151)

Preunkert S, Wagenbach D, Legrand M and Vincent C (2000) Col du Dome (Mt Blanc Massif, French Alps) suitability for ice-core studies in relation with past atmospheric chemistry over Europe. Tellus, Ser. B Chem. Phys. Meteorol. 52, 993–1012 (doi:10.1034/j.1600-0889.2000.d01-8.x)

Regmi AD, Devkota KC, Yoshida K, Pradhan B, Pourghasemi HR, Kumamoto T and Akgun A (2013) Application of frequency ratio, statistical index, and weights-of-evidence models and their comparison in landslide susceptibility mapping in Central Nepal Himalaya. Arab. J. Geosci. 7(2), 725–742 (doi:10.1007/s12517-012-0807-z)

Regmi NR, Giardino JR and Vitek JD (2010) Modeling susceptibility to landslides using the weight of evidence approach: Western Colorado, USA. Geomorphology 115(1-2), 172–187 (doi:10.1016/j.geomorph.2009.10.002)

Remondo J, Gonzalez A, De JRD, Cendrero A and Fabbri A (2003) Validation of Landslide Susceptibility Maps ; Examples and Applications from a Case Study in Northem Spain. Nat. Hazards 30(3), 437–449 (doi:10.1023/B:NHAZ.0000007201.80743.fc)

Saaty TL (1980) The Analytic Hierarchy Process. McGraw-Hill Inc, 17–34 (doi:0070543712)

Saaty TL (2008) Decision making with the analytic hierarchy process. Int. J. Serv. Sci. 1(1), 83 (doi:10.1504/IJSSCI.2008.017590)

Saidi S, Bouri S and Ben Dhia H (2011) Sensitivity analysis in groundwater vulnerability assessment based on GIS in the Mahdia-Ksour Essaf aquifer, Tunisia: a validation study. Hydrol. Sci. J. 56(755239602), 288–304 (doi:10.1080/02626667.2011.552886)

Sakai A, Nuimura T, Fujita K, Takenaka S, Nagai H and Lamsal D (2015) Climate regime of Asian glaciers revealed by GAMDAM glacier inventory. Cryosph. 9(2014), 865–880 (doi:10.5194/tc-9-865-2015)

Salo AA and Hämäläinen RP (1997) On the measurement of preferences in the analytic hierarchy process. J. Multi-Criteria Decis. Anal. 6, 309–319 (doi:10.1002/(SICI)1099-1360(199711)6:6<309::AID-MCDA163>3.0.CO;2-2)

Schuster PF, Krabbenhoft DP, Naftz DL, Cecil LD, Olson ML, Dewild JF, Susong DD, Green JR and Abbott ML (2002) Atmospheric Mercury Deposition during the Last 270 Years: A Glacial Ice Core Record of Natural and Anthropogenic Sources. Environ. Sci. Technol. 36(11), 2303–2310 (doi:10.1021/es0157503)

Schwikowski M, Brütsch S, Gäggeler HW and Schotterer U (1999) A high-resolution air chemistry record from an Alpine ice core: Fiescherhorn glacier, Swiss Alps. J. Geophys. Res. 104(D11), 13709 (doi:10.1029/1998JD100112)

Schwikowski M, Döscher a., Gäggeler HW and Schotterer U (1999) Anthropogenic versus natural sources of atmospheric sulphate from an Alpine ice core. Tellus, Ser. B Chem. Phys. Meteorol. 51, 938–951 (doi:10.1034/j.1600-0889.1999.t01-4-00006.x)

Sener E and Davraz A (2012) Assessment of groundwater vulnerability based on a modified DRASTIC model, GIS and an analytic hierarchy process (AHP) method: the case of Egirdir Lake basin (Isparta, Turkey). Hydrogeol. J. 21(3), 701–714 (doi:10.1007/s10040-012-0947-y)

Shirazi SM, Imran HM and Akib S (2012) GIS-based DRASTIC method for groundwater vulnerability assessment: a review. Journal of Risk Research 15, 991–1011 (doi:10.1080/13669877.2012.686053)

Sorichetta A, Masetti M, Ballabio C and Sterlacchini S (2012) Aquifer nitrate vulnerability assessment using positive and negative weights of evidence methods, Milan, Italy. Comput. Geosci. 48, 199–210 (doi:10.1016/j.cageo.2012.05.021)

Steig E (2003) Ice Cores. Paleoclimatology. 1673–1680

Sterlacchini S, Ballabio C, Blahut J, Masetti M and Sorichetta A (2011) Spatial agreement of predicted patterns in landslide susceptibility maps. Geomorphology 125(1), 51–61 (doi:10.1016/j.geomorph.2010.09.004)

Stevenazzi S, Masetti M, Nghiem S V. and Sorichetta A (2015) Groundwater vulnerability maps derived from a time-dependent method using satellite scatterometer data. Hydrogeol. J. 23(4), 631–647 (doi:10.1007/s10040-015-1236-3)

Stocker TF, Qin D, Plattner G-K, Tignor M, Allen SK, Boschung J, Nauels A, Xia Y, Bex V, Midgley PM and (eds.) (2013) IPCC, 2013: Climate Change 2013: The Physical Science Basis. Contribution of Working Group I to the Fifth Assessment Report of the Intergovernmental Panel on Climate Change. Cambridge University Press, Cambridge, United Kingdom and New York, NY, USA,

Strigaro D, Mattavelli M, Frigerio I and De Amicis M (2014) PaleoProxy Data Base (PPDB): A comprehensive geodatabase to archive and manage paleoproxies data. Rend. Online Soc. Geol. It. Suppl. n. 1 al Vol. 31 118

Thevenon F, Anselmetti FS, Bernasconi SM and Schwikowski M (2009) Mineral dust and elemental black carbon records from an Alpine ice core (Colle Gnifetti glacier) over the last millennium. J. Geophys. Res. 114(D17), D17102 (doi:10.1029/2008JD011490)

Thiery Y, Malet JP, Sterlacchini S, Puissant a. and Maquaire O (2007) Landslide susceptibility assessment by bivariate methods at large scales: Application to a complex mountainous environment. Geomorphology 92(1-2), 38–59 (doi:10.1016/j.geomorph.2007.02.020)

Thirumalaivasan D, Karmegam M and Venugopal K (2003) AHP-DRASTIC: software for specific aquifer vulnerability assessment using DRASTIC model and GIS. Environ. Model. Softw. 18(7), 645–656 (doi:10.1016/S1364-8152(03)00051-3)

Thompson LG (1996) Climatic changes for the 2000 years inferred from ice-core evidence in tropical ice cores. NATO Adv. Res. Ser. I 41, 281–295

Thompson LG (2000) Ice core evidence for climate change in the Tropics: implications for our future. Quat. Sci. Rev. 19(1-5), 19–35 (doi:10.1016/S0277-3791(99)00052-9)

Thompson LG (2010) Understanding global climate change: paleoclimate perspective from the world's highest mountains. Proc. Am. Philos. Soc. 154(2), 133–57 http://www.ncbi.nlm.nih.gov/pubmed/21553594

Thompson LG, Davis ME, Mosley-Thompson E, Lin PN, Henderson KA and Mashiotta TA (2005) Tropical ice core records: Evidence for asynchronous glaciation on Milankovitch timescales. J. Quat. Sci. 20, 723–733 (doi:10.1002/jqs.972)

Thompson LG, Mosley-Thompson E, Davis ME and Brecher HH (2011) Tropical glaciers, recorders and indicators of climate change, are disappearing globally. Ann. Glaciol. 52(59), 23–34 (doi:10.3189/172756411799096231)

Thompson LG, Mosley-Thompson E, Davis ME, Henderson KA, Brecher HH, Zagorodnov VS, Mashiotta TA, Lin P-N, Mikhalenko VN, Hardy DR and Beer J (2002) Kilimanjaro ice core records: evidence of holocene climate change in tropical Africa. Science 298(OCTOBER), 589–593 (doi:10.1126/science.1073198)

Thompson LG, Mosley-Thompson E, Davis ME, Lin PN, Henderson K and Mashiotta T a. (2003) Tropical glacier and ice core evidence of climate change on annual to millennial time scales. Clim. Change 59, 137–155 (doi:10.1023/A:1024472313775)

Thompson LG, Mosley-Thompson E, Davis ME, Zagorodnov VS, Howat IM, Mikhalenko VN and Lin P-N (2013) Annually Resolved Ice Core Records of Tropical Climate Variability over the Past 1800 Years. Science (80-.). 340(6135), 945–950 (doi:10.1126/science.1234210)

Tian L, Yao T, Schuster PF, White JWC, Ichiyanagi K, Pendall E, Pu J and Yu W (2003) Oxygen-18 concentrations in recent precipitation and ice cores on the Tibetan Plateau. J. Geophys. Res. 108(D9), 1–10 (doi:10.1029/2002JD002173)

Vaidya OS and Kumar S (2006) Analytic hierarchy process: An overview of applications. Eur. J. Oper. Res. 169(1), 1–29 (doi:10.1016/j.ejor.2004.04.028)

Vimeux F, Ginot P, Schwikowski M, Vuille M, Hoffmann G, Thompson LG and Schotterer U (2009) Climate variability during the last 1000 years inferred from Andean ice cores: A review of methodology and recent results. Palaeogeogr. Palaeoclimatol. Palaeoecol. 281(3-4), 229–241 (doi:10.1016/j.palaeo.2008.03.054)

Vincent C, Ribstein P, Favier V, Wagnon P, Francou B, Le Meur E and Six D (2005) Glacier fluctuations in the Alps and in the tropical Andes. Comptes Rendus Geosci. 337(1-2), 97–106 (doi:10.1016/j.crte.2004.08.010)

Vogt J V., Colombo R and Bertolo F (2003) Deriving drainage networks and catchment boundaries: A new methodology combining digital elevation data and environmental characteristics. Geomorphology 53, 281–298 (doi:10.1016/S0169-555X(02)00319-7)

Wang B, Wu R and Fu X (2000) Pacific–East Asian Teleconnection: How Does ENSO Affect East Asian Climate? J. Clim. 13(9), 1517–1536 (doi:10.1175/1520-0442(2000)013<1517:PEATHD>2.0.CO;2)

Williams RSJ and Ferrigno JG (2006) Glaciers of Europe - Glaciers of the Alps: satellite image atlas of glacier of the world. U.S. Geol. Surv. Prof. Pap. 1386-E-1, 444

Wilson JP and Gallant JC (2000) Terrain Analysis: Principles and Applications. John Wiley & Sons (doi:0471321885)

You-Hailin, Xu-Ligang, Ye-Chang and Xu-Jiaxing (2011) Evaluation of Groundwater Vulnerability with Improved DRASTIC Method. Procedia Environ. Sci. 10, 2690–2695 (doi:10.1016/j.proenv.2011.09.418)

Youssef AM, Pourghasemi HR, El-Haddad B a. and Dhahry BK (2015) Landslide susceptibility maps using different probabilistic and bivariate statistical models and comparison of their performance at Wadi Itwad Basin, Asir Region, Saudi Arabia. Bull. Eng. Geol. Environ. (doi:10.1007/s10064-015-0734-9)

Zhang Q, Kang S, Gabrielli P, Loewen M and Schwikowski M (2015) Vanishing High Mountain Glacial Archives: Challenges and Perspectives. Environ. Sci. Technol. 49(16), 9499–9500 (doi:10.1021/acs.est.5b03066)

3. COLLECTING FIELD SPECTROSCOPY DATA WITH A NON-IMAGING HYPERSPECTRAL UAV

Abstract

A light UAV for collecting visible to near-infrared spectral measurements, in support of common field spectroscopy surveys, is presented in this study. The system, namely HyUAV, is based on a four-rotors platform with hovering capability, equipped with the non-imaging spectrometer and the RGB camera. The HyUAV collects hyperspectral data (350-1000 nm with ~1.5 nm FWHM of spectral resolution) of Earth reflected radiance and RGB images simultaneously. The Entrance Optics Receptor (EOR) was specifically developed to optimize the spectrometer field of view and to collect in-flight dark current. The geometric, radiometric and spectral performances of the system were characterized through dedicated laboratory tests. The accuracy and the precision of hyperspectral data were evaluated during flight tests, in which spectral data collected from HyUAV, were compared with ground-based measurements over the same targets. Furthermore, two methods to estimate surface reflectance from HyUAV data: i) reference tarp; and ii) ground dual spectrometer approach; were investigated and discussed with the aim of providing further suggestions for an accurate retrieval of surface reflectance. The RGB images were processed and products (i.e. orthomosaic image, 3D model, Digital Surface Model) were created and integrated with hyperspectral measurements. The results achieved shown: i) good systems stability (in terms of geometric, radiometric and spectral features), with negligible effect of UAV rotors vibrations on hyperspectral data; ii) accurate spectra measurements (in terms of radiance and reflectance), with RRMSE < 10%; iii) similar results for the methods to calculate reflectance. The HyUAV demonstrated to be a reliability systems for supporting field spectroscopy surveys and a promising platform for a wide range of environmental applications.

3.1 Introduction

Field spectroscopy is an essential technique in remote sensing to gain valuable insight on Earth surface optical properties. These data are important to characterize natural surfaces, to support the calibration and validation of airborne and satellite measurements, and to provide essential information for scaling-up measurements from local to regional scale (Morisette and others, 2002; Schaepman and others, 2009; Masek and others, 2015).

In general, the common way to collect field spectroscopy data during field surveys is based on manual measurements by using non-contact devices operated close (few meters) from the target (Milton, 1987; Milton and others, 2009). This approach could result not practical for collecting spectral over certain types of targets, limiting the exploitation of field spectroscopy. For example, the collection of top of canopy spectral measurements, on high trees forest (i.e. tens of meters), requires dedicated facilities such as scaffolding towers or hydraulic platforms. Sometime, this can limit or at least make difficult, sampling spatial heterogeneity or monitoring temporal dynamic of ecosystem. Analogous complications can arise when field spectroscopy measurements must be collected in hardly accessible ecosystems such as glaciers, volcanoes, lakes etc.

In the last decade, the Unmanned Aerial Vehicles (UAVs) are becoming a commonly used platform for collecting proximal sensing data, useful for Earth observation studies, and more in general to a wide range of scientific disciplines (Ma and others, 2013; Colomina and Molina, 2014). In particular, the UAVs provide a high level of flexibility, in fact, they might be employed for autonomous/routinely operations, to collect data with different observation requirements (i.e. different scale/resolution, view angle and revisit time), and to facilitate data collection in hardly accessible targets.

The multi-scale acquisitions can be performed varying the flight parameters: detailed resolution data can be collected with proximal target measurements, as well as medium scale data can be collected increasing the flight altitude above the targets.

These data can be useful to improve the upscaling between field and airborne (or satellite) observations. The autonomous and routinely surveys can be replicated in time to have a better insight of processes temporal evolution. Actually, the major limits of light-UAVs are the restriction in terms of weight and payload dimensions, the power duration of the battery, and legislative constraints. However, an increasing number of hyperspectral sensors compatible with light-UAV limitations, is becoming available recently.

Several systems were developed and used in several scientific disciplines. Several authors exploited the use of UAV systems for vegetation monitoring and precision farming (Zhang and Kovacs, 2012; Link and others, 2013; Uto and others, 2013; Salamí and others, 2014; Candiago and others, 2015; von Bueren and others, 2015). The UAVs are used in photogrammetry for creation of orthophoto and 3D models (Westoby and others, 2012; Lucieer, Turner, and others, 2014; Turner and others, 2014; Zarco-Tejada and others, 2014). Some authors exploited the advantages of UAV in geomorphology, glaciers and landslides monitoring (Niethammer and others, 2012; Whitehead and others, 2013; Immerzeel and others, 2014; Aasen and others, 2015; Dall'Asta and others, 2015; Fugazza and others, 2015; Turner and others, 2015). Furthermore unmanned systems are becoming useful tools also in ecology (Getzin and others, 2012; Anderson and Gaston, 2013; van Andel and others, 2015).

In field spectroscopy, hyperspectral sensors measure hundreds of spectral bands with bandwidths usually less than 10 nm, up to sub-nanometer level, providing the possibility to exploit spectral indices for bio-geophysical variable estimation. The hyperspectral measurements can be used for monitoring phenological and physiological traits of the vegetation (Gitelson and others, 2003; Rossini and others, 2010; Clevers and Kooistra, 2012; Deery and others, 2014) and also for a wide range of environmental applications (e.g. mineral dust investigation, water quality, asbestos cement mapping, etc.) (Olmanson and others, 2013; Cilia and others, 2015; Kudela and others, 2015; Di Mauro and others, 2015; Hestir and others, 2015).

In recent years, two indicators derived from hyperspectral data have been proposed and investigated: the Photochemical Reflectance Index (PRI) and the Sun-induced Chlorophyll fluorescence (SIF) (Meroni and others, 2008; Guanter and others, 2013; Panigada and others, 2014; Cogliati and others, 2015; Damm and others, 2015; Rossini, Nedbal, and others, 2015; Rossini, Panigada, and others, 2015).

The UAVs can be considered new platform to investigate Earth surfaces optical properties. The hyperspectral cameras integrated on UAVs allow collecting high spectral resolution data with high spatial and temporal resolution. Some authors developed UAV systems based on multispectral or hyperspectral sensor to monitoring quantitative biochemical and biophysical characteristics of vegetation (Laliberte and others, 2011; Zarco-Tejada and others, 2012; Burkart and others, 2014; Lucieer, Malenovský, and others, 2014; Bareth and others, 2015). Non-imaging sensors were chosen to have the best spectral quality (signal to noise ratio) respecting the required weight of the payload and an affordable cost.

The objective of this study is the development of a novel UAV, equipped with a non-imaging spectrometer, for collecting near-range Earth reflected radiance in the visible to near-infrared (VIS-NIR) spectral domain, coupled with RGB images. Detailed and accurate spectral data (i.e. radiance, reflectance), from which environmental parameters (e.g. biochemical and biophysical traits of vegetation) can be retrieved, required an accurate calibration and characterization of the sensors in terms of spectral and radiometric characteristics. This process is essential in order to obtain high quality data and repeatable and comparable measurements. In this study accuracy and capability to collect high quality spectral data of HyUAV are evaluated by dedicated laboratory tests and flight tests, in order to obtain enhanced radiometric data. Two method to measure reflectance from HyUAV (using a white calibrated tarp or reference spectrometer to collect incoming solar irradiance) were delineated and compared. The possibility to integrate hyperspectral data, RGB images and RGB products is also described in this study.

3.2 The HyUAV system

3.2.1 UAV platform

The Hyperspectral UAV (HyUAV) concept combines a multirotor platform and a specifically developed hyperspectral payload. The Anteos UAV (Aermatica, Italy), powered by four electric rotors (quadcopters), allows autonomous vertical take-off and landing (VTOL), high stability (hovering over target) and high manoeuvrability. These are essential characteristics for an accurate and precise collection of spectral measurements.

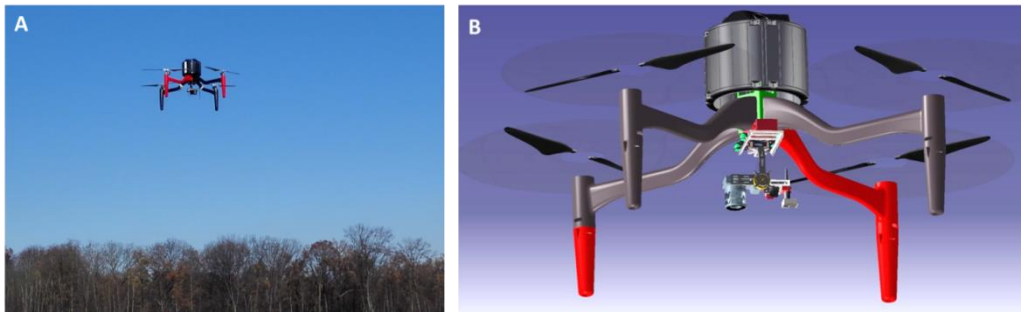

Figure 3.1: The HyUAV. A) picture of the HyUAV during field survey; B) schematic drawing.

The Anteos (Figure 3.1) has a maximum take-off weight of 9 Kg and is able to carry a maximum payload about of 2 Kg, with a flight autonomy of 20 min. The UAV features a width of 200 cm, a length of 200 cm, and a height of 55 cm when rotors' blades are unfolded. The maximum forward flight speed is about 5 m/s. The Anteos uses a full Inertial Navigation Systems (INS) and with a Global Positioning System (GPS). The position data are calculated in cinematic mode during the flight and are used to precisely control the flight, locate the UAV, and tag all the data collected from the payload. The system is also composed by the Ground Control Station (GCS): an essential transportable dedicated hardware/software devices, radio-connected to the UAV, used to monitor and command the HyUAV by a Graphic User Interface (GUI). Lastly, the security and safety of UAV platforms is an important issue to be considered.

HyUAV implements security procedures in case of malfunctioning (e.g. connection error, flight instability) that are essential to the safety of the operators and to preserve the UAV and the sensors from possible damages.

3.2.2 Hyperspectral payload

The HyUAV is equipped with a payload specifically developed for field spectroscopy measurements that combines a high-resolution spectrometer with a RGB digital camera. The Figure 3.2 shows the instruments set-up aboard the UAV platform.

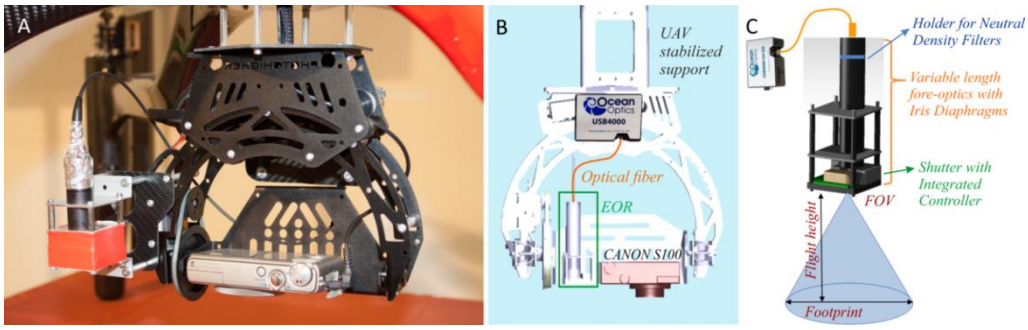

Figure 3.2: (A) RGB image of the HyUAV payload; (B) Schematic illustration of the HyUAV payload, it includes USB4000 spectrometer, Entrance Optic Receptor, and RGB camera (not in scale); (C) Detailed drawing of the Entrance Optic Receptor (not in scale).

The miniaturized VIS-NIR USB4000 is a non-imaging fiber optic spectrometer (190 grams of weight), able of collecting hyperspectral data in the 350 to 1000 nm spectral range, with a Full Width at Half Maximum (FWHM) of about 1.5 nm. The 0.1 m long fiber optic connects the spectrometer with the customized Entrance Optic Receptor (EOR). The latter is composed by a number of lens tubes, with iris diaphragms (Thorlabs, USA), that allows adapting the spectrometer field of view (FOV) in the range between ~2.5° to ~15°, according to the target dimension and flight altitude. Consequently, the dimension of the sampled area at ground can vary from ~50 cm to 15 m, considering an indicative target-sensor distance (i.e. flight altitude) between 5 and 10 m. The EOR includes also the RDI131 shutter (Melles Griot, USA), mounted at the end of the fore-optics, which allows the regular and systematic measurement of

dark current (DC). In fact, the DC signal can substantially change during in-flight conditions because it depends on the sensor temperature and integration time (IT). Therefore, the DC measurements are systematically recorded during flight and are used in the data-processing phase to correct the spectral data.

The spectrometer IT can be either set manually or automatically during the flight in order to collect optimal data at different light conditions (i.e. low/high light intensity, typical for different solar zenith angles and atmospheric conditions). The Integration Time Optimisation (ITO) algorithm (Cogliati and others, 2015) is implemented for automatically set the IT, on the base of the light intensity, obtaining the maximum of the spectrum at 70-80% of the spectrometer dynamic range. Furthermore, the EOR provides a holder for Reflective neutral Density Filters (Thorlabs, Inc. USA) that help in optimizing the intensity of light that reaches the spectrometer. Firstly it avoids spectrometer saturation even for high light intensities (i.e. measurements over high albedo surfaces as snow covered area); and secondly it serves as additional degree of freedom, in optimizing light intensity, to achieve spectrometer IT compatible with the platform motion during data collection. Three lens with different transmittance: 79%, 63% and 40% are available. The spectrometer can be operated according to the defined acquisition scheme protocol. The experimental protocol for collecting spectral data usually follows these steps: i) ITO, ii) DC acquisition, iii) target spectrum measurements (S). Two data collection schemes are implemented: i) the *way-points* measurements, where the user defines a set of way-points and for each of them all the spectrometer operations; ii) the *transect* scheme, where the spectrometer collect continuous measurements along a defined path. However, the HyUAV is able to operate in manual mode: the pilot drive the UAV and the spectrometer operations are manually operated; or in autonomous mode based on the pre-defined mission planning procedure.

The PowerShot S100 (Canon, Italy) is a compact digital camera with a 12.1 Megapixel CMOS sensor, combined with the DIGIC 5 Image Processor, that records high-

resolution images (4000 x 3000 pixels). The RGB camera is automatically triggered (1 image/s) during the flight. Both the sensors are installed on a stabilized platform (Photohigher, AV200 Gimbal) to reduce the impact of platform vibrations.

3.2.3 Data collection

Two software were developed to define the flight plan and the payload data collection over the targets of interest, and to visualize and control in real-time the HyUAV during in-flight operations. The mission plan consists in defining both the platform path and the data collection scheme. These tasks are facilitated by the Mission Planning software which helps in defining the mission specifications before the flight. As first step, a map of the area can be loaded in the software user interface, afterwards the operator defines the so-called *flight-space*. It delimits the surface area to be covered and the platform flight height. Consecutively, the *flight-path* can be automatically created as a series of flight lines and gridded way-points covering the study area according to flight height, RGB camera coverage, and USB4000 sampling area.

In general, the HyUAV can collect spectral data in two distinct modes: i) in static mode platform hovers a specific way-point until spectra are collected; ii) in dynamic mode platform flies between two way-points and spectra are collected continuously (Figure 3.3).

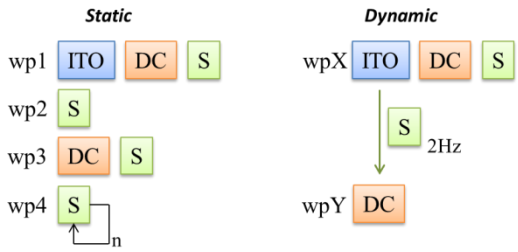

Figure 3.3: Flow chart of the two possible data collection modes for HyUAV.

The static mode allows to select measurements to be collected for each way-point in terms of optimization of the spectrometer IT, dark-current or target measurement in agreement with the widely used field spectroscopy techniques. On the contrary, the

dynamic mode is configured so that optimization and dark-current are collected only at the beginning of the data collection along the transect. Additionally, the user can manually edit and modify the mission plan adding, deleting or varying way-points. Once the mission-plan has been defined and uploaded, the HyUAV is ready to lift for collecting data.

During the flight operations, the Mission Control software allows to monitor and command the HyUAV. Both RGB images and hyperspectral data are digitized and sent through the radio link directly to the GCS. A dedicated GUI for the spectrometer was developed (Figure 3.4).

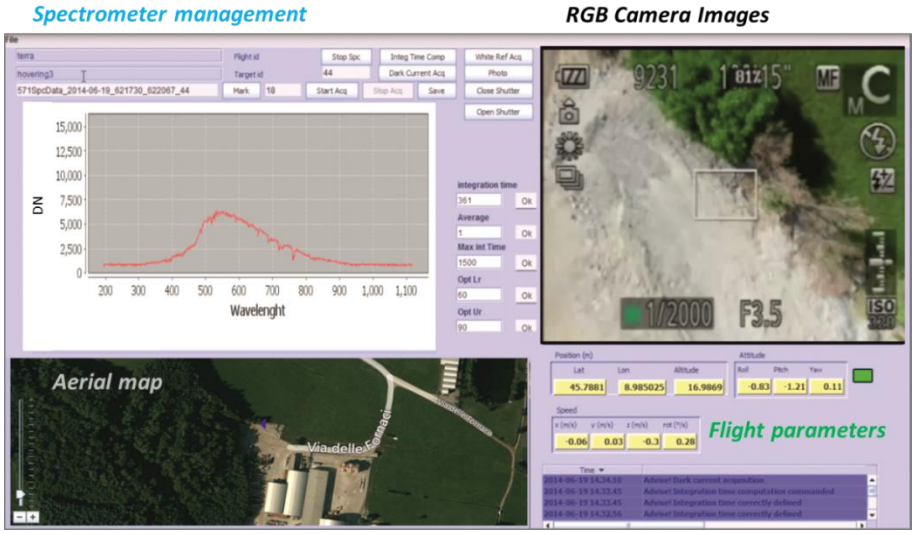

Figure 3.4: Graphic user interfaces of the Mission Control software that allows to manage the USB4000 spectrometer data collection. Upper left panel: interactive view of DN spectra and parameters setting of spectrometer. Lower left panel: aerial map and UAV position. Right panel: real-time RGB image acquired from the UAV and telemetry data.

The GUI continuously displayed in real-time, the sensor data (spectral signature and RGB image) and the flight parameters (latitude and longitude position, horizontal and vertical speed, roll, pitch and yow), which are useful during the data collection process for interactively operating the HyUAV, and an aerial map (or thematic map) of the area with the UAV position. In particular: i) the flight and the target ID can be chosen in order to mark the collected data; ii) the user can collect DC and “white reference”

spectra; iii) IT is computed automatically or could be set manually; iv) a single spectrum acquisition or a continuous spectra collection could be operated (static / dynamic mode).

The system associates to each spectrum acquired the corresponding RBG image and the set of navigation data collected. In particular, spectrum file names, target ID name, positioning data (latitude, longitude, elevation), telemetry data (relative displacements, roll, pitch, yaw, vertical and horizontal speed) and RGB image filename are associated and saved in .CSV file.

3.2.4 Data processing

A dedicated software packages were developed for the systematic processing the hyperspectral data collected. In particular, processing functions were implemented in MATLAB® language in order to: i) calibrate the spectral radiance (DC subtraction, non-linearity correction, radiometric and spectral calibrations), ii) calculate the surface reflectance and iii) calculate widely used spectral indices related to biophysical and biochemical vegetation process from reflectance data such as the Normalized Difference Vegetation Index (NDVI), the Enhanced Vegetation Index (EVI), the MERIS Terrestrial Chlorophyll Index (MTCI) and the Photochemical Reflectance Index (PRI).

Furthermore, RGB images acquired from the UAV are processed with Structure From Motion (SFM) algorithms (Westoby and others, 2012) implemented in the Agisoft Photoscan© package. A 3D textured model, a georeferenced orthomosaic image and a high-resolution digital surface model (DSM) were created using ground control points positions collected using the Differential GPS (DGPS). Finally, the georeferenced data were imported and overlapped to spectral measurements in a GIS.

From single channels RGB data, we estimated the reflectance by normalizing for incident radiation (calculated considering the calibrated tarp image). Values relative to the UAV footprint were extracted from the orthomosaic and compared with USB4000 spectra in order to evaluate the coherence between RGB and hyperspectral data from HyUAV.

3.3 Material and methods

3.3.1 Laboratory characterization and calibration

Dedicated laboratory tests were performed to characterize and calibrate geometric, radiometric and spectral properties of the system, and to verify the its stability during in-flight conditions. In fact, the mechanical vibrations due to platform engines can affect the spectral data collected, in terms of position and width of the spectral bands, radiometric response, etc. For this reason, a test-bed was realized for simulating the in-flight conditions (Figure 3.5).

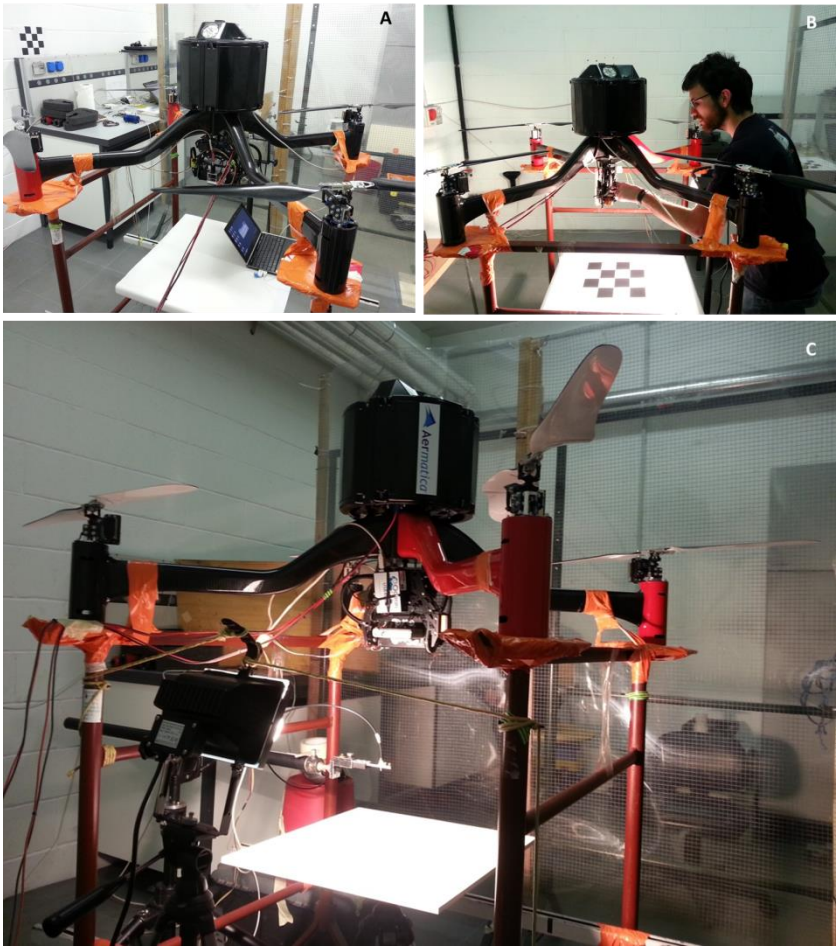

Figure 3.5:Test bed used during the laboratory tests to simulate in- flight conditions (A): Geometric (B) and radiometric set-up (C).

This set-up permits turning on engines in laboratory and operate them as during normal flight, in fact the platform lifts from its support (less than 1 cm) keeping the payload centered on the test bed. Furthermore, the four platform rotors were operated at different regimes emulating diverse manoeuvres such as take-off (i.e. maximum thrust and consequently maximum vibrations), hovering (i.e. minimum thrust), and flying between way-points. The data were acquired before, during and after a series of flight simulations and differences in terms of geometric, radiometric and spectral stability were evaluated.

Geometric

The geometric test aims to determining the dimension of the spectrometer FOV, its relative position in the RGB image, and evaluating the effect of UAV rotors vibration on these parameters. In fact, vibrations can slightly modify the mechanical set-up of some elements of the optical system (in particular of the EOR) that might translate in variations of the dimension of the area sampled at ground. The test was carried out as follows. A halogen lamp was focused directly into the fiber optic connected to the EOR fore-optic projecting the FOV on a levelled surface. A RGB images of FOV footprint (light circle) are collected in dark conditions. The footprint diameters were measured counting the number of lighted pixel and estimating its dimension by using a reference chessboard and validating its dimension measuring manually the circle. The center of the spectrometer footprint within the RGB image is also estimated. Measurements were taken during repeated flight simulations in order to evaluate the geometrical stability (FOV dimension and center position).

Radiometric

The radiometric calibration required to convert raw digital counts recorded by the HyUAV to radiance spectrum ($Wm^{-2}sr^{-1}nm^{-1}$). It was achieved by cross-calibration with a reference, well calibrated, FieldSpec HH (ASD Inc., USA) spectrometer, following Cogliati et al., 2015. In particular, spectral measurements of a stabilized halogen lamp

were collected over a calibrated reference Lambertian Spectralon® panel, placed in the test-bed, in order to obtain nadiral observations from HyUAV. Measures from HyUAV were compared with those collected by FieldSpec in order to calibrate and evaluate the radiometric stability of the USB4000 spectrometer.

Spectral

The center and width of the 3648 spectral bands detected by HyUAV must be characterized and calibrated, and the stability during in-flight conditions must be verified. The spectral accuracy were evaluated according to the typical laboratory methods, pointing the calibrated mercury-argon (Hg-Ar) CAL-2000 light source (Ocean Optics, USA) directly in the EOR. The Hg-Ar lamp emits very narrow and sable peaks at certain wavelengths in the VIS-NIR spectral domain. The spectra of the lamp were collected by USB4000 during and after flights simulations. The wavelength positions of the peaks were extracted and differences in spectral position were evaluated.

3.3.2 Flight tests

A flight test were performed to verify accuracy and precision of the spectral data collected by the HyUAV. The test area was a small pit with different land cover types located in Gironico (CO, Italy, LAT/LON: 45.7878, 8.9840). The data were collected on different land cover types: forest, corn, grassland, gravel, sand and asphalt. The FOV was set to 6°, while the flight altitude during the tests was adjust, from 10 to 35 m above the ground level, for sampling almost the same area over targets with different heights. Using this configuration, the area sampled by the spectrometer was about 1.15 m at 10 m of distance from the target. Simultaneous ground-based measurements were collected over the same targets (unless for the trees) with the FieldSpec HH spectrometer.

Retrieval of surface reflectance

The surface reflectance $\rho(\lambda)$ was calculated normalizing the reflected radiance $L_{ref}(\lambda)$ measured over the surface of interest by the incident solar irradiance $L_{inc}(\lambda)$. In formula:

$$\rho(\lambda) = \frac{L_{ref}(\lambda)}{L_{inc}(\lambda)}$$

During the flight test the reference $L_{inc}(\lambda)$ and $L_{ref}(\lambda)$ were collected manually using the FieldSpec HH spectrometer over a calibrated Lambertian Spectralon® panel and over the target of interest, respectively.

Two method were tested to estimate $\rho(\lambda)$ from HyUAV which differ in the measure of the $L_{inc}(\lambda)$ term. In the first method (*HyUAV-tarp*) only the HyUAV spectrometer was used, in fact the $L_{inc}(\lambda)$ was collected directly from UAV over a calibrated white tarp (6x6 m), before and after target measurements. A linear interpolation was applied in order to improve the estimation of the $L_{inc}(\lambda)$ exactly during the HyUAV measurements and the reflectance was calculated (Figure 3.6, A).

In the second method (*HyUAV-spec*) a dual spectrometer approach was implemented. In fact, $L_{inc}(\lambda)$ was recorded continuously during the HyUAV flight by FieldSpec HH spectrometer over a calibrated Lambertian Spectralon® panel. The spectra collected simultaneously were coupled in time and the reflectance was estimated. The cross calibration between two spectrometer introduce artefacts due to the difference in the spectral resolution (FWHM) and in the Point Spread Function (PSF). In particular, relative shifts in wavelength between spectrometers generate peaks in the estimated signal (radiance or radiance) (Bachmann and others, 2012). To correct this effect, the method described by Bachmann was implemented introducing a multiplicative factor in the estimation of reflectance (Figure 3.6, b).

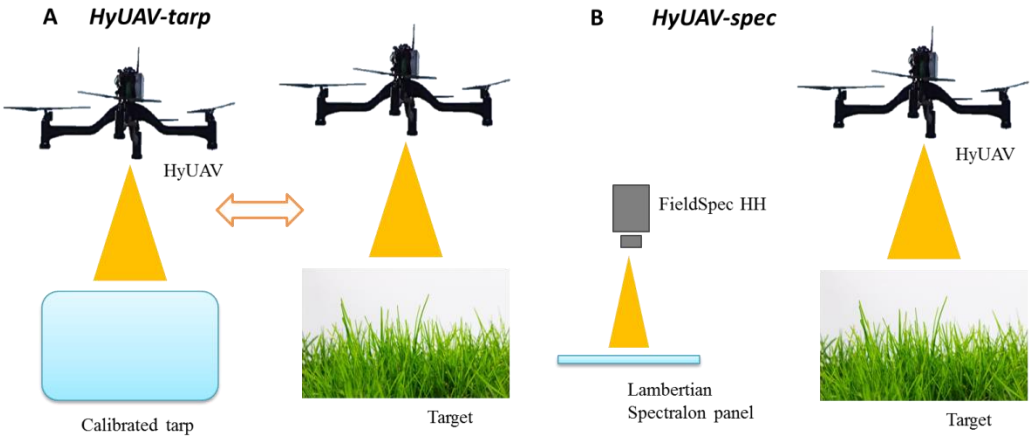

$$\rho_{tarp}(\lambda) = \frac{L_{ref\_UAV}(\lambda)}{L_{inc\_UAV}(\lambda)} \qquad \rho_{spec}(\lambda) = \frac{L_{t\_HH}(\lambda)}{L_{t\_UAV}(\lambda)} * \frac{L_{ref\_UAV}(\lambda)}{L_{inc\_UAV}(\lambda)}$$

Figure 3.6: Methods to estimate reflectance. In the HyUAV-tarp method only the HyUAV spectrometer was used, while the HyUAV-spec method combine two spectrometers measurements. The equations for the calculation of the reflectance are shown in the figure.

The accuracy of spectral data collected by the HyUAV can be assessed by comparing measured radiance and estimated reflectance against data collected from ground-truth by FieldSpec HH spectrometer. The statistical indexes considered were the Root Mean Square Error (RMSE), which quantifies the differences between predicted values (HyUAV data) and assumed true values (FieldSpec HH data), and the Relative RMSE (RRMSE%) that represents the percentage of error with respect to the actual values.

3.4 Results and discussion

3.4.1 Laboratory tests

Figure 3.7 shows the footprint of the spectrometer, as observed by RGB camera in dark condition (left), and the reference chessboard used for determining the spatial resolution (right). The mean values and the standard deviation calculated to retrieve dimension of spectrometer footprint (and estimated FOV), and its position within the RGB image are reported in table. The low standard deviations values demonstrates

that the typical platform vibration have negligible effect of the geometric characteristics of HyUAV. Additionally, spatial transects of blue, green and red channels detected by the RGB camera, extracted along the x and y directions of the image are reported in Figure 3.7 (left). These profiles can be considered in term of spectrometer Point Spread Function (PSF). The shape similar to a square wave and the not-blurred image indicate a very delineated focal plane: the spectra collected from USB4000 (with EOR mounted at the entrance of optical fiber) are well focused on the plane with a limited effect of energy coming from surrounding area. Therefore, the EOR can be considered good to reduce common fiber optics diffraction and collect good quality focused data.

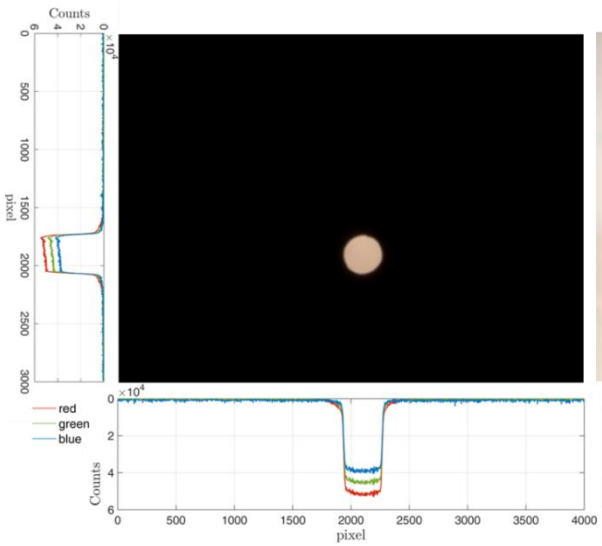

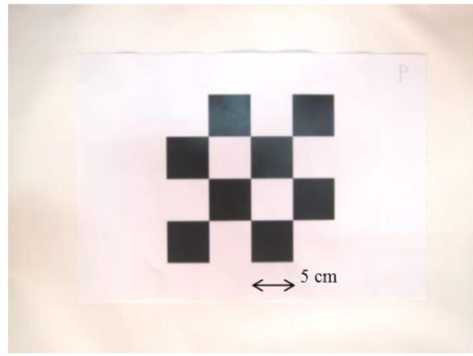

	Footprint parameters		RGB image coordinates	
	Diameter (cm)	FOV (deg)	x (pixel)	y (pixel)
mean (std)	4.64 (0.06)	6.56 (0.01)	2100 (5)	1894 (5)

Figure 3.7: RGB images of spectrometer footprint (with related graph of RBG signal) and reference chessboard. The table show the mean value end the standard deviation of the geometric parameters calculated from images.

The radiometric signal measured from HyUAV shown only limited variations that can be related to the common variability of the USB4000 spectrometer and not to the switch on/off of the rotors. As an example, Figure 3.8 shows the radiometric stability evaluated at 628 nm. The HyUAV measurements show a correlation with corresponding ASD radiance data (physical units). The observed liner relationship (R-square 0.83) indicates the accuracy of the collected data. A small standard deviation

between replicated HyUAV measurements (error bars) is also shown in the graph. Similar results were observed for all the wavelengths.

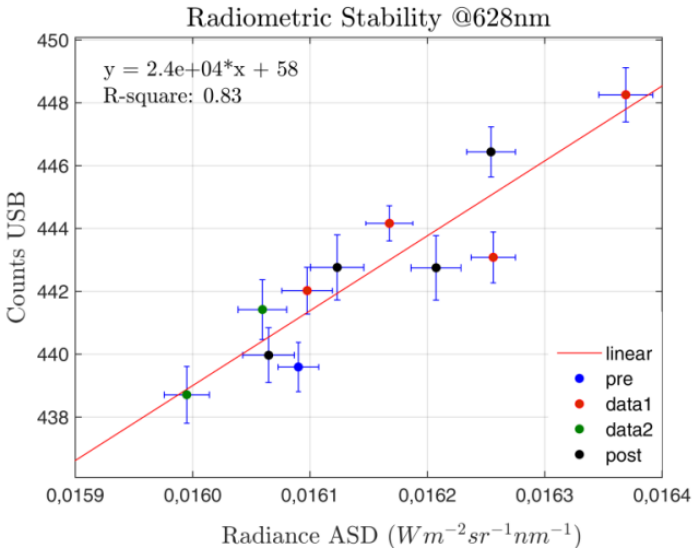

Figure 3.8: Scatterplot between USB4000 (raw digital counts) and FieldSpec HH spectrometers at 628 nm. Blue, red/green and black dots refer to measurements acquired before, during and after vibrations, respectively.

An example, spectral peaks emitted by the CAL-2000 Hg-Ar light source as detected by the HyUAV in presence/absence of vibrations are shown in Figure 3.9 (left). The absolute differences in wavelength position of the extracted peaks, calculated between stand and in-flight measurements, are depicted in Figure 3.9 (right). The maximum difference value observed is about ± 0.1 nm, at 404, 696 and 800 nm, and it can be considered negligible compared with the spectrometers FWHM. This result demonstrates the good spectral stability of the HyUAV, in fact spectral pikes estimation from in-flight measurements are not significantly affected by rotors platform vibrations. The laboratory tests performed on USB4000 spectrometer on-board on the HyUAV demonstrated good stability in terms of geometric, radiometric and spectral features of the systems. In particular, negligible effect of HyUAV platform vibrations are observed on the collected data.

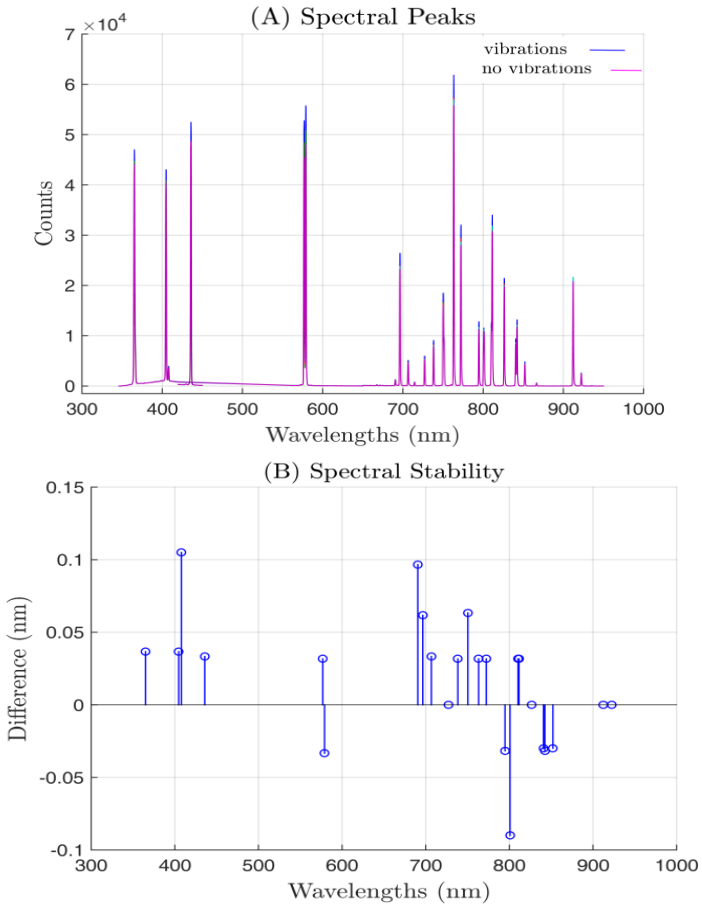

Figure 9: Spectral peaks of calibrated light source (CAL-2000 Hg-Ar) and spectral stability of HyUAV measurements.

3.4.2 Flight tests

The reliability of the data collected from HyUAV was tested through a field survey. The RGB images of the targets sampled from HyUAV (forest, corn, grassland, gravel, sand) are depicted in Figure 3.10 (the sampled area coincides with the center of the image). Reflectance signatures calculated for each sample (shown in the graph) describe the typical features of the different land covers types. Expected behaviours are present between the different targets: forest and corn have a similar signatures, grassland has an higher reflectance especially in the NIR domain and gravel show the lowest reflectance.

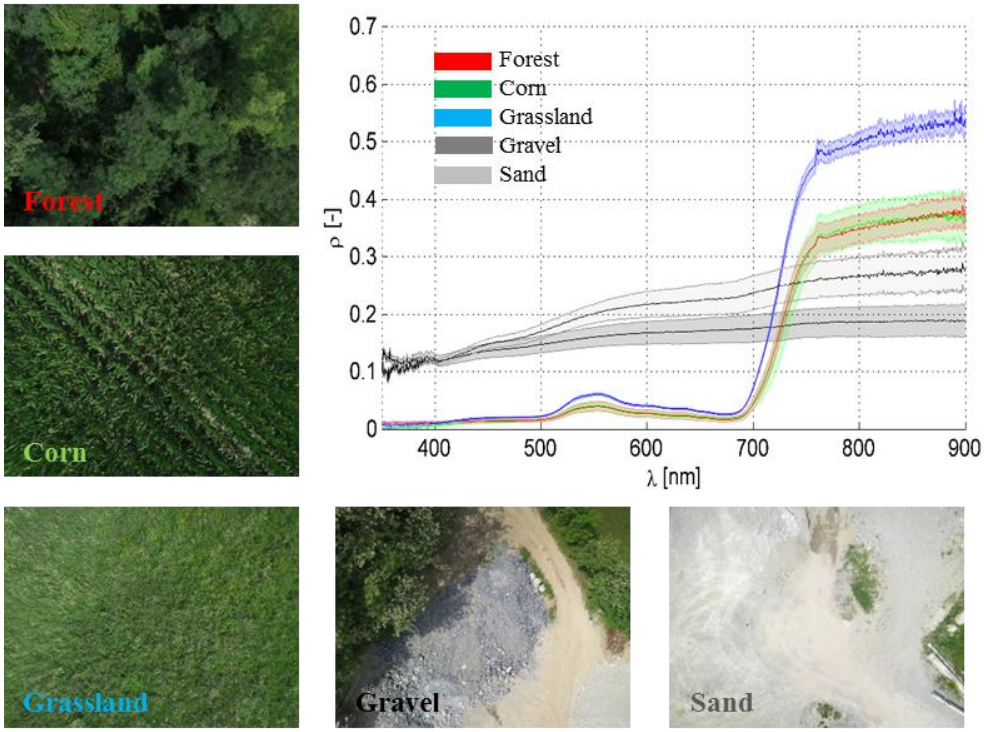

Figure 3.10: RGB images of sampled area collected simultaneously to spectral data. Graph of calculated spectral reflectance related to each sample.

The reflectance signature estimated from HyUAV were compared with those collected using the FieldSpec HH spectrometer, hereafter referred as ground-truth. The Figure 3.11 proves a good agreement between ground-truth (green line) and reflectance estimated from HyUAV considering both methods: HyUAV-tarp (blue line) and HyUAV-spec (red line). In particular spectral signatures (mean value and relative standard deviation) of measure collected from UAV are inside the variability of spectra collected by FieldSpec. The FieldSpec HH has a spectrometer footprint smaller than the HyUAV, so it is able to capture spatial variability at a small scale; this results in a greater standard deviation in the reflectance of the investigated targets (Figure 3.11). In any case, we show that, for all the spectral bands and for all targets, reflectance measured with the HyUAV exhibits a high correlation (R^2 = 0.98 for both methods) with those measured at the ground with the FieldSpec HH (Figure 3.12).

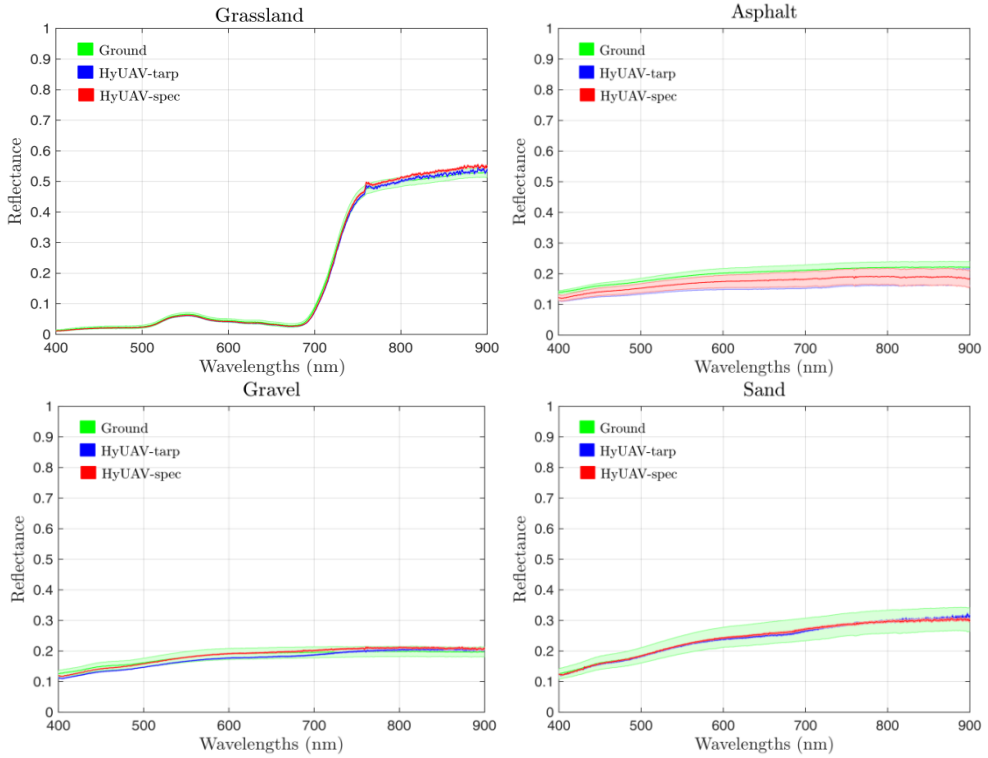

Figure 3.11: Comparison between reflectance measured from ground FielSpec HH spectrometer (green line) and from HyUAV using the two methods: HyUAV-tarp (blue line) and HyUAV-spec (red line).

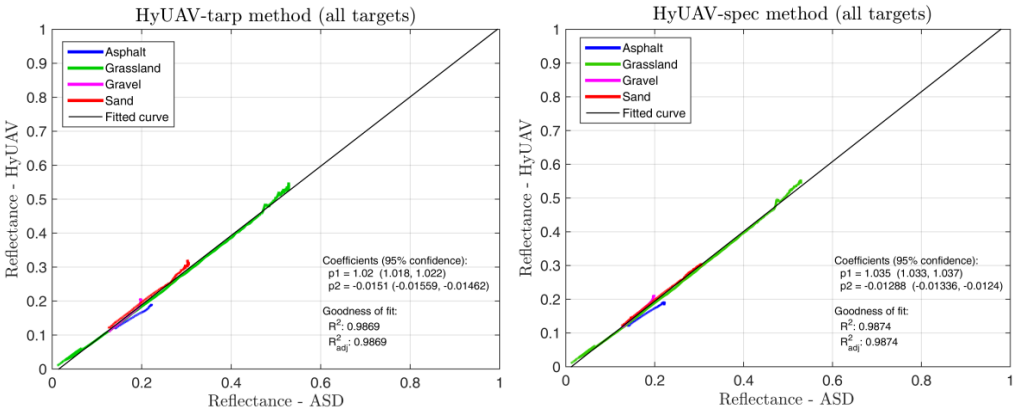

Figure 3.12: Scatter plot of reflectance measured from HyUAV and from FieldSpec for all targets and all spectral bands.

The RMSE and the RRMSE calculated are shown in Table 2. Considering all targets, RRMSE values are lower than 15% and 10% for radiance and reflectance, respectively. The HyUAV-spec method shows lower RMSE and RRMSE compared with HyUAV-spec

methods. In particular, RRMSE values are equal to 7.88% and 9.62%. These results indicate the good accuracy and reliability of HyUAV measurements for both radiance and reflectance. Similar results can be observed between HyUAV-tarp and HyUAV-spec methods, with slightly better results (expressed in term of RMSE, RRMSE) for the second one.

	Radiance		Reflectance			
	HyUAV		HyUAV-tarp		HyUAV-spec	
	RMSE	RRMSE%	RMSE	RRMSE%	RMSE	RRMSE%
Grassland	*0.0050*	*19.44*	*0.0065*	*7.99*	*0.0096*	*6.78*
Asphalt	*0.0018*	*6.46*	*0.0319*	*15.88*	*0.0273*	*13.50*
Gravel	*0.0011*	*4.13*	*0.0116*	*6.99*	*0.0079*	*4.29*
Sand	*0.0077*	*20.79*	*0.0052*	*2.29*	*0.0021*	*1.16*
All targets	*0.0047*	*14.74*	*0.0174*	*9.62*	*0.0150*	*7.88*

Table 2: RMSE and RRMSE% of radiance and reflectance (HyUAV-tarp and HyUAV-spec methods) calculated from comparison between HyUAV data and FieldSpec ground-truth for all the sampled targets.

Some differences can be delineated in the process to collect data and calculate reflectance between HyUAV-tarp and HyUAV-spec methods. In order to collect in-flight accurate incoming solar irradiance, the first method required a calibrated tarp, (larger than the spectrometers footprint, i.e. 6x6 m considering a footprint of 2 m), placed over a flat area near the targets of interests. In same conditions or in particular environments (mountains areas, glaciers, forest, urban areas etc.) this requirement is not easy to fulfil. Furthermore, the flight-path/mission-path are more complicated to define, because of the need to measure, with high frequency, the incoming solar irradiance on the tarp. Using the dual spectrometers approach (HyUAV-spec) a continuous measurements of solar irradiance variation is obtained using a calibrated Spectralon® panel. Instead, the HyUAV-spec methods require an inter-calibration between the two spectrometers, in particular the spectral sampling interval and FWHM have to been considered. The inter-calibration coefficients, estimated from simultaneous measurements of solar irradiance (Bachmann and others, 2012), depends on the atmosphere characteristics (i.e. spectral absorption, gasses, aerosol,

etc.) and the relative position of the sun. Daily variations (and seasonal differences) have to be considered to ensure an accurate inter-calibration with the need to simultaneously measurements of incoming solar irradiation before the flight.

The dedicated software packages developed allow the systematic import of data, calibration to spectral radiance, estimation of reflectance (both methods) and calculate spectral indices. The figure 3.13 shows the value of common vegetation indexes (NDVI, PRI, MTCI and EVI) for different vegetated (i.e. forest, corn, grass) and not-vegetated (asphalts) surfaces. The mean and dispersion values of this indices are in agreement to the different canopy characteristics while they are close to zero for the asphalt.

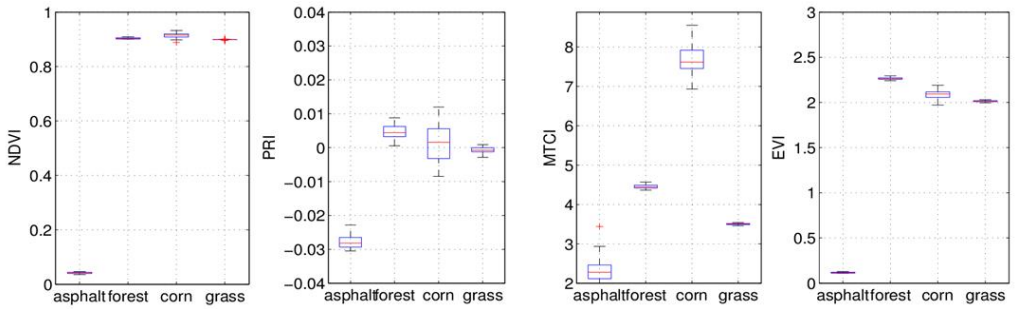

Figure 3.13: Calculated vegetation indices for the different surfaces.

A comparison between the way-points and the transect scheme can be delineated from the telemetry data. In particular, during transect acquisitions, higher pitch and roll variations cause off-nadir measurements. Figure 3.14 shows a maximum variation of roll/pitch of 8° during the transect (continuous) measurements; while, it is lower than 2° in way-points acquisition (during hovering). As an example, a pitch/roll equal to 5° causes a shift of 2 m from nadiral acquisition, considering a flight altitude of 20 m. The impact of the acquisition scheme (way point or transect) on spectral data must be considered in order to define the proper mission planning as a function of the environmental applications.

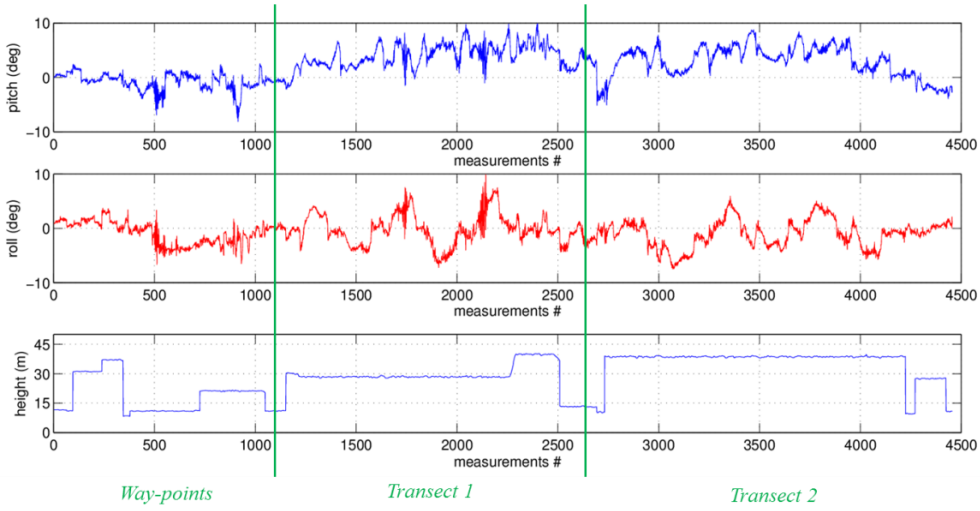

Figure 3.14: Telemetry data saved during the acquisition of spectra using way-points and transect scheme.

The RGB images collected were used to create an orthomosaic image, a textured 3D model (Figure 3.15) and a Digital Surface Model (DSM). Using the GPS data, the position of collected spectra (or calculated indices) can be easily imported in a GIS software and overlapped on RGB product and other cartographic georeferenced data.

Figure 3.15: Textured 3D model created with SFM algorithms (A) and orthomosaic of the test site with the location of the spectra collected with the HyUAV (B, points dimension reflect the estimated footprint of the spectrometer).

Figure 3.15A shows a detailed textured 3D model of the study area, created with the SFM algorithms. From this output, several morphometric parameters (such as, pit volume, tree heights and canopy structure, etc.) can be extracted. Figure 3.15B shows

the position of the spectra acquired during the flight test over the study area. The collected spectra are well positioned with respect to the investigated targets and allow the possibility to effectively analyse the optical features of small targets for environmental applications. To evaluate this aspect, we also compared the reflectance calculated from RGB data with that estimated with the USB4000 spectrometer, results are showed in Figure 3.16.

RGB images allow to observe overall characteristics of different land cover (e.g. greenness of vegetation) and to create 3D models from which surface structure can be extracted and used in environmental modelling. For studies that aim to describe specific characteristics of the surfaces (e.g. precision farming, stress detection, etc.), multi- or hyper-spectral systems are needed. In facts, many optical features of natural surfaces are located outside classical RGB wavelengths, and this represents a big advantage of using multi- and hyper-spectral systems.

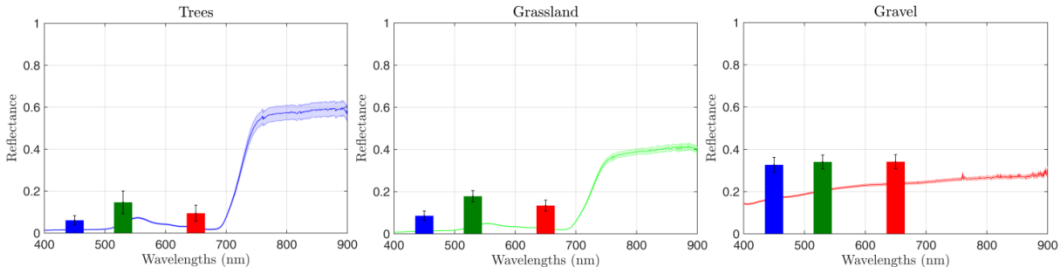

Figure 3.16: Comparison between reflectance calculated from single RGB channel and HyUAV spectrometer.

3.5 Conclusions

The HyUAV, a novel hyperspectral non-imaging UAV system, was developed and presented as a new tool for environmental monitoring. The HyUAV was based on a four-rotors UAV and was developed providing systematic collection of RGB images coupled with VIS-NIR hyperspectral data. We first evaluate the geometric, radiometric and spectral stability of the systems, through laboratory tests, then we flew over a small pit and we tested the accuracy of HyUAV spectra compared with ground-truth data collected with a FieldSpec HH spectrometer. A dedicated software packages was

developed for: i) mission planning; ii) data collection; iii) processing and geolocation of hyperspectral data and RGB images. The possibility to integrate hyperspectral data and RGB product is also considered. Two method for retrieving reflectance from HyUAV were proposed and discussed.

The results from the laboratory tests on USB4000 demonstrate that the typical platform vibrations do not significantly affect the geometric (FOV dimension and position of its center in the RBG image), radiometric and spectral quality of collected hyperspectral data. The flight tests showed a good agreement between HyUAV and FieldSpec HH spectral measurements for all the sampled land cover types. In particular, both the method to calculate reflectance showed a good accuracy with reflectance estimated from FieldSpec spectrometer (RRMSE% < 10). Different spectral indices (i.e. NDVI, EVI, MTCI, PRI) were calculated and they are in agreement with the canopy characteristics. Reflectance collected from hyperspectral HyUAV, allows to investigate spectral features in the VNIR domain suitable to describe specific characteristics of the surfaces. Created 3D textured model and orthomosaic image are promising results that can be further investigated to gain useful information on surface properties and volume (e.g. canopy structure model for vegetation studies).

The HyUAV demonstrated to be a promising platform for supporting field spectroscopy surveys. With the possibility to integrate hyperspectral data (in the VIS-NIR spectrum) to RGB product (orthomosaic, 3D model, DTM) it can be considered an advance in remote sensing, filling the gap in current instrument capabilities. HyUAV is able to provide relevant environmental data (i.e. radiance/reflectance, spectral indices and RGB products) at very detailed spatial and temporal resolutions with a valuable potential for a wide range of monitoring activities and environmental applications. Future applications of this platform can be regard: precision farming, species mapping in forest, phenological modelling, vegetation stress (e.g. fluorescence estimation), snow albedo monitoring, inland waters quality (i.e. turbidity), asbestos roof mapping, landslide movements and estimation of mass volume.

Acknowledgments:

The research was supported by the SINOPIAE project funded by the Regione Lombardia. A final version of this chapter will be submitted to *IEEE Transactions on Geoscience and Remote Sensing*.

I wish to thank the Aermatica S.P.A. for collaboration and the team of the Geomatic Laboratory (University of Milano-Bicocca) and M. Celesti for their support in the field campaign.

Bibliography

Aasen H, Burkart A, Bolten A and Bareth G (2015) Generating 3D hyperspectral information with lightweight UAV snapshot cameras for vegetation monitoring: From camera calibration to quality assurance. ISPRS J. Photogramm. Remote Sens. 108, 245–259 (doi:10.1016/j.isprsjprs.2015.08.002)

Van Andel AC, Wich S a., Boesch C, Koh LP, Robbins MM, Kelly J and Kuehl HS (2015) Locating chimpanzee nests and identifying fruiting trees with an unmanned aerial vehicle. Am. J. Primatol. (June), n/a–n/a (doi:10.1002/ajp.22446)

Anderson K and Gaston KJ (2013) Lightweight unmanned aerial vehicles will revolutionize spatial ecology. Front. Ecol. Environ. 11(3), 138–146 (doi:10.1890/120150)

Bachmann CM, Montes MJ, Parrish CE, Fusina R a, Nichols CR, Li R-R, Hallenborg E, Jones C a, Lee K, Sellars J, White S a and Fry JC (2012) A dual-spectrometer approach to reflectance measurements under sub-optimal sky conditions. Opt. Express 20(8), 8959–73 (doi:10.1364/OE.20.008959)

Bareth G, Aasen H, Bendig J, Gnyp ML, Bolten A, Jung A, Michels R and Soukkamäki J (2015) Low-weight and UAV-based Hyperspectral Full-frame Cameras for Monitoring Crops: Spectral Comparison with Portable Spectroradiometer Measurements. Photogramm. - Fernerkundung - Geoinf. 2015(1), 69–79 (doi:10.1127/pfg/2015/0256)

Von Bueren SK, Burkart a., Hueni a., Rascher U, Tuohy MP and Yule IJ (2015) Deploying four optical UAV-based sensors over grassland: challenges and limitations. Biogeosciences 12(1), 163–175 (doi:10.5194/bg-12-163-2015)

Burkart A, Cogliati S, Schickling A and Rascher U (2014) A Novel UAV-Based Ultra-Light Weight Spectrometer for Field Spectroscopy. IEEE Sens. J. 14(1), 62–67 (doi:10.1109/JSEN.2013.2279720)

Candiago S, Remondino F, De Giglio M, Dubbini M and Gattelli M (2015) Evaluating Multispectral Images and Vegetation Indices for Precision Farming Applications from UAV Images. Remote Sens. 7(4), 4026–4047 (doi:10.3390/rs70404026)

Cilia C, Panigada C, Rossini M, Candiani G, Pepe M and Colombo R (2015) Mapping of Asbestos Cement Roofs and Their Weathering Status Using Hyperspectral Aerial Images. ISPRS Int. J. Geo-Information 4(2), 928–941 (doi:10.3390/ijgi4020928)

Clevers J and Kooistra L (2012) Using Hyperspectral Remote Sensing Data for Retrieving Canopy Chlorophyll and Nitrogen Content. Ieee J. Sel. Top. Appl. Earth Obs. Remote Sens. 5(2), 574–583 (doi:10.1109/JSTARS.2011.2176468)

Cogliati S, Rossini M, Julitta T, Meroni M, Schickling a., Burkart a., Pinto F, Rascher U and Colombo R (2015) Continuous and long-term measurements of reflectance and sun-induced chlorophyll fluorescence by using novel automated field spectroscopy systems. Remote Sens. Environ. 164, 270–281 (doi:10.1016/j.rse.2015.03.027)

Colomina I and Molina P (2014) Unmanned aerial systems for photogrammetry and remote sensing: A review. ISPRS J. Photogramm. Remote Sens. 92, 79–97 (doi:10.1016/j.isprsjprs.2014.02.013)

Dall'Asta E, Delaloye R, Diotri F, Forlani G, Fornari M, Morra di Cella U, Pogliotti P, Roncella R and Santise M (2015) Use of Uas in a High Mountain Landscape: the Case of Gran Sommetta Rock Glacier (Ao). ISPRS - Int. Arch. Photogramm. Remote Sens. Spat. Inf. Sci. XL-3/W3, 391–397 (doi:10.5194/isprsarchives-XL-3-W3-391-2015)

Damm A, Guanter L, Paul-Limoges E, van der Tol C, Hueni A, Buchmann N, Eugster W, Ammann C and Schaepman ME (2015) Far-red sun-induced chlorophyll fluorescence shows ecosystem-specific relationships to gross primary production: An assessment based on observational and modeling approaches. Remote Sens. Environ. 166, 91–105 (doi:10.1016/j.rse.2015.06.004)

Deery D, Jimenez-Berni J, Jones H, Sirault X and Furbank R (2014) Proximal Remote Sensing Buggies and Potential Applications for Field-Based Phenotyping. (doi:10.3390/agronomy4030349)

Di Mauro B, Fava F, Ferrero L, Garzonio R, Baccolo G, Delmonte B and Colombo R (2015) Mineral dust impact on snow radiative properties in the European Alps combining ground, UAV and satellite observations. J. Geophys. Res. Atmos., n/a–n/a (doi:10.1002/2015JD023287)

Fugazza D, Senese A, Azzoni RS, Smiraglia C, Cernuschi M, Severi D and Diolaiuti GA (2015) High resolution mapping of glacier surface features . The UAV survey of the Forni Glacier (Stelvio National Park , Italy). Geogr. Fis. e Din. Quat. 38(AUGUST), 25–33 (doi:10.4461/GFDQ.2015.38.03)

Getzin S, Wiegand K and Schöning I (2012) Assessing biodiversity in forests using very high-resolution images and unmanned aerial vehicles. Methods Ecol. Evol. 3(2), 397–404 (doi:10.1111/j.2041-210X.2011.00158.x)

Gitelson AA, Gritz Y and Merzlyak MN (2003) Relationships between leaf chlorophyll content and spectral reflectance and algorithms for non-destructive chlorophyll assessment in higher plant leaves. J. Plant Physiol. 160(3), 271–282 (doi:10.1078/0176-1617-00887)

Guanter L, Rossini M, Colombo R, Meroni M, Frankenberg C, Lee JE and Joiner J (2013) Using field spectroscopy to assess the potential of statistical approaches for the retrieval of sun-induced chlorophyll fluorescence from ground and space. Remote Sens. Environ. 133(September), 52–61 (doi:10.1016/j.rse.2013.01.017)

Hestir EL, Brando VE, Bresciani M, Giardino C, Matta E, Villa P and Dekker AG (2015) Measuring freshwater aquatic ecosystems: The need for a hyperspectral global mapping satellite mission. Remote Sens. Environ. 167, 181–195 (doi:10.1016/j.rse.2015.05.023)

Immerzeel WW, Kraaijenbrink PDA, Shea JM, Shrestha AB, Pellicciotti F, Bierkens MFP and de Jong SM (2014) High-resolution monitoring of Himalayan glacier dynamics using unmanned aerial vehicles. Remote Sens. Environ. 150, 93–103 (doi:10.1016/j.rse.2014.04.025)

Kudela RM, Palacios SL, Austerberry DC, Accorsi EK, Guild LS and Torres-Perez J (2015) Application of hyperspectral remote sensing to cyanobacterial blooms in inland waters. Remote Sens. Environ. 167, 196–205 (doi:10.1016/j.rse.2015.01.025)

Laliberte AS, Goforth M a., Steele CM and Rango A (2011) Multispectral remote sensing from unmanned aircraft: Image processing workflows and applications for rangeland environments. Remote Sens. 3(11), 2529–2551 (doi:10.3390/rs3112529)

Link J, Senner D and Claupein W (2013) Developing and evaluating an aerial sensor platform (ASP) to collect multispectral data for deriving management decisions in precision farming. Comput. Electron. Agric. 94, 20–28 (doi:10.1016/j.compag.2013.03.003)

Lucieer A, Malenovský Z, Veness T and Wallace L (2014) HyperUAS-Imaging Spectroscopy from a Multirotor Unmanned Aircraft System. J. F. Robot. 31(4), 571–590 (doi:10.1002/rob.21508)

Lucieer A, Turner D, King DH and Robinson S a. (2014) Using an unmanned aerial vehicle (UAV) to capture micro-topography of antarctic moss beds. Int. J. Appl. Earth Obs. Geoinf. 27(PARTA), 53–62 (doi:10.1016/j.jag.2013.05.011)

Ma L, Li M, Tong L, Wang Y and Cheng L (2013) Using unmanned aerial vehicle for remote sensing application. 2013 21st International Conference on Geoinformatics. IEEE, 1–5 (doi:10.1109/Geoinformatics.2013.6626078)

Masek JG, Hayes DJ, Joseph Hughes M, Healey SP and Turner DP (2015) The role of remote sensing in process-scaling studies of managed forest ecosystems. For. Ecol. Manage. (doi:10.1016/j.foreco.2015.05.032)

Meroni M, Rossini M, Picchi V, Panigada C, Cogliati S, Nali C and Colombo R (2008) Assessing Steady-state Fluorescence and PRI from Hyperspectral Proximal Sensing as Early Indicators of Plant Stress: The Case of Ozone Exposure. Sensors 8(3), 1740–1754 (doi:10.3390/s8031740)

Milton EJ (1987) Review Article Principles of field spectroscopy. Int. J. Remote Sens. 8(12), 1807–1827 (doi:10.1080/01431168708954818)

Milton EJ, Schaepman ME, Anderson K, Kneubühler M and Fox N (2009) Progress in field spectroscopy. Remote Sens. Environ. 113, S92–S109 (doi:10.1109/IGARSS.2006.509)

Morisette JT, Privette JL and Justice CO (2002) A framework for the validation of MODIS Land products. Remote Sens. Environ. 83(1-2), 77–96 (doi:10.1016/S0034-4257(02)00088-3)

Niethammer U, James MR, Rothmund S, Travelletti J and Joswig M (2012) UAV-based remote sensing of the Super-Sauze landslide: Evaluation and results. Eng. Geol. 128, 2–11 (doi:10.1016/j.enggeo.2011.03.012)

Olmanson LG, Brezonik PL and Bauer ME (2013) Airborne hyperspectral remote sensing to assess spatial distribution of water quality characteristics in large rivers: The Mississippi River and its tributaries in Minnesota. Remote Sens. Environ. 130, 254–265 (doi:10.1016/j.rse.2012.11.023)

Panigada C, Rossini M, Meroni M, Cilia C, Busetto L, Amaducci S, Boschetti M, Cogliati S, Picchi V, Pinto F, Marchesi a. and Colombo R (2014) Fluorescence, PRI and canopy temperature

for water stress detection in cereal crops. Int. J. Appl. Earth Obs. Geoinf. 30(1), 167–178 (doi:10.1016/j.jag.2014.02.002)

Rossini M, Meroni M, Migliavacca M, Manca G, Cogliati S, Busetto L, Picchi V, Cescatti A, Seufert G and Colombo R (2010) High resolution field spectroscopy measurements for estimating gross ecosystem production in a rice field. Agric. For. Meteorol. 150(9), 1283–1296 (doi:10.1016/j.agrformet.2010.05.011)

Rossini M, Nedbal L, Guanter L, Ač A, Alonso L, Burkart A, Cogliati S, Colombo R, Damm A, Drusch M, Hanus J, Janoutova R, Julitta T, Kokkalis P, Moreno J, Novotny J, Panigada C, Pinto F, Schickling A, Schüttemeyer D, Zemek F and Rascher U (2015) Red and far red Sun-induced chlorophyll fluorescence as a measure of plant photosynthesis. Geophys. Res. Lett. 42, 1632–1639 (doi:10.1002/2014GL062943)

Rossini M, Panigada C, Cilia C, Meroni M, Busetto L, Cogliati S, Amaducci S and Colombo R (2015) Discriminating Irrigated and Rainfed Maize with Diurnal Fluorescence and Canopy Temperature Airborne Maps. ISPRS Int. J. Geo-Information 4(2), 626–646 (doi:10.3390/ijgi4020626)

Salamí E, Barrado C and Pastor E (2014) UAV flight experiments on the remote sensing of vegetation areas. Remote Sens. 6, 11051–11081 (doi:10.3390/rs61111051)

Schaepman ME, Ustin SL, Plaza AJ, Painter TH, Verrelst J and Liang S (2009) Earth system science related imaging spectroscopy-An assessment. Remote Sens. Environ. 113(SUPPL. 1), S123–S137 (doi:10.1016/j.rse.2009.03.001)

Turner D, Lucieer A and de Jong S (2015) Time Series Analysis of Landslide Dynamics Using an Unmanned Aerial Vehicle (UAV). Remote Sens. 7(2), 1736–1757 (doi:10.3390/rs70201736)

Turner D, Lucieer A and Wallace L (2014) Direct georeferencing of ultrahigh-resolution UAV imagery. IEEE Trans. Geosci. Remote Sens. 52(5), 2738–2745 (doi:10.1109/TGRS.2013.2265295)

Uto K, Seki H, Saito G and Kosugi Y (2013) Characterization of rice paddies by a UAV-mounted miniature hyperspectral sensor system. IEEE J. Sel. Top. Appl. Earth Obs. Remote Sens. 6(2), 851–860 (doi:10.1109/JSTARS.2013.2250921)

Westoby MJ, Brasington J, Glasser NF, Hambrey MJ and Reynolds JM (2012) 'Structure-from-Motion' photogrammetry: A low-cost, effective tool for geoscience applications. Geomorphology 179, 300–314 (doi:10.1016/j.geomorph.2012.08.021)

Whitehead K, Moorman BJ and Hugenholtz CH (2013) Brief Communication: Low-cost, on-demand aerial photogrammetry for glaciological measurement. Cryosphere 7(6), 1879–1884 (doi:10.5194/tc-7-1879-2013)

Zarco-Tejada PJ, Diaz-Varela R, Angileri V and Loudjani P (2014) Tree height quantification using very high resolution imagery acquired from an unmanned aerial vehicle (UAV) and automatic 3D photo-reconstruction methods. Eur. J. Agron. 55, 89–99 (doi:10.1016/j.eja.2014.01.004)

Zarco-Tejada PJ, González-Dugo V and Berni J a J (2012) Fluorescence, temperature and narrow-band indices acquired from a UAV platform for water stress detection using a micro-hyperspectral imager and a thermal camera. Remote Sens. Environ. 117, 322–337 (doi:10.1016/j.rse.2011.10.007)

Zhang C and Kovacs JM (2012) The application of small unmanned aerial systems for precision agriculture: A review. Precis. Agric. 13(6), 693–712 (doi:10.1007/s11119-012-9274-5)

4. A NEW HYPERSPECTRAL SYSTEM FOR ICE CORE IMAGING

Abstract

Paleoclimatic information recorded in polar and mountain glaciers are fundamental to study climate and environmental changes. New advanced techniques can be developed to improve the accuracy of ice core measurements. In this context, we developed a new system based on hyperspectral imaging to collect data from ice cores. The system is composed by a high-precision linear stage which embeds an imaging hyperspectral sensor and a dedicated halogen light source. It is designed to scan a whole ice core collecting high resolution hyperspectral data. Several tests were performed on the camera and on the components of the system. Then, hyperspectral image of an ice core was collected and analysed. The Snow Darkening Index (SDI) was calculated observing its spatial relation with impurity layers. The research provided important results in the development of a new system. Applied to ice cores, hyperspectral imaging can be considered an innovative technique, powerful to analyse past atmospheric depositions.

4.1 Introduction

Ice cores provide paleoclimate records essential to study climate change. Polar ice sheets (i.e. Greenland or Antarctica), as well as non-polar high mountain glaciers, preserve in each ice layer differences in chemical and physical properties of the atmosphere, and ice structure related to past environmental and climatic conditions. The most important information collected from ice cores comprehends: local air temperature and precipitation rate; origin of the precipitation; regional atmospheric

circulation and dust transportation; chemical composition of the atmosphere including greenhouse gas concentrations; volcanic and solar activity.

A variety of chemical and physical measurements are traditionally performed on ice core samples. Common ice core measurements of stable isotopic are used as paleo-temperature indicator; greenhouse and trace gasses trapped in air bubbles (such as carbon dioxide, methane, nitrous oxide, etc.) are extracted in order to study past climate variability; mineral dust, elemental black carbon and tephra from volcanic eruption are investigated from ice core stratigraphy (Petit and others, 1999; Alley, 2000; Brook, 2007; Jouzel and Masson-Delmotte, 2010). This information allows scientists to reconstruct past climate at very high time-resolution, on time scales of thousands of millennia to the last few decades. Particularly, long time series were provided by large polar ice sheets (especially Antarctica where precipitation rate are very low); whereas, detailed seasonal records collected from mountain glaciers are informative regarding to climate and environmental variability.

Visual stratigraphy is the oldest technique in ice core studies (Alley and others, 1997). High-resolution profiles can be obtained since the development of digital scanners for optical imaging of ice cores (Ortiz and others, 1999; Takata and others, 2004; Svensson and others, 2005; Kipfstuhl and others, 2006; Sjögren and others, 2007; Kinnard and others, 2008; McGwire, Hargreaves, and others, 2008; McGwire, Mcconnell, and others, 2008). In particular, an end-to-end system for imaging ice cores, was developed at the United States National Ice Core Laboratory (NICL) (McGwire, Hargreaves, and others, 2008). This system is based on a RGB line-scan camera that collects images of brightness across the ice core. Svensson and others, 2005, fund relations between mineral dust concentrations and brightness on NorthGRIP ice core.

Visual stratigraphy techniques were used to analyse various stratigraphic information such as: identification of annual layers, that provide useful interpretation of chronology (essential to compare ice core from different locations); layers thickness as estimation of snowfall variations and past precipitation rates; distribution of summer melt layers

associated with warmer summer temperature; location of chemical impurities (mineral dust, volcanic ash, Ca^{2+} ion concentrations); physical properties such as size and the orientation of ice crystals (related to ice flow and glacier dynamics), distribution of bubbles and density profile. Visual stratigraphy is fundamentally based on RGB images of transmitted light intensity. This technique provides a detection of stratigraphic features with high spatial resolution that and can be improved developing tools based on imaging spectroscopy camera (Svensson and others, 2005; McGwire, Mcconnell, and others, 2008).

Imaging spectroscopy is a powerful technique used to characterised surfaces properties. Images are collected in hundreds of wavelengths simultaneously, permitting spectral analysis of each discrete pixel (Goetz and others, 1985). Distinct materials reflect and absorb light differently as a function of wavelength, creating unique spectra that are used to identify and map compositional units remotely. Hyperspectral imaging, traditionally used for airborne remote sensing, is now becoming a valuable tool for in-line inspection and quality control (Bannon, 2009). The development of miniaturized hyperspectral imaging cameras (e.g. produced by Headwall Photonics or SPECIM) improves the possibility to developed novel systems with exiting potential for several scientific disciplines such as geology, vegetation and crops monitoring, chemometrics and food quality, etc. (Kim and others, 2001; Bannon, 2009; Lucieer and others, 2014; Bareth and others, 2015; Greenberger and others, 2015; He and Sun, 2015). The characterisations of material composition with very high spectral and spatial resolution (sub- centimetre pixel size) provide a unique possibility to analyse optical surface properties.

Applied to ice cores analysis hyperspectral imaging can be considered an innovative technique. In this context, the object of this research is the development of a fully automated Hyperspectral system for Imaging Ice core (HYCE) in a cold room environment to inspect the potential of hyperspectral imaging for quantitatively estimate past atmospheric deposition of light-absorbing impurities (such as mineral dust, volcanic ash and black carbon).

4.2 The HYCE system

4.2.1 Architecture of the system

The HYCE system (Figure 4.1) is composed by a high-precision linear stage, which embeds an imaging hyperspectral sensor and a dedicated halogen light source. The sensor is the HeadWall Photonics VINR imaging spectrometer, that is able to collect spectral radiance (in 810 spectral bands, range from 380 to 1000 nm, with 2-3 nm of spectral resolution of Full Width at Half Maximum, FWHM) along 1004 spatial pixels (24 deg. of field of view). The ice core is lighted with a halogen stable light source (600 or 1000 W, LOT Quantum Design). The lamp produces a uniform collimated output beam (with 50 mm diameter) that provides an homogenous stable illumination of the sampled area. The camera and the lamp are mounted on a custom-designed linear stage (1.5 m length, moved by a steeper motors), designed to work in a cold room laboratory (i.e. -20°C). A case was realised to hold the camera maintaining it at fixed temperature (i.e. 10°C), to preserve functionality and ensuring the optimal collection of hyperspectral data. The system is designed to ensure the optimal high-resolution hyperspectral imaging of the whole ice core, preventing changes in chemical and physical properties (e.g. ice grain metamorphism).

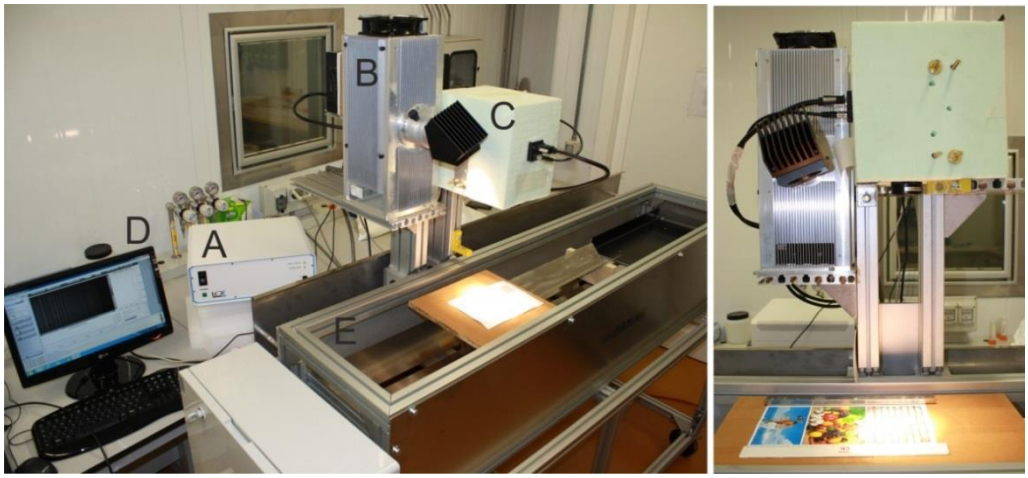

Figure 4.1: The HYCE system. A) Power supply; B) Halogen lamp; C) Headwall camera; D) PC; E) Sample holder.

The camera mounts two different lenses: the Schneider Xenoplan F/1.4, 17 mm allows a maximum resolution of ~90 µm of pixel size (Figure 4.2A) ; instead the CoastalOpt UV-VIS-IR Apo Macro lens (F/4, 60 mm) provides an high-macro hyperspectral images with ~25 µm of pixel size (Figure 4.2B) (both the pixels size are calculated considering 20 cm the distance from the sample). Although standard lens is optimal to analyse ice ore stratigraphy (compared with common geophysics methods), grain features and single layers structure could be investigated with the macro lens. Results presented in this paper were obtained only with the Schneider Xenoplan lens.

Figure 4.2: Lens. Standard Schneider Xenoplan 17 mm (A) and the CoastalOpt UV-VIS-IR Macro 60 mm (B).

The architecture of the system was designed to integrate all these components (Figure 4.3). A dedicated PC is connected to the Headwall sensor and it based on high speed frame grabber that provides the collection of a large amount of data in high speed velocity. The Single-Board RIO (sbRIO, National Instrument) is used to monitor and adjust the temperature of the camera, and to interface stepper drivers with the PC. All the components are linked by an Ethernet TCP/IP connection. A dedicated software was developed to command the acquisition of spectral measurement synchronising the motion of the camera. This configuration of the system is suitable for future development and for the integration with other sensors and software routines.

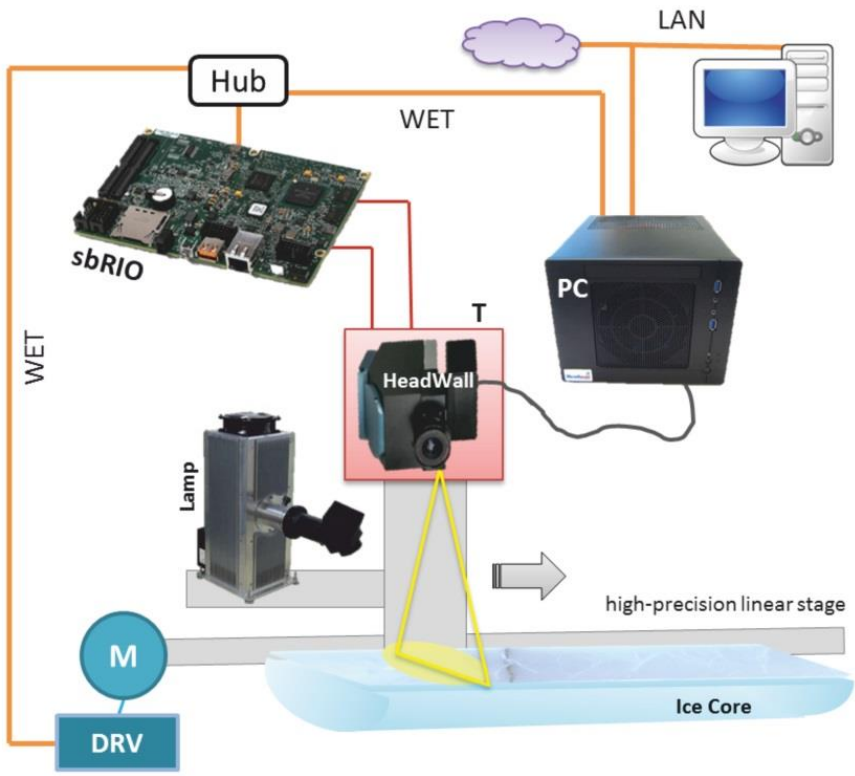

Figure 4.3: Architecture of the HYCE system.

4.2.2 Hyperspectral measurement

Hyperspectral data allows the investigation of the visible-infrared spectrum identifying individual features that provide information related to surface materials. Different authors investigated spectral features of snow and ice collecting data with hyperspectral sensors during laboratory experiments, field surveys, or using satellite sensors (Wiscombe and Warren, 1980; Warren, 1982; Nolin and Dozier, 2000; Casacchia and others, 2001, 2002; Nakamura and others, 2001; Dozier and Painter, 2004; Lei and others, 2012; Di Mauro and others, 2015; Negi and others, 2015). The study of spectral properties of snow and ice is generally based on the analysis of the reflectance. Reflectance is defined as the ratio between the radiation reflected by the surface and the incident radiation, common measured using a calibrated Lambertian Spectralon panel. The spectral reflectance in the VNIR domain decreases with the

increasing of the grains size, when the snow is metamorphosed to granular snow. Different degrees of metamorphism and density profiles can be distinguished from hyperspectral data. The high reflectance of snow in the visible domain is particularly affected by the presence of impurities and other contaminants, such as: mineral dust, tephra volcanic eruption, nuclear fallout, anthropogenic particulate matter (black carbon or elemental carbon), vegetation traces, pollens and other organic matters. These impurities absorb radiation in specific wavelengths ranges producing specific spectral features. The potential of hyperspectral imaging can be used to estimate impurities concentration in ice core samples with high spectral resolution. In addition, HYCE collects high resolution images of morphological features and microstructure details that can be used to investigate annual layers thickness, density, grains, discontinuity and air bubbles.

Hyperspectral imaging can be considered a non-destructive technique. It can produce highly resolved analysis, if compared with traditional geophysical methods. It provides valuable information for climate studies that can be integrated in the traditional ice core analysis.

4.2.3 Data collection

The system is designed to collect hyperspectral images of reflected radiance. The ice core is illuminates directly and uniformly by the stable halogen lamp. Both the distance between the camera and the lamp from the sample, can be set up manually in order to modify the spatial resolution of the camera (pixel size) and the area lighted by the lamp. The exposure time of the sensor can be set to collect optimal hyperspectral data over different surfaces, using different light intensity (600/1000 W lamp). The system is designed to scan a core section that have a half-round shape with just one side cut. In order to collect optimal hyperspectral data, the ice surface should be as smooth as possible. Discontinuity and roughness, in fact, produce differences in the light reflection and scattering phenomena.

To calculate spectral reflectance the incident radiation of the lamp is measured using a calibrated Lambertian Spectralon panel before sample measurements. The reflectance measured can be considered mainly due to the reflection of the surface and secondary as the contribution of the light scattering in the core section. Motion speed and camera frame period are automatically synchronised with the exposure time by developed software. The system can be operated manually collecting images of a portion of the ice core, or in an automatic way collecting systematic images of the whole ice core.

4.3 Material and methods

4.3.1 Laboratory characterisation and calibration

Dedicate laboratory tests were performed to calibrate the camera and define the best configuration of the system. In particular, tests were finalised to evaluate the performances of the lamp, to verify the collection of very high-resolution hyperspectral images (synchronising frame periods and motor speeds) and to collect good quality ice core hyperspectral data in cold room environment.

Lamp test

The lamp test was performed to measure the intensity of the 600/1000 W lamps (Figure 4.4). Variation in the light intensity during the measurements affect the accuracy of the hyperspectral data. Therefore, the spatial and temporal uniformity of the lamp was evaluated with the test. The performances of the lamps are also tested in a cold laboratory. An ice core was lighted during the experiment and the ice melting was evaluated in order to ensure the complete preservation of the ice core stratigraphy.

Figure 4.4: Set-up of the lamp tests. The images below show the sample of ice core lighted by the lamp.

The camera collect the light beam reflected by a calibrated Lambertian Spectralon panel. The lamp was adjusted to produce a collimated light beam that illuminate uniformly the surface. The distance between the camera and the lamp from the panel was ~30 cm. To reproduce the configuration of the system, the panel was lighted with an angle of ~20 deg. and the spectra were collected at nadir (i.e. viewing zenith angle at 0°). The intensity of the lamps was calculated in term of radiance. The spatial uniformity of the sensor was evaluated considering the data collect by the 1004 pixels, while the temporal stability was assessed during an hour of experiment measuring intensity every 10 minutes. Then, the performances of the lamp were tests in cold room environment (air temperature was -18°C). An ice core sample was lighted using the 600 W lamp (and after with the 1000 W) from a distance of about 30 cm.

HeadWall test

In the first experiment, hyperspectral data were collected over vegetation and soil samples, to evaluate the spectral signature on traditional surfaces. Three different samples were analysed: a young magnolia leaf, an old magnolia leaf and a dark soil sample. Setup of the experiment reflect the setting used in the lamp test. Reflectance was calculated and compared among different surfaces. For the young magnolia spectra, the Normalized Difference Vegetation Index (NDVI) was also calculated.

A test was also performed to confirm the possibility to measure reflectance from ice core. The camera and the lamp were brought in cold room laboratory (- 20 °C). A test bed was realised according the designed system (i.e. distance, light intensity, angles) (Figure 4.5) and a single-line hyperspectral data were collected from firn and ice core (the camera is fixed and scans a line placed within the red box in the Figure 4.5). Lamp radiance was collected using a calibrated Spectralon panel before and after ice core measurements. The reflectance was calculated and analysed to investigate spectral features of firn and ice.

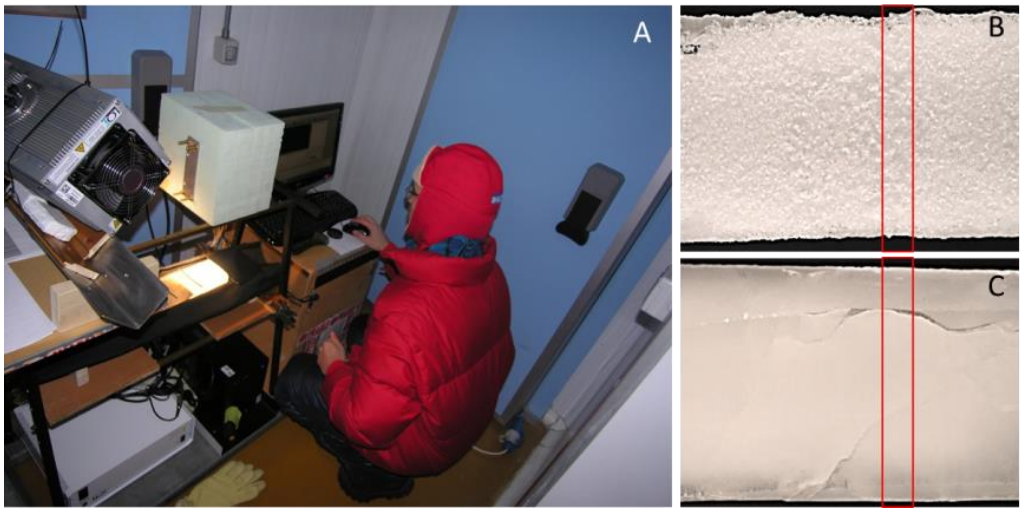

Figure 4.5: Collection of hyperspectral ice core data in cold room laboratory (A). Sampled firn core (B) and ice core (C) with the indication of the area where the measure were collected (red box).

Collection of high-resolution images

The system was tested in order to analyse the capability to reconstruct high-resolution images. The collection of spectra (exposure time and fame period) were synchronised with the stepper motor velocity that determine the movement of the sample under the sensor. Different test images were scanned in laboratory producing hyperspectral images. The first is a RGB figure that represents geometric shapes such as square and circles; the second is a RGB image with different texture and colours. The camera collected spectra with a velocity of 40 frame/ms and with a spatial resolution of about 160 µm. Consequently, the speed of the motors was set to 24 cm/min, synchronizing the motion of the camera and the spectral measurements. Collected hyperspectral images were visually analysed in order to evaluate their geometrical accuracy.

4.3.2 Hyperspectral imaging

Hyperspectral imaging of different targets were performed to evaluate the quality of the collected spectra. The frame rate and the motor velocity was setting as described in the previous paragraph. First, an image of leaves and coins were captured. Then, the system was carried in the cold room laboratory and an hyperspectral image of an ice core was collected. The reflectance was calculated for both the images, measuring incident radiation using a calibrated Lambertian Spectralon panel before the scan.

The ice sample was the ice core extracted from the Mt. Canin ice cave. Ice caves are found in areas without permafrost regime (i.e. at altitudinal al latitudinal ranges with an annual air temperature above 0 C) (Obleitner and Spötl, 2011). The Canin massif (2.587 m., Julian Alps) is located in the Eastern Alps (46°21’ N, 13°26’ E) along the borderline between Italy and Slovenia. The higher peaks reach altitudes slightly higher than 2500 m. On the northern slope few small glaciers still persist. The area of Canin massif hosts a large number of karst cavities and an intense speleological research activity developed since several decades. Climatic conditions are peculiar in the area, especially with regard to the precipitation. The Mean Annual Precipitation reaches

values up to 3300 mm representing one of the highest mean values for the European Alps (Colucci and others). Several layers of impurities and difference in ice layers density can be observed in the ice core (Figure 4.6). The test aims to map these features using from reflectance data.

Figure 4.6: RGB image of the Ice core collected from Mount Canin ice cave.

A novel spectral index, the Snow Darkening Index (SDI) proposed by Di Mauro and others, 2015 was calculated on ice core image. This index combines different wavelengths showing non-linear correlation with mineral dust concentrations. It is formalized as follows:

$$SDI = \frac{\rho(640; 670nm) - \rho(550; 590nm)}{\rho(640; 670nm) + \rho(550; 590nm)}$$

Values higher than zero indicate impurity layers and the values increase with dust concentration. An image of SDI was created in order to map the impurities on Canin ice core.

4.4 Results and discussion

4.4.1 Lamp test

The Figure 4.7 shows the intensity of the 600 W lamp (blue line) and the 1000 W lamp (red line) express in radiance. The intensity of the 1000 W lamp show a value of 0.45 W/m^2sr^{-1} at 550 nm of wavelength; this value can be considered similar to the intensity of solar irradiance common measured during spectroscopy field surveys. The standard deviation of the values (showed in the graph) is calculated considering 100 central pixels of the sensors and, it is larger from 900 to 1000 nm.

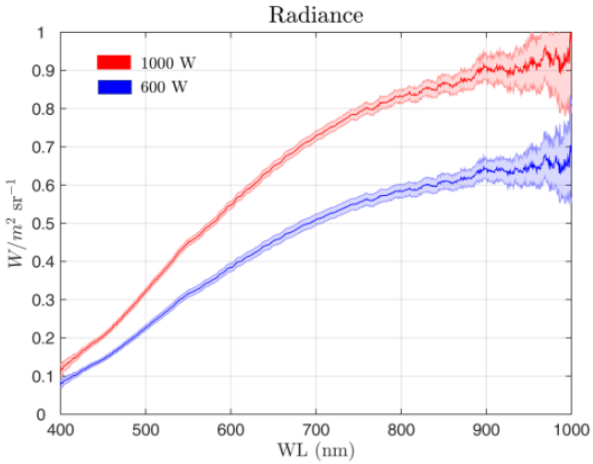

Figure 4.7: Halogen stable 600/1000 W lamps Intensity

The spatial and the temporal uniformity of the lamps can be observed in Figure 4.8. The images show the intensity (colour bars, W/m^2sr^{-1}) of the radiance range from 400 to 1000 nm for each of the 1004 spatial pixel. The two graphs show: the spatial uniformity refer as the radiance variability observed for some specific wavelengths (i.e. 460, 550, 650, 805 nm); and the temporal stability calculated as variability of the six measurements collected every 10 min (i.e. t0-t5).

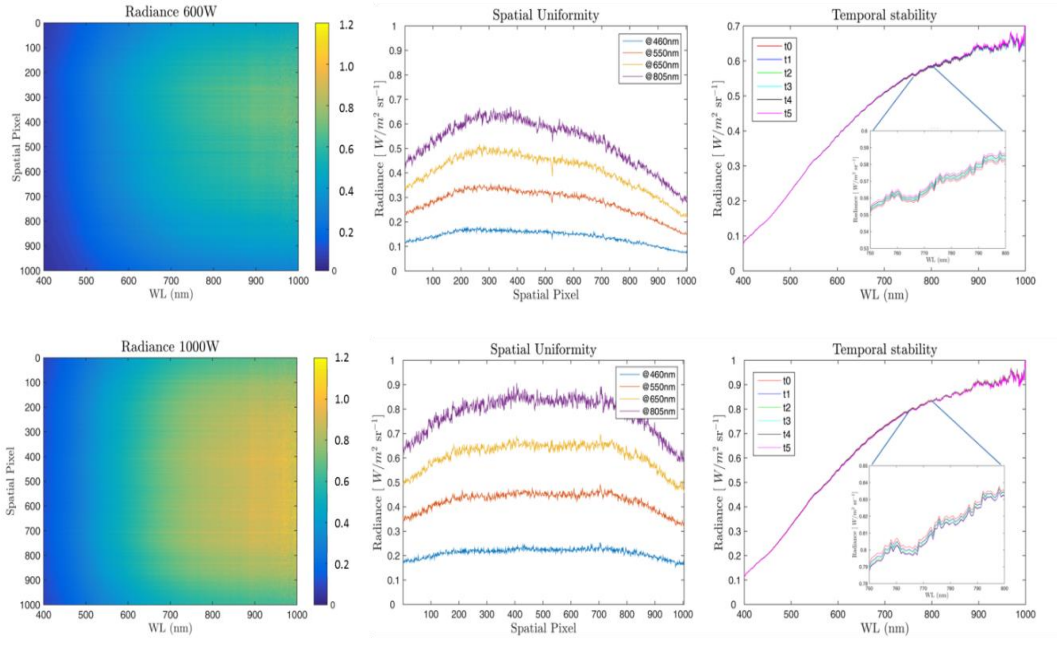

Figure 4.8: Spatial and the temporal stability of the halogen lamps

A good spatial uniformity was observed for both lamps. The maximum difference was found at 805 nm and it is about 25%. Successive radiance measurements demonstrate that the stability of the lamp is very high so can be considered negligible.

The test on the halogen lamp performed in the cold room laboratory show that the lamp works fine in cold conditions. In fact, during 3 hours of experiment at temperature of -18°C no effects were found on the spectral radiance and on the lamp surface. Furthermore the test aims to analyse the conservation of the ice core stratigraphy lighted by the 600/1000 W lamp. Using the 600 W lamp no effect was found on ice core samples while a slight melting was found on the surface using the 1000 W lamp. The results allow the use of the 600 W lamp to directly lighted the ice cores (in cold room laboratory at temperature lower than -18°C) ensuring the preservation of the stratigraphy.

4.4.2 HeadWall test

Figure 4.9 shows the result of the experiment on the magnolia leaves. The image (A) shows the data collected on the young magnolia (the images show replicated measurements on the leaf over the same line). The top of the images show the difference between the leaf and the white surface that held the sample. The graph (B) shows the spectral reflectance calculated for the three different target. The spectral signatures show the expected behaviours.

The results of hyperspectral data collected from firn and ice cores are shown in Figure 4.10. The RGB images show the area in which the line scan were performed. The Figure 4.10A show the values of reflectance (colour bars) from 400 to 1000 nm for each spatial pixel. Its spatial variability calculated for some specific wavelengths (i.e. 460, 550, 650, 805, 840, 900, 925) and the spectral signatures of some spatial pixel (range from 200 to 800) are showed in the graphs B and C, respectively.

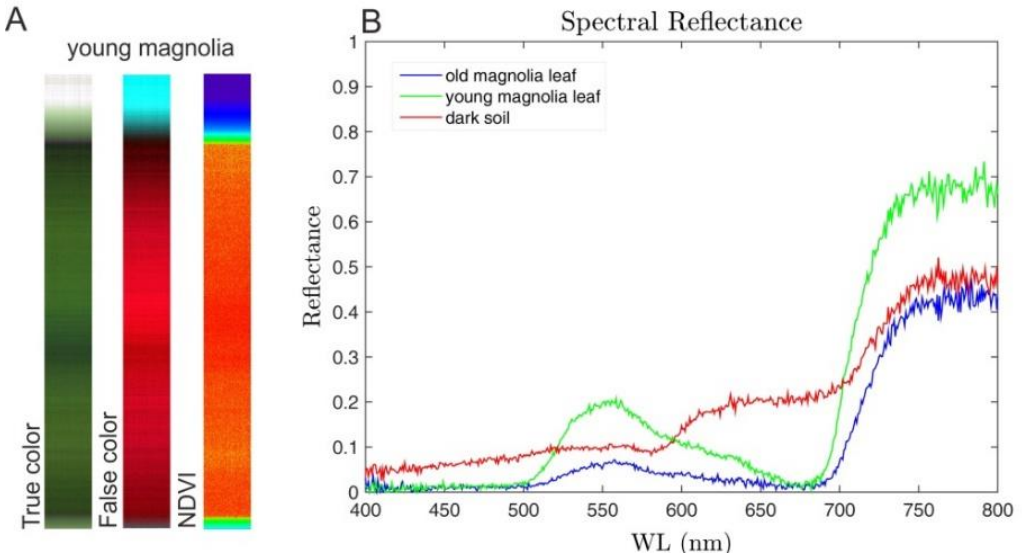

Figure 4.9: Images of young magnolia leaf (replicated measurements) and calculated NDVI index (A). Spectral reflectance of different target (B).

Differences in the firn/ice structure are visible in the RGB images and can be observed (Figure 4.10) also in the spectral data. Particularly, the typical grain texture of the firn core produce spectral spikes that are uniformly spatially distributed. Otherwise, spikes are less visible on ice core and they are the result of ice discontinuities and fractures. The graphs in Figure 4.10C snows the typical spectral signatures of ice and snow. The anisotropic effect of the grains orientation produce some anomalous spectral signatures. The ice core shows spectral signatures more uniform than firn core and lower values of reflectance with respect to firn. The anomaly observed (blue spectrum) refers to a discontinuity in the surface of the core.

The results show that is possible to analyses ice core spectral reflectance to characterize features related to ice characteristics. The camera (and the lighting position) have to be as nadiral as possible in order to reduce the influence of anisotropic directional effects. Tests shown promising results that have to be further investigated to map ice core properties from hyperspectral imaging or quantitatively evaluate components correlated to past environmental and climate depositions.

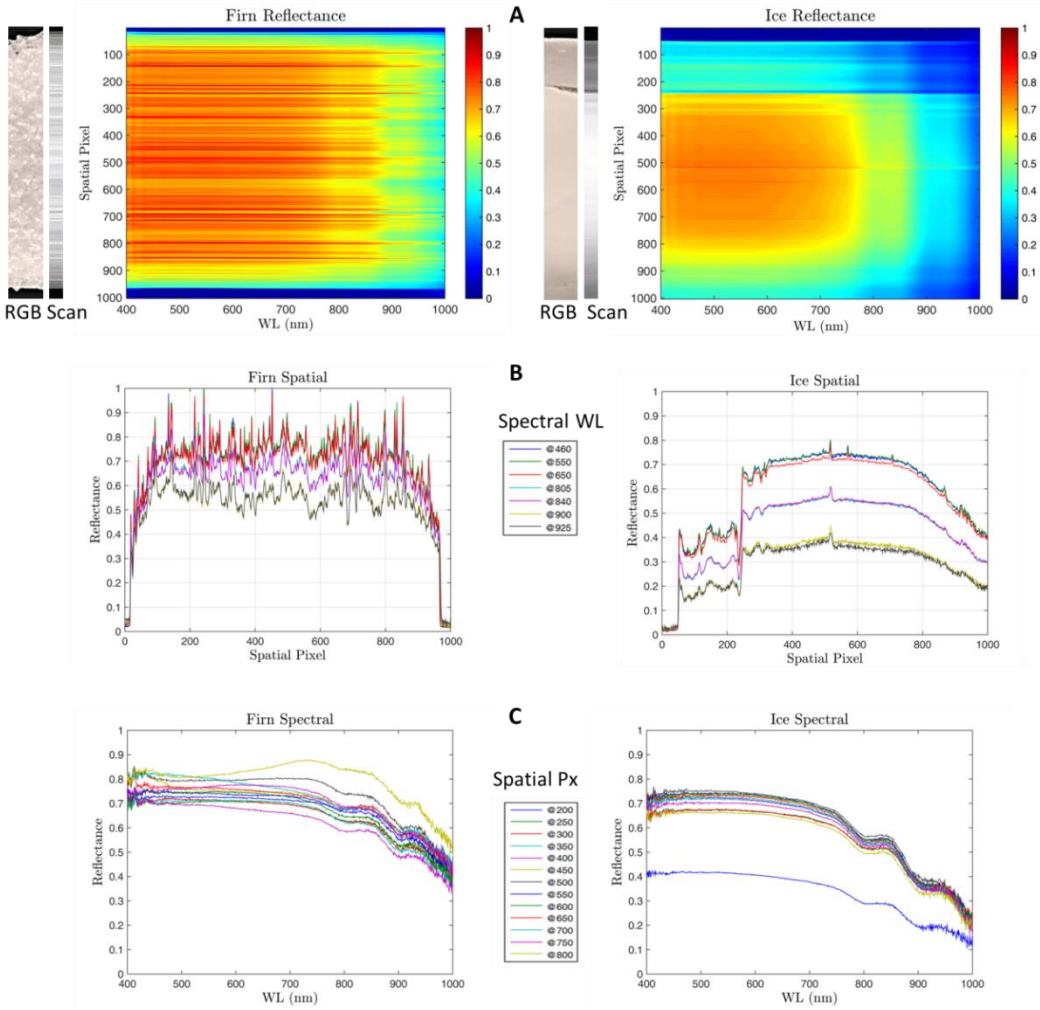

Figure 4.10: Results of spectra data collected from firn and ice cores.

4.4.3 High-resolution images

The images collected with the scanning system (RGB synthesis) are showed in Figure 4.11. The first image shows geometrical shapes and the second coloured textured objects. A good accuracy of the represented images can be observed. These results demonstrate a good capability to reconstruct high resolution hyperspectral images of the systems.

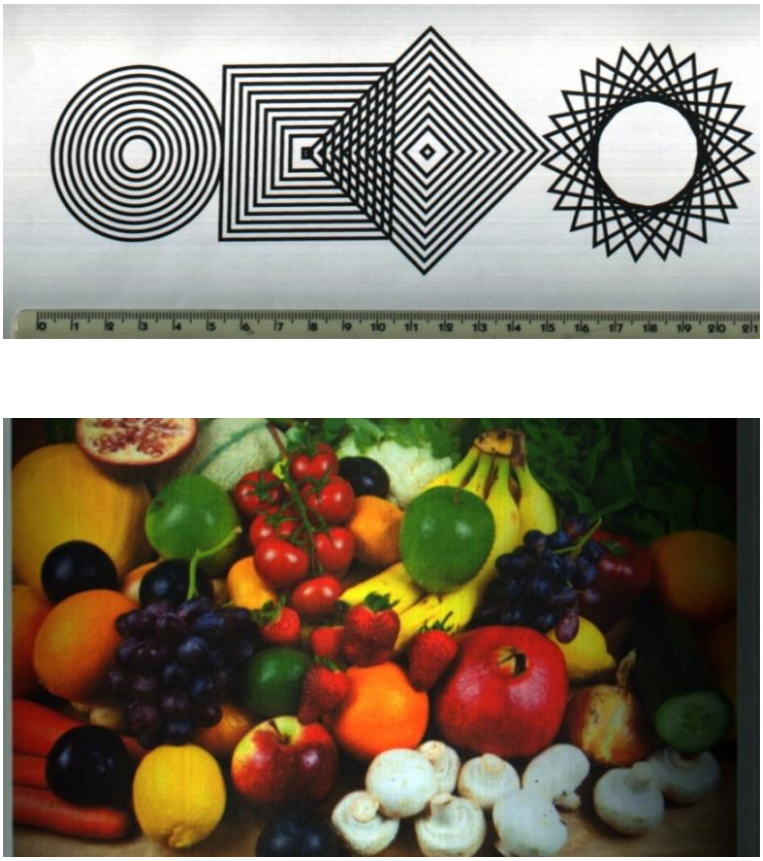

Figure 4.11: High resolution images reconstructed with the HYCE system.

4.4.4 Hyperspectral imaging

Figure 4.12 shows the hyperspectral images of leaves and coins. The graph shows the spectral reflectance of the two leaves (a dark green leaf and a light senescent leaf) and different coins (silver, golden, bronze). The circles in the image indicate the plotted pixel in the image. The spectral differences that can be observed are related to the health state of the leaves and to the different materials of the coins. The reflectance showed the typical behaviours of the leaves. If compared with the dark green leaf, the light leaf shows a lower absorption around 650 nm of wavelength that can be related to the reduction in photosynthetic pigments.

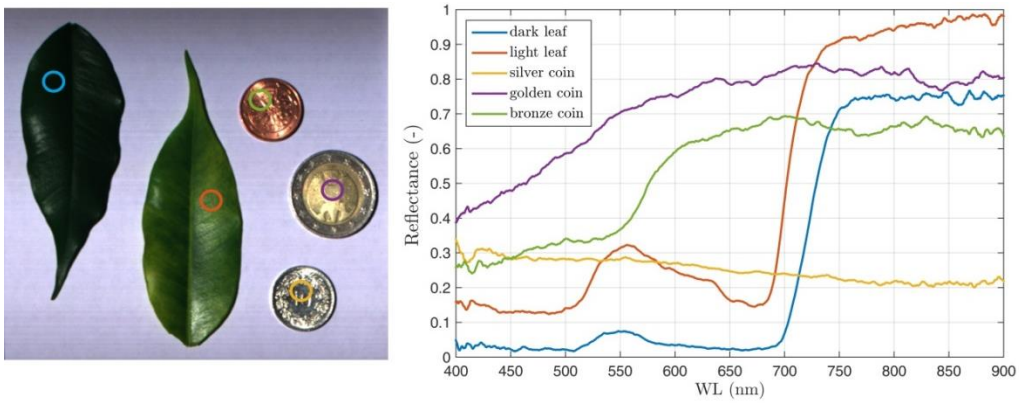

Figure 4.12: Hyperspectral image of different targets. The graph shows the spectral reflectance within the circles.

The spectral signatures of some pixel of the Canin ice core image are shown in Figure 4.13. The plotted pixels are circled in the Figure 4.14A with the corresponding colours. We can observe the difference between ice (red spectra) and dust layers (blue and green spectra). The presence of impurities reduce the reflectance in the VIS domain under 700 nm. This difference is considered in the definition of the SDI and it is used to identify layers of impurities or mineral dust.

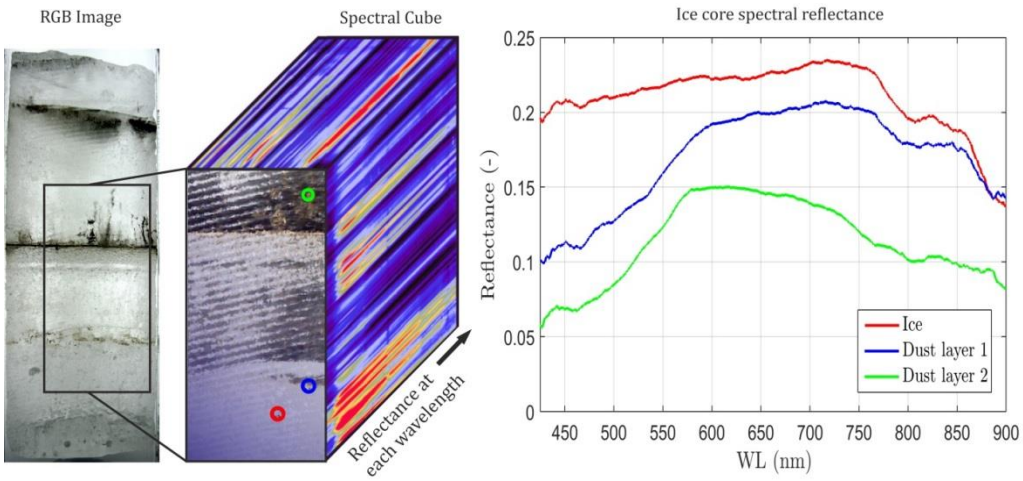

Figure 4.13: Spectral reflectance of ice core and dust layers. The square in the RGB image show the scanned area. The graph shows the spectral signature of ice and dust impurities (420 to 900 nm). Sampled pixel are circled in the cube image with corresponding colours.

Figure 4.14 shows a section of the hyperspectral image of the Canin ice core. From the RGB image (Figure 4.14A) we can observed: i) two layers of impurities (brown colour);

ii) ice with different density that reflects light differently; iii) a brightness lines texture can be related to the anisotropic reflectance of the rough surface. The SDI of the same section of the core is shown in the image below (Figure 4.14B). SDI values increase with higher concentration of impurities (i.e. mineral dust). Higher value of SDI are referred with red colours. From this image the two main layers of impurities can be identified. Furthermore, a higher level of impurities can be observed in the structure of the left part of the core (spatially range from 200 to 500) compared with the right ones. These results show the possibility to investigate layers of impurities present in ice cores samples using hyperspectral imaging.

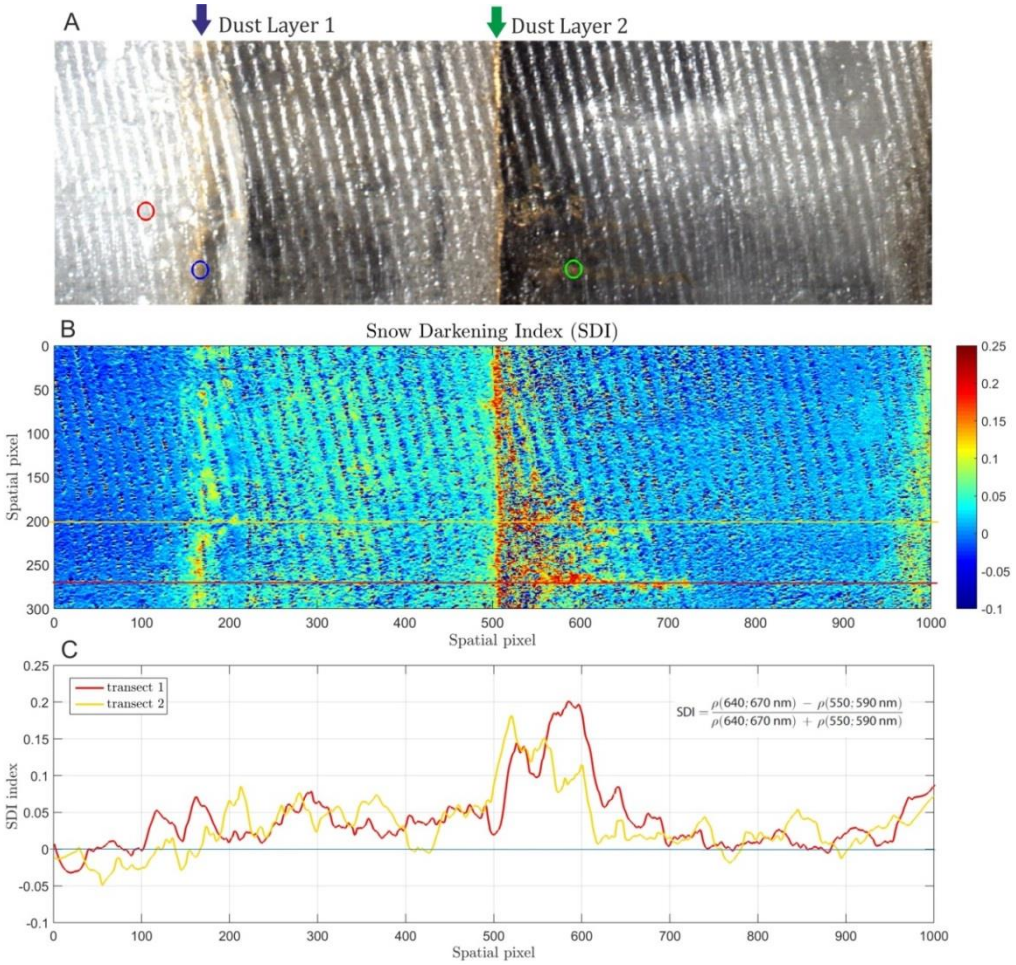

Figure 4.14: Investigation of impurity layers in the Canin ice core. A) RGB image of the area investigated using the hyperspectral camera. B) Calculated SDI index: red colours are associated with impurities. C) Spatial transect of SDI evidence the presence of these layers.

4.5 Conclusions and perspectives

A new system for hyperspectral imaging of ice cores was developed. It is based on a hyperspectral VIS-NIR imaging spectrometer carried by a high-precision linear stage, which embeds the HeadWall Photonics camera and a dedicated halogen stable light source (600/1000 W, LOT Quantum Design). The system was designed to have the best quality of imaging and the components were tested in laboratory and in cold room environment. The system can provide different resolution, adjusting the distance between the sensor and the target. Furthermore, two light intensity (600/1000 W) and two different lens (a standard lens; 17mm, and a macro lens: 60mm) can be mounted on the camera on the basis of the application requirements.

Dedicate laboratory tests were performed to calibrate the camera. Then, the performances of the lamps and the capability to collect very high-resolution hyperspectral images were tested. The experiments demonstrated that the stability of the lamp is very high and it is optimal for the collection of quality spectral data. Furthermore, the setup of the lamp allows a uniform illumination of the section of the core that is measured by the sensor. The intensity of the 600 W lamp ensures the preservation of the ice core stratigraphy. This was verified performing a test in cold room laboratory at a temperature of - 18 °C: no ice metamorphism was observed on the surface of the ice core. The system provides a collection of spectra data synchronizing the frame rate of the camera with the velocity of the stepper motor. This capability to create an hyperspectral image was tested capturing high resolution images (around 160 µm of pixel size) of different targets. Results show that the system provided an accurate imaging of the target.

Hyperspectral imaging was performed on different targets to observe difference in the spectral reflectance and first ice core hyperspectral image was collected. The experiment confirmed the possibility to measure reflectance from ice core to characterize ice core components. To reduce the influence of anisotropic directional effects, the surface of the ice core must be as smooth as possible. Test hyperspectral

images were collected from the Canin ice cave core to evaluate the presence of fine debris deposits and impurities. The SDI index was calculated on the image. This index was developed comparing satellite image and field spectral spectroscopy to quantitavely estimate mineral dust concentration on glaciers surfaces. Results suggest the possibility to use the SDI to evaluate concentration of impurities in the ice cores with high spatial resolution.

Imaging spectroscopy allows a quantitative analysis of optical properties, enabling new science investigations. This technique can be considered innovative in ice core studies since no attempt to hyperspectral imaging an ice core before. It can be used to map automatically ice core components, improving chemical analysis on ice cores. Tests showed promising results, those can be further investigate to map ice core components related to past depositions with high spatial resolution. Future studies will aims to analyse spectral feature to estimate layers thickness, ice density, grains structures and concentration of dust, black carbon, or other impurities. These information will be integrated with traditional geophysics methods for understanding past climatic and environmental conditions. Furthermore, the system can be used for other scientific application such as studying compositional material, food quality, geologic and biologic samples.

Acknowledgements:

The final version of this chapter will be submitted to *Cold Regions Science and Technology Journal*.

I wish to kindly thank Andrea Passerini, Sandro Baù, Stefano Banfi for their support in the development of the system. Biagio Di Mauro and Barbara Delmonte for their scientific support.

Bibliography

Alley RB (2000) Ice-core evidence of abrupt climate changes. *Proc. Natl. Acad. Sci.* 97(4), 1331–1334 (doi:10.1073/pnas.97.4.1331)

Alley RB, Shuman CA, Meese DA, Gow AJ, Taylor KC, Cuffey KM, Fitzpatrick JJ, Grootes PM, Zielinski GA, Ram M, Spinelli G and Elder B (1997) Visual-stratigraphic dating of the GISP2 ice core: Basis, reproducibility, and application. *J. Geophys. Res.* 102, 26367–26381 (doi:10.1029/96JC03837)

Bannon D (2009) Hyperspectral imaging: Cubes and slices. *Nat. Photonics* 3(11), 627–629 (doi:10.1038/nphoton.2009.205)

Bareth G, Aasen H, Bendig J, Gnyp ML, Bolten A, Jung A, Michels R and Soukkamäki J (2015) Low-weight and UAV-based Hyperspectral Full-frame Cameras for Monitoring Crops: Spectral Comparison with Portable Spectroradiometer Measurements. *Photogramm. - Fernerkundung - Geoinf.* 2015(1), 69–79 (doi:10.1127/pfg/2015/0256)

Brook EJ (2007) Ice Core Methods. *Encycl. Quat. Sci.*, 1145–1156 (doi:10.1016/B0.44.452747.8/00328-8)

Casacchia R, Lauta F, Salvatori R, Cagnati A, Valt M andOrbæk JB (2001) Radiometric investigation of different snow covers in Svalbard. *Polar Res.* 20(1), 13–22 (doi:10.1111/j.1751-8369.2001)

Casacchia R, Salvatori R, Cagnati a, Valt M and Ghergo S (2002) Field reflectance of snow/ice covers at Terra Nova Bay, Antarctica. *Int. J. Remote Sens.* 23(21), 4653–4667 (doi:Doi 10.1080/01431160110113863)

Colucci RR, Forte E and Fontana D Characterization Of Two Permanent Ice Cave Deposits In The Southeastern Alps (Italy) By Means Of Ground Penetrating Radar (Gpr). *The International Workshop on Ice Caves (IWIC)*. 33–39

Di Mauro B, Fava F, Ferrero L, Garzonio R, Baccolo G, Delmonte B and Colombo R (2015) Mineral dust impact on snow radiative properties in the European Alps combining ground, UAV, and satellite observations. *J. Geophys. Res. Atmos.*, 1–18 (doi:10.1002/2015JD023287)

Dozier J and Painter TH (2004) Multispectral and Hyperspectral Remote Sensing of Alpine Snow Properties. *Annu. Rev. Earth Planet. Sci.* 32(1), 465–494 (doi:10.1146/annurev.earth)

Goetz a F, Vane G, Solomon JE and Rock BN (1985) Imaging spectrometry for Earth remote sensing. *Science* 228(4704), 1147–1153 (doi:10.1126/science.228.4704.1147)

Greenberger RN, Ehlmann BL, Blaney DL, Cloutis E a, Wilson JH, Green RO and Fraeman A a (2015) Imaging spectroscopy of geological samples and outcrops: Novel insights from microns to meters. *Gsa Today* (12) (doi:10.1130/GSATG252A.1)

He H and Sun D (2015) Trends in Food Science & Technology Hyperspectral imaging technology for rapid detection of various microbial contaminants in agricultural and food products. *Trends Food Sci. Technol.* 46(1), 99–109 (doi:10.1016/j.tifs.2015.08.001)

Jouzel J and Masson-Delmotte V (2010) Paleoclimates: what do we learn from deep ice cores? *Wiley Interdiscip. Rev. Clim. Chang.* 1(5), 654–669 (doi:10.1002/wcc.72)

Kim MS, Chen YR and Mehl PM (2001) Hyperspectral reflectance and fluorescence imaging system for food quality and safety. *Am. Soc. Agric. Eng.* 44(3), 721–729

Kinnard C, Koerner RM, Zdanowicz CM, Fisher DA, Zheng J, Sharp MJ, Nicholson L and Lauriol B (2008) Stratigraphic analysis of an ice core from the Prince of Wales Icefield, Ellesmere Island, Arctic Canada, using digital image analysis: High-resolution density, past summer warmth reconstruction, and melt effect on ice core solid conductivity. *J. Geophys. Res. Atmos.* 113(24), 1–14 (doi:10.1029/2008JD011083)

Kipfstuhl S, Hamann I, Lambrecht A, Freitag J, Faria SH, Grigoriev D and Azuma N (2006) Microstructure mapping: a new method for imaging deformation-induced microstructural features of ice on the grain scale. *J. Glaciol.* 52(178), 398–406

Lei R, Zhang Z, Matero I, Cheng B, Li Q and Huang W (2012) Reflection and transmission of irradiance by snow and sea ice in the central Arctic Ocean in summer 2010. *Polar Res.* 31(0), 1–17 (doi:10.3402/polar.v31i0.17325)

Lucieer A, Malenovský Z, Veness T and Wallace L (2014) HyperUAS-Imaging Spectroscopy from a Multirotor Unmanned Aircraft System. *J. F. Robot.* 31(4), 571–590 (doi:10.1002/rob.21508)

McGwire KC, Hargreaves GM, Alley RB, Popp TJ, Reusch DB, Spencer MK and Taylor KC (2008) An integrated system for optical imaging of ice cores. *Cold Reg. Sci. Technol.* 53(2), 216–228 (doi:10.1016/j.coldregions.2007.08.007)

McGwire KC, Mcconnell JR, Alley RB, Banta JR, Hargreaves GM and Taylor KC (2008) Instruments and Methods Dating annual layers of a shallow Antarctic ice core with an optical scanner. *J. Glaciol. Instrum. Methods* 54(188), 831–838 (doi:10.3189/002214308787780021)

Nakamura T, Abe O, Hasegawa T, Tamura R and Ohta T (2001) Spectral reflectance of snow with a known grain-size distribution in successive metamorphism. *Cold Reg. Sci. Technol.* 32(1), 13–26 (doi:10.1016/S0165-232X(01)00019-2)

Negi HS, Shekhar C and Singh SK (2015) Snow and glacier investigations using hyperspectral data in the Himalaya. *Curr. Sci.* 108(5)

Nolin AW and Dozier J (2000) A hyperspectral method for remotely sensing the grain size of snow. *Remote Sens. Environ.* 74(2), 207–216 (doi:10.1016/S0034-4257(00)00111-5)

Obleitner F and Spötl C (2011) The mass and energy balance of ice within the Eisriesenwelt cave, Austria. *Cryosph.* 5(1), 245–257 (doi:10.5194/tc-5-245-2011)

Ortiz J, Mix A, Harris S and O'Connell S (1999) Diffuse spectral reflectance as a proxy for percent carbonate content in North Atlantic sediments. *Paleoceanography* 14(2), 171–186 (doi:10.1029/1998PA900021)

Petit JR, Jouzel J, Raynaud D, Barkov NI, Barnola JM, Basile I, Bender M, Chappellaz J, Davis M, Delaygue G, Delmotte M, Kotlyakov VM, Legrand M, Lipenkov VY, Lorius C, PEpin L, Ritz C, Saltzman E and Stievenard M (1999) Climate and atmospheric history of the past 420,000 years from the Vostok ice core, Antarctica. *Nature* 399(6735), 429–436 (doi:10.1038/20859)

Sjögren B, Brandt O, Nuth C, Isaksson E, Pohjola V, Kohler J and Van de Wal RSW (2007) Determination of firn density in ice cores using image analysis. *J. Glaciol.* 53(182), 413–419 (doi:10.3189/002214307783258369)

Svensson A, Nielsen SW, Kipfstuhl S, Johnsen SJ, Steffensen JP, Bigler M, Ruth U and Rothlisberger R (2005) Visual stratigraphy of the North Greenland Ice Core Project (NorthGRIP) ice core during the last glacial period. *J. Geophys. Res.* 110(D2), D02108 (doi:10.1029/2004JD005134)

Takata M, Iizuka Y, Hondoh T, Fujita S, Fujii Y and Shoji H (2004) Stratigraphic analysis of Dome Fuji Antarctic ice core using an optical scanner. *Ann. Glaciol.* 39(1), 467–472 (doi:10.3189/172756404781813899)

Warren SG (1982) Optical properties of snow. *Rev. Geophys.* 20(1), 67 (doi:10.1029/RG020i001p00067)

Wiscombe WJ and Warren SG (1980) A model for the spectral albedo of snow. I: Pure snow. *Journal of Atmospheric Sciences* 37, 2712–2733 (doi:10.1175/1520-0469(1980)037)

5. Summary and Conclusions

In my thesis, I proposed a methodology to maps potential drilling sites of mountain glaciers in order to collect new ice cores with preserved stratigraphy. To date, the issue of the identification of the suitable areas for ice core drilling has not been addressed quantitatively in scientific literature. Nevertheless, new ice cores from non-polar mountain glaciers are essential to study climate change. The methods presented were applied for mapping the SICD in the European Alps and in the Asian High Mountains. The most potential glaciers were identified and their interest was discussed. Whereas, in the Alps the major part of suitable drilling sites have been already exploited, in the Asian High Mountains as well as in other remote regions (i.e. North and South America Mountains), a large number of potential drilling sites are still available. More ice cores should be collected with the purpose to study regional climate behaviours, such as: variability of circulation patterns, improving accuracy of global circulation model, extreme events, environmental impacts of emerging economy, etc. Results provide useful information to facilitate the selection of the future drillings. Furthermore, the method can easily applied in the other mountain chains to collect ice core, providing a global view of climate and environmental change.

In the second part of my research I proposed new tools that can be used for studying glaciers and ice cores properties. The HyUAV, a novel hyperspectral non-imaging UAV, is a promising platform for field spectroscopy surveys. We evaluate the geometric, radiometric and spectral stability of the systems and then we tested the accuracy of collected spectra through flight tests. HyUAV is able to collect RGB images coupled with VIS-NIR hyperspectral data. Reflectance data allow to investigate spectral features related to surface properties. The system can provide relevant environmental data at

very detailed spatial and temporal resolutions. Furthermore, hyperspectral data were integrated with RGB products (orthomosaic, 3D model, DTM) and telemetry data providing new advantages for environmental applications. The HyUAV can be considered a potential tool for studying glaciers and for a wide range of monitoring activities. For example, the system can be used to collect snow/ice reflectance in order to evaluate the impact of light-absorbing impurities on glaciers mass balance. Seasonal mineral dust depositions, in fact, can strongly alter their radiative properties. This produce a radiative forcing that accelerate the melting of seasonal snow increasing the absorption of incident solar radiation. Other applications of this platform can be regard: precision farming, species mapping in forest, phenological modelling and stress vegetation estimation, inland waters quality, landslide monitoring, asbestos roof mapping, etc.

In order to study climate change, new collection of ice cores have to be accompanied with the development of advanced techniques to analysed ice core components. An innovative hyperspectral imaging system was developed for this purpose. Hyperspectral imaging, in fact, can be used to quantitatively estimate atmospheric components contained in the ice core stratigraphy. The system is based on a hyperspectral VINR imaging spectrometer, that is carried by an high-precision linear stage. This embeds also a dedicated halogen stable light source (600/1000 W). The system was tested in laboratory and in cold room environment. The experiments confirmed the possibility to collect high resolution imaging of ice cores. First hyperspectral data (i.e. reflectance) were collected with promising results. Further studies can be performed to evaluate the concentration of different components related to past climatic and environmental conditions such as: mineral dust, elemental black carbon, tephra from volcanic eruption, etc. Furthermore, the system can be considered a valuable tool for other scientific applications and disciplines, range from studying compositional materials, food quality control, analysing geologic or biologic samples.

In conclusion, ice cores are essential for understanding the past improving the prediction of future climate change. For this propose, new ice core should be globally collected in the next years. Nonetheless, is fundamental understanding the environment, through the observation of the natural processes and dynamics. The development of new promising systems is the first step towards these challenges. Environmental variability such as temperature and precipitation trends, as well as anthropogenic impacts of populations dynamics, affect the natural ecosystems of many regions of the planet and the Earth's populations. Preserve glaciers and ecosystems, through the efforts of the sciences, the society and the politics is one of the our main responsibilities to ensure the conservation of the environments and their beauty to the new generations.

Appendix 1: Research output

Published papers:

Di Mauro B., Fava F., Ferrero L., Garzonio R., Baccolo G., Delmonte B. and Colombo R., 2015. Mineral dust impact on snow radiative properties in the European Alps combining ground, UAV and satellite observations. Journal of Geophysical Research: Atmospheres. doi: 10.1002/2015JD023287.

Papers in review and in preparation:

Garzonio R., Di Mauro B., Strigaro D., Colombo R., De Amicis M. and Maggi V., Mapping the suitability for ice core drilling of glaciers in the European Alps and in the Asian High Mountains. In review for Journal of Glaciology.

Garzonio R., Cogliati S., Di Mauro B., and Colombo R., Collecting field spectroscopy data with a non-imaging hyperspectral UAV. On submission to: IEEE Transaction on Geoscience and Remote Sensing.

Communications to conferences:

Di Mauro B., Baccolo G., Garzonio R., Colombo R. Glaciers darkening in the European Alps: a comparative satellite analysis. Submitted to ESA Living Planet Symposium, Prague, Czech Republic. 9-13 May 2016.

Di Mauro B. , Baccolo G. , Garzonio R. , Piazzalunga A. , Massabò D. , Colombo R. Mountain glaciers darkening: geochemical characterization of cryoconites and radiative impact for the Vadret da Morteratsch (Swiss Alps). Geophysical Research Abstracts. Submitted to European Geosciences Union (EGU), Vienna, Austria.17-22 April 2016.

Di Mauro B., Fava F., Ferrero L., Garzonio R., Baccolo G., Delmonte B. and Colombo R. Mineral dust radiative effect on snow in European Alps. Geophysical Research Abstracts. European Geosciences Union (EGU), Vienna, Austria. Vol. 17, EGU2015-3416, 2015.

Cogliati S., Garzonio R., Di Mauro B., Tattarletti B., Zacchello F., Marras P. and Colombo R. The Hyperspectral UAV (HyUAV) a novel UAV-based spectroscopy tool. ESSEM COST Action ES1309 OPTIMISE, Milan, Italy, October 2014.

Garzonio R., Di Mauro B., Strigaro D., De Amicis M., Maggi V. and Colombo R. Definition of a methodology to map the suitability of mountain glaciers for ice core drilling using morphometric and climatic indicators. International Symposium on The Future of the Glaciers: From the past to the next 100 years. Turin, Italy, September 2014.

Garzonio R., Cogliati S., Di Mauro B., Zanin A., Tattarletti B., Zacchello F., Marras P. and Colombo R. The HYUAV: a novel UAV-based spectroscopy tool for environmental monitoring. Unmanned Aerial Vehicles (UAVs) in Environmental Research, University of Exeter's, Environment and Sustainability Institute (ESI), Cornwall, United Kingdom, June 2014.

Di Mauro B., Delmonte B., Fagnani M., Fava F., Garzonio R. and Colombo R. Model simulation and hyperspectral measurement of snow albedo and light absorbing impurities. International Conference on Atmospheric Dust, Session He-13, Castellaneta Marina (TA), Italy, June 2014.

Fussi F., Barry H., Beavogui M., Garzonio R., Keita A., Patra L., Sartorelli M., and Vogt M. L. Characterization of shallow geology based on direct borehole data and field reports and identification of suitable zones for manual drilling in Guinea. Geophysical Research Abstract. European Geosciences Union (EGU), Vienna, Austria. Vol. 15, EGU2013-10662, 2013.

Ober G., Di Nicolantonio W., Colombo R., Maffeis G., Cazzaniga I., Brumana R., Marras P., Ferrero L., Cacciari A., Marmorale N., Rampini A., Bresciani M., Cogliati S. , Di Mauro B., Garzonio R., Gianfreda R., Ferrari F., Barazzetti L., Previtali M., Tattarletti B., Bolzacchini E., Sangiorgi G., Perrone M.G., Pastore S., Casini F., Fiorentino N., 2015. Il progetto SINOPIAE, impiego di dati telerilevati multisorgente per applicazioni ambientali innovative. Conferenza Nazione ASITA 2015, Lecco, Italy, pp. 619-626.

Taaac fatto!

- fun and exciting -

Roberto Garzonio

Ph.D. Dissertation